Wormholes and islands

Nikolakopoulou, T.

Publication date
2023
Document Version
Final published version

[Link to publication](#)

Citation for published version (APA):
Nikolakopoulou, T. (2023). *Wormholes and islands*. [Thesis, fully internal, Universiteit van Amsterdam].

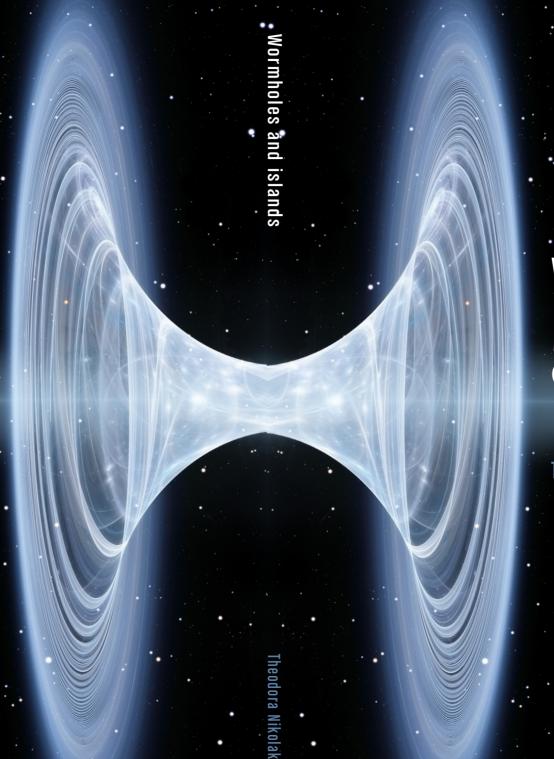Download date:19 Sep 2023

Wormholes
and islands

Theodora Nikolakopoulou

Wormholes and Islands

UNIVERSITEIT VAN AMSTERDAM

European Research Council
Established by the European Commission

Cover: Tamira Theunissen

WORMHOLES AND ISLANDS

ACADEMISCH PROEFSCHRIFT

ter verkrijging van de graad van doctor

aan de Universiteit van Amsterdam

op gezag van de Rector Magnificus

prof. dr.ir. P.P.C.C. Verbeek

ten overstaan van een door het College voor Promoties ingestelde commissie,

in het openbaar te verdedigen in de Aula der Universiteit

op vrijdag 29 September 2023, te 14:00 uur

door

THEODORA NIKOLAKOPOULOU

geboren te Athens

Promotiecommissie

Promotor

dr. B. W. Freivogel   Universiteit van Amsterdam

Copromotor

dr A. Castro Anich   Universiteit van Amsterdam

Overige leden

prof. dr. E.P. Verlinde   Universiteit van Amsterdam

dr. J.P. van der Schaar   Universiteit van Amsterdam

dr. E. Caceres   The University of Texas at Austin

dr. W.J. Waalewijn   Universiteit van Amsterdam

dr. A.D. Rolph   Universiteit van Amsterdam

prof. dr. S.J.G Vandoren   Universiteit Utrecht

Faculteit der Natuurwetenschappen, Wiskunde en Informatica

Publications

THIS THESIS IS BASED ON THE FOLLOWING PUBLICATIONS:

Presented in chapter 2:

[1] B. Freivogel, D.A. Galante, D. Nikolakopoulou, A.F. Rotundo

Traversable Wormholes in AdS and Bounds on Information Transfer

JHEP 01 (2020) 050, arXiv: 1907.13140

Presented in chapter 3:

[2] S. Bintanja, R. Espíndola, B. Freivogel, D. Nikolakopoulou

How to make traversable wormholes: eternal AdS_4 wormholes from coupled CFT's

JHEP 10 (2021) 173, arXiv: 2102.06628

Presented in chapter 4:

[3] R. Espíndola, B. Najian, D. Nikolakopoulou

Islands in FRW Cosmologies

arXiv: 2203.04433

OTHER PUBLICATIONS BY THE AUTHOR:

[1] B. Freivogel, D. Nikolakopoulou, A.F. Rotundo

Wormholes from Averaging over States

SciPost Phys. 14, 026 (2023) , arXiv: 2105.12771

The publications that are included in this thesis are a result of close collaboration with the co-authors. Most of the ideas were borne out of the numerous discussions and most of the calculations were performed by more than one author, together or separately. Below I describe the parts where my contribution had been the biggest.

[1] B. Freivogel, D.A. Galante, D. Nikolakopoulou, A.F. Rotundo

Traversable Wormholes in AdS and Bounds on Information Transfer

JHEP 01 (2020) 050, arXiv: 1907.13140

I participated in all the conceptual discussions. This paper was based on research that I conducted for my master thesis. I performed all the calculations before section 2.2.3.

[2] S. Bintanja, R. Espíndola, B. Freivogel, D. Nikolakopoulou

How to make traversable wormholes: eternal AdS_4 wormholes from coupled CFT's

JHEP 10 (2021) 173, arXiv: 2102.06628

I participated in all the conceptual discussions. I also contributed to most of the calculations up to section 3.3.2.

[3] R. Espíndola, B. Najian, D. Nikolakopoulou

Islands in FRW Cosmologies

arXiv: 2203.04433

I participated in all the conceptual discussions, in all the calculations and in writing the entire paper.

Contents

Contents

Contents

1
Main Findings and Introduction

Before diving in the introduction and the background material, for the impatient and excited reader, the main findings of this thesis are presented and briefly discussed. Some familiarity with the concepts presented is assumed.

1.1 Main findings

The main topic of this thesis is wormholes. These can be thought of as smooth bridges between two far away points in spacetime. These points can be disconnected from each other, in the sense that they are spacelike separated. If a wormhole allows information to travel through it, we call it traversable. In the opposite case we have a non-traversable wormhole, a famous example of which is the Einstein-Rosen bridge. In order for a wormhole to be traversable it needs to be sourced by an exotic stress tensor. More precisely, the stress tensor must violate the null energy condition (NEC), which is respected in classical physics. However, in quantum physics the NEC is violated. There is now a whole zoo of wormhole constructions that use various techniques to achieve traversability. However, the work that changed the landscape of wormholes is [1], by Gao, Jafferis and Wall (GJW). The authors constructed the first traversable holographic wormhole by starting from a BTZ black hole and coupling the two boundaries with a non-local coupling. Without too much detail, this coupling has the form

$$\delta S = -\int h \mathcal{O}_R \mathcal{O}_L \,, \tag{1.1.1}$$

where $\mathcal{O}_{L,R}$ is a primary operator in the left and right boundary respectively, and h is the coupling constant. This creates two negative shock waves that propagate in the black hole background. After some lengthy calculations one finds that the average null energy condition (ANEC) is violated so that the wormhole opens up. The opening of the wormhole, is calculated to be

$$\Delta V \propto \frac{h G_N}{\ell} \,, \tag{1.1.2}$$

where ℓ is the AdS radius, G_N is Newton's constant and ΔV is the difference of V coordinate (in Kruskal metric) between the future horizon and the first lightray which can get through the wormhole. In Chapter 2 we study the amount of information that can be sent through this type of wormhole. In the GJW case, we find that the number of particles that go through the wormhole is

$$N \propto \frac{h r_h}{\ell} \, , \tag{1.1.3}$$

where r_h is the black hole horizon radius. To obtain this estimate we impose that we are in the probe limit, which means that the signal does not backreact too much on the geometry. Moreover, instead of only coupling one $\mathcal{O}$ field, we couple K of them as in [2]. This enhances the negative energy and the amount of particles we can send the wormhole in a linear way. We also find that there is an upper bound on how many fields we are allowed to couple

$$K \lesssim \ell^{d-1}/G_N \, . \tag{1.1.4}$$

We also calculate that the maximum amount of information we can send through this type of wormhole, using various techniques is

$$N \lesssim \frac{f_h}{G_N} = S_{\text{BH}} \, . \tag{1.1.5}$$

Finally, we compare the aforementioned bulk results we obtained with a crude boundary estimate, and find them compatible.

In Chapter 3, we stay in the same spirit. Once again we use the non-local coupling for traversability. The goal of this chapter is to make an eternal AdS$_4$ traversable wormhole. We have drawn inspiration from [3]. In a nutshell, we start with two magnetically charged Reissner-Nordstrom (RN) black holes with opposite charges. In order to render the wormhole traversable we add a non-local coupling of the same type as GJW between the two CFTs that are dual to our black holes. The term we add to our action is of the form

$$\delta S = i \int d^3x \; h \left(\bar{\Psi}^R_- \Psi^L_+ + \bar{\Psi}^L_+ \Psi^R_- \right) \, , \tag{1.1.6}$$

where $\Psi_{R,L}$ is the bulk field that is dual to the charged fermions in the right and left CFT respectively and h is the coupling constant. This added term modifies the boundary conditions. By solving the Einstein equations with these new boundary conditions we get the quantum correction of the stress tensor to linear order in h

$$\langle T_{++}(x) \rangle = -\frac{1}{2\pi^3} \frac{q\lambda(h)}{R^2} \, . \tag{1.1.7}$$

2

For $h \geq 0$ the stress tensor is negative and we can violate the ANEC and open up the wormhole. We then use this result to solve the Einstein equations numerically and pertubatively in order to find the geometry. From far away the resulting geometry looks like two AdS$_4$ RN black holes. However in the middle the two black holes are connected by a throat that is nearly AdS$_2 \times \mathcal{S}^2$. So, an infalling observer would not hit a singularity but instead they would travel from one mouth to the other through this nearly AdS$_2 \times \mathcal{S}^2$ throat.

Finally, we find that there is a Hamiltonian whose ground state is dual to this wormhole

$$H = H_L + H_R - \frac{ih}{\ell} \int d\Omega_2 \left(\bar{\boldsymbol{\Psi}}_-^R \boldsymbol{\Psi}_+^L + \bar{\boldsymbol{\Psi}}_+^L \boldsymbol{\Psi}_-^R \right) + \mu(Q_L - Q_R), \qquad (1.1.8)$$

for some small values of μ, the chemical potential and h, the coupling constant.

In Chapter 4 we switch gears and focus on recent developments in the information paradox front. In a number of papers [4–9] the Page curve of Hawking radiation was recovered within semi-classical gravity. This was managed by recognizing that the fine grained entropy of the radiation receives a contribution from a disconnected piece of spacetime that usually lives in the black hole, called the island. The so-called island formula is

$$S(\mathbf{R}) = \min_I \left\{ \underset{I}{\text{ext}} \left[\frac{A(\partial I)}{4G_N} + S_{\text{mat}}(R \cup I) \right] \right\}, \qquad (1.1.9)$$

where $A(\partial I)$ is the area of the boundary of the island I, and $S_{\text{mat}}(R \cup I)$ is the renormalized entropy of the quantum fields on the union of the regions R and I. In short, the way we acquire the Page curve goes as follows. Before the evaporation starts there is no island, so the first term in (4.1.1) is zero and thus the entropy follows the curve $S(\mathbf{R}) \approx S_{\text{mat}}(R)$. Later, when the evaporation of the black hole has progressed, a new extremal surface appears, which is the island. Its boundary is close to the horizon and it contains almost all the partners of the Hawking radiation that has escaped. These partners in the island purify the external ones and hence the entropy decreases, following the curve $S(\mathbf{R}) \approx \frac{A(\partial I)}{4G_N}$ and the Page curve is recovered.

By now, islands have been studied in various different ways and in a number of geometries. In this thesis we study them in Friedmann–Lemaître–Robertson–Walker (FRW) cosmologies. Usually islands are associated with black holes, in the context of which the information paradox is well-defined. We explore what happens in four dimensional cosmological spacetimes. We extend the work of [10], where the authors derived three necessary conditions for the existence of an island and applied them to spatially flat $k = 0$ FRW supported by radiation and curvature and cosmological constant Λ. They found that for flat slicing and $\Lambda < 0$ there is

an island that starts at a large radius and extends to infinity. For $\Lambda \geq 0$ no islands were found.

We expand to the cases of open and closed slicing. We find that for closed universes irrespective of the cosmological constant there is always an island that is the whole Cauchy slice. However, this is not the exciting case. When $\Lambda > 0$, for open universes there are no islands. However, for $\Lambda < 0$ there are non-trivial islands for both the open and closed slicing. In the case of a closed universe, there is an island region around the half-sphere point. This island is finite in size. For open universes, an island region shows up for large enough radius and extends all the way to infinity, in a similar fashion as in the flat slicing case in [10].

With this we conclude the main findings of this thesis. We proceed with giving a more general overview concerning wormholes and discussing background material needed for the rest of the thesis.

1.2 Wormholes

Wormholes have been, for over a century, an object of fascination both for physicists and the wider public. They are depicted as spacetime shortcuts that a traveler can take in order to traverse distances that otherwise would be impossible to cross. Usually the travelers are shown to go through one side and appear unharmed on the other. However, in reality, it is still unclear whether or not such objects exist, and if they do, if the trip through them would be a safe one.

For a wormhole to be traversable, it is necessary that geodesics entering from one side (and hence, focusing) defocus upon reaching the other in order to escape. This defocusing of the geodesics is contrary to the usual effect of gravity. In the presence of ordinary positive energy, geodesics tend to focus. Thus, for the geodesics to defocus, the presence of negative energy is required in the throat region.

This conclusion was first arrived at by Morris and Thorne [11] in 1998. They constructed the one of the first traversable wormholes by choosing an adequate, well-behaved metric and solving for the stress tensor.[1] The resulting stress tensor indicated that negative energy is essential to prevent the wormhole throat from collapsing upon a traveler. This type of unusual energy violates the energy conditions, which are requirements that capture the expectation that energy should be positive. Despite this, there exist a number of theoretical and experimental examples, classically and quantumly, where the energy conditions are violated. In

---

[1]The first traversable wormhole was constructed by Ellis and independently by Bronnikov in 1973, and it was a nongravitating, purely geometric wormhole.

subsection 1.2.2, we will briefly examine a case where the null energy condition (the most useful energy condition in the study of wormholes) is violated, and in 1.2.3 we will review a famous non-traversable wormhole, namely, the Einstein-Rosen bridge.

In the years following Morris and Thorne's publication, a plethora of papers on the topic of traversable wormholes were published. The construction most relevant to this thesis is the Gao-Jafferis-Wall (GJW) wormhole [1]. This was the first traversable wormhole in holography. One appealing aspect of the GJW construction is that the negative energy necessary to open up the wormhole is not artificially put there "by hand," but instead arises as a consequence of a non-local coupling that connects the two boundaries. Once this coupling is done, two negative energy shock waves start propagating in the bulk of the geometry. In subsection 1.3.3 we will briefly review how shock waves work and in 1.3.4 we will examine the GJW construction.

1.2.1   Pointwise and averaged null energy condition

The essence of General Relativity can be captured by the Einstein Equations

$$G_{\mu\nu} = 8\pi G_N T_{\mu\nu} \,, \tag{1.2.1}$$

where $G_{\mu\nu}$ is the Einstein tensor and $T_{\mu\nu}$ is the stress tensor. The left hand side of (1.2.1) represents the curvature of our spacetime and the right hand side encapsulates all the energy contained in it. In general, one can pick their favorite metric, calculate the Einstein tensor and then demand that it is equal to the stress tensor. Even though this procedure is formally correct, it does not ensure that the resulting stress tensor will be a realistic energy source. Thus, in order to avoid having nonphysical stress tensors we impose energy conditions.

As Carroll [12] explains: "*The energy conditions are coordinate-invariant restrictions on the energy-momentum tensor*". To gain more physical intuition we will consider the stress tensor of the perfect fluid and examine how the energy conditions look in this case. The perfect fluid stress tensor has the form

$$T_{\mu\nu} = (\rho + p)U_\mu U_\nu + p g_{\mu\nu} \,, \tag{1.2.2}$$

where U^μ is the four-velocity of the fluid, ρ is the energy density and p the pressure. In what follows ℓ^μ is a null vector. The most popular energy condition, at least for the topic of wormholes, is the null energy condition (NEC)

$$T_{\mu\nu}\ell^\mu\ell^\nu \geq 0 \,, \tag{1.2.3}$$

which in the case of the perfect fluid can be written as

$$\rho + p \geq 0\,. \tag{1.2.4}$$

There are more energy conditions, but this one will be the only one that we will be using in this thesis. Moreover, it is the hardest one to violate. Notice that the energy density can be negative as long as there is compensating positive pressure. The aforementioned condition is otherwise called pointwise null energy condition because it only refer to specific points in spacetime. Most classical matter obeys NEC, not all. Additionally, all pointwise energy conditions are necessarily violated by essentially any quantum field theory [13]. This led Tipler [14] to suggest an averaged version of the pointwise energy conditions. He proposed averaging the weak energy condition (yet another energy condition) over an observer's worldline

$$\int_{\gamma} T_{\mu\nu} u^{\mu} u^{\nu} d\tau \geq 0\,, \tag{1.2.5}$$

where γ is a timelike curve, u^{μ} is a tangent vector and τ the proper time. The energy density is not measured on a single point, rather averaged over a geodesic. In this case, we are allowed to have negative energy density on some portions of the geodesic, as long as overall the positive energy density "wins". We can do the same for NEC

$$\int_{\gamma} T_{\mu\nu} k^{\mu} k^{\nu} d\lambda \geq 0\,, \tag{1.2.6}$$

where γ is now a lightlike curve, k^{μ} is a tangent null vector and λ the affine parameter. This type of energy condition is called averaged null energy condition (ANEC) and this is the one whose violation can lead to a traversable wormhole. The success of averaging is that these non-local conditions do, in general, hold for quantum field theories, unlike their local counterparts [15–19] .

An alternative approach to the averaged energy conditions are the quantum inequalities, first introduced by Ford [20]. They are constraints on the magnitude and duration of the negative energy fluxes and densities, measured by an inertial observer. They resemble the uncertainty principle because they state that the duration of a negative energy pulse is inversely related to its magnitude. In this thesis, we will not explore the quantum inequalities further.

1.2.2 The Casimir effect

The most prominent example of violation of the energy conditions, in the quantum realm, is the Casimir effect, which has been experimentally observed [21–23]. In 1948 Hendrik Casimir showed that the presence of two perfectly reflecting plates distorts the vacuum energy of the electromagnetic (EM) field [24,25]. Specifically, he found that it is negative relative to the normal zero point energy. The EM field

becomes quantized due to the presence of the plates. The modes of the field that are longer than the distance between the plates cannot fit between them. So, to put it simply, between the plates we are "missing" some of the modes. As a result, the vacuum energy we calculate is lower than that of the Minkowski vacuum, which contains all modes.

Following [26], the electromagnetic Casimir stress tensor, in four dimensional Minkowski spacetime $ds^2 = -dt^2 + dx^2 + dy^2 + dz^2$ with plates at $z = 0$ and $z = a$, can be written as

$$T^{\mu\nu}_{Casimir} = \frac{\pi^2}{720a^4} \begin{pmatrix} -1 & 0 & 0 & 0 \\ 0 & 1 & 0 & 0 \\ 0 & 0 & 1 & 0 \\ 0 & 0 & 0 & -3 \end{pmatrix}. \tag{1.2.7}$$

It is easy to see that the EM Casimir stress tensor violates NEC for all null vectors (except when they are parallel to the plates) since $\rho + p_z < 0$. By ρ we denote T^{00} and p_z is T^{33}. On the other hand, ANEC is harder to violate. Up to this point of the analysis we have assumed perfectly conducting plates, but in realistic scenarios the mass of the plates far exceeds the negative energy. Since we integrate along a complete null geodesic, the integral takes contributions from the matter composing the plates too. So, even though NEC is violated everywhere between the plates, ANEC is in general satisfied.

In Visser's book [27] there is an explicit analysis about what happens with the averaged energy conditions. In a nutshell, he defines another Casimir stress tensor, similar to (1.2.7), that corresponds to having realistic metal plates:

$$T^{\mu\nu}_{Casimir} = \sigma \hat{t}^\mu \hat{t}^\nu [\delta(z) + \delta(z-a)] + \Theta(z)\Theta(a-z)\frac{\pi^2}{720a^4} \left[\eta_{\mu\nu} - 4\hat{z}^\mu \hat{z}^\nu \right], \tag{1.2.8}$$

where $\hat{t}^\mu$ is the unit vector in the time direction and the plates are not ideal and have surface mass density σ. Then he writes down ANEC and immediately infers that the only way it can be violated is when σ is physically unreasonable. So, it's safe to say that ANEC is obeyed in the case of physical plates.

However, there is another variation of the electromagnetic Casimir effect. The Casimir effect can also arise when our spacetime does not have trivial topology. A simple example is the following. Assume that we have a two dimensional flat spacetime and a free massless scalar field on which we impose periodic boundary conditions. In this case, the Casimir stress tensor is found to be

$$T^{Casimir}_{tt} = -\frac{\pi}{6L^2}, \tag{1.2.9}$$

where L is the period. In this case, since there are no physical plates to contribute, ANEC is violated. Thus, the topological Casimir effect is a better candidate for the

construction of traversable wormholes. There is a number of papers dedicated to building traversable wormholes by using the topological Casimir effect, indicatively [3,28–34]. One study that stands out is [3]. The set-up includes fermions that give rise to Casimir energy, which renders the wormhole traversable. We will review this construction in detail in chapter 3.

1.2.3   Einstein-Rosen bridge

The first theoretical example of a non-traversable wormhole lives in the maximally extended Schwarzschild black hole. It was first noticed by Ludwig Flamm [35], in 1916, and later by Einstein and Rosen [36]. They realized that besides the usual Schwarzschild black hole solution, there is a second solution, the white hole. It can be thought as the reverse of the black hole. Things can escape to us from the white hole, but we can never reach it.
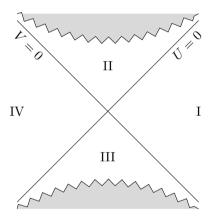
Figure 1.1: Kruskal diagram of the Schwarzschild black hole. The zig-zag lines represents the singularities ($UV = 1$).

One can start from the usual form of the Schwarzschild black hole metric

$$ds^2 = -\left(1 - \frac{2G_N M}{r}\right) dt^2 + \left(1 - \frac{2G_N M}{r}\right)^2 + r^2 d\Omega^2 \,, \qquad (1.2.10)$$

and bring it to the following form

$$ds^2 = \frac{32 G_N^3 M^3}{r} e^{-r/2G_N M} dU dV + r^2 d\Omega^2 \,, \qquad (1.2.11)$$

where

$$UV = \left(1 - \frac{r}{2G_N M}\right) e^{r/2G_N M} \,. \qquad (1.2.12)$$

These cooridnates in (1.2.12) are known as the Kruskal coordinates. The Kruskal diagram of the Schwarzschild black hole is shown in fig. 1.1. Depending on the signs of U and V we can be in either of the four quadrants. From region I we can travel to region II, but we can could never reach III or IV. Signals can travel to I and II from IV. Of course, anything moving in region II has its fate sealed; it will unavoidably hit the future singularity.

In this geometry there is a non-static, non-traversable wormhole connecting the two asymptotically flat regions. The throat of the wormhole has its shortest length at the bifurcation point, in the middle. However, even if we send a photon from region I, almost hugging the horizon, it will never make it to region IV.

1.3   Wormholes in holography

The new era of wormholes came a few years ago, with the work of Gao, Jafferis and Wall (GJW) [1]. In this work the first traversable wormhole in holography was constructed. After the publication of this paper, many others followed. Here we review the GJW wormhole and some of its follow-up papers, in subsection 1.3.4. For now, we are going to review some necessary background material before diving into the wormholes.

1.3.1   AdS/CFT

Wormholes had been the topic of study of physicists for a long time. The game changer, however, was when they were put in the context of AdS/CFT. The AdS/CFT correspondence was proposed by Juan Maldacena in 1997 [37]. Simply put, it is a duality between a gravitational system with negative cosmological constant (AdS) in $d + 1$ dimensions and a quantum field theory (specifically a CFT) in d dimensions. The CFT lives on the boundary of AdS and the gravitational theory lives in the bulk of AdS.

In path integral language we can express the AdS/CFT correspondence as

$$Z_{CFT}[J] = Z_{bulk}[\phi_b]\,, \tag{1.3.1}$$

where J is the source of an operator $\mathcal{O}$ in the CFT and ϕ_b is the boundary condition of a field ϕ in the bulk. This is one version of the dictionary between the quantities on the boundary and the bulk [38,39]. One can differentiate the partition functions with respect to the sources, acquire the desired correlators and then set the sources to zero.

There is a second version [40,41] of the dictionary that is obtained by extrapolating

correlators in the bulk to the boundary as follows

$$\langle \mathcal{O}_1(x_1)\mathcal{O}_2(x_2)\cdots\mathcal{O}_n(x_n)\rangle = \lim_{z\to 0} z^{-\Delta}\,\langle \phi_1(z,x_1)\phi_2(z,x_2)\cdots\phi_n(z,x_n)\rangle\,, \quad (1.3.2)$$

where $\mathcal{O}$ are CFT operators of conformal weight Δ_i, and Δ is the sum of conformal weights of all the $\mathcal{O}$ operators. The z appearing above is the one holographic direction. In Poincare coordinates AdS_{d+1} is written as

$$ds^2 = \frac{\ell^2}{z^2}(dz^2 + \eta_{\mu\nu}dx^\mu dx^\nu)\,, \quad (1.3.3)$$

where ℓ^2 is the AdS length. Two important limits of z are $z \to 0$ at the boundary and $z \to \infty$ in the bulk. The two dictionaries are equivalent [42, 43]. Using these dictionaries, one can translate between quantities between the bulk and those on the boundary.

For example, a useful lemma of the AdS/CFT dictionary is the scalar field in AdS. The dictionary tells us that a scalar field of mass m in the bulk is dual to a scalar operator $\mathcal{O}$ with scaling dimension

$$\Delta = \frac{d}{2} + \sqrt{\frac{d^2}{4} + m^2\ell^2}\,. \quad (1.3.4)$$

There are many entries in the AdS/CFT dictionary and discovering more remains an active area of research.

Since the appearance of AdS/CFT there have been hundreds of studies on it. It has proven a very useful tool in the pursuit of understanding quantum gravity.

1.3.2 The BTZ black hole

There are many different black holes relevant to holography. Here we focus our attention on the BTZ black hole, as it is necessary for the following material and importantly, because it has a favorite holographic dual, the thermofield double state. The BTZ black hole is asymptotically AdS and three-dimensional. Its metric in "Schwarzschild"-like coordinates is

$$ds^2 = -\frac{r^2 - r_h^2}{\ell^2}dt^2 + \frac{\ell^2}{r^2 - r_h^2}dr^2 + r^2 d\phi^2\,, \quad r_h = \sqrt{8G_N\ell M} \quad (1.3.5)$$

where r_h is the horizon radius, ℓ is the radius of AdS and M is the mass of the black hole. Another set of useful coordinates is Kruskal coordinates. In Kruskal

coordinates the BTZ metric becomes

$$ds^2 = \frac{4\ell^2 dU dV + r_h^2 \left(1 - UV\right)^2 d\phi^2}{\left(UV + 1\right)^2}, \qquad (1.3.6)$$

where

$$\exp\left(2\frac{r_h t}{\ell^2}\right) = -\frac{U}{V}, \qquad \frac{r}{r_h} = \frac{1 - UV}{1 + UV}. \qquad (1.3.7)$$

The horizons live at $U = 0$ and $V = 0$, the boundaries at $UV = -1$, and the singularities at $UV = 1$. In this geometry, there exists a non-traversable wormhole, as in the maximally extended Schwarzschild black hole. The Penrose diagram is shown in Fig. 1.2. Once again, even if we send a signal from the right side, very far in the past, it can never make it to the left side.
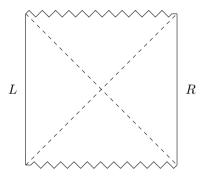
Figure 1.2: Penrose diagram of the BTZ black hole. The vertical lines represent the boundaries and the zigzag lines represent the singularities.

In 2001, Maldacena proposed that this geometry is dual to two copies of the CFT in the thermofield double state [44], which has the form

$$|TFD\rangle = \frac{1}{\sqrt{Z(\beta)}} \sum_n e^{-\beta E_n/2} |n\rangle_1 |n\rangle_2. \qquad (1.3.8)$$

The thermofield double state was first introduced in [45], as a trick to treat the thermal mixed state $\rho = e^{-\beta H}$ as a pure one in a bigger system. The trick involves doubling the degrees of freedom (dof) of one theory and entangling the two resulting systems.

The propagators of the BTZ black hole are known analytically [46, 47]

$$K_\Delta\left(t, r, \phi\right) = \left(\frac{r_h}{\ell^2}\right)^\Delta \frac{1}{2^{\Delta+1}\pi} \left(-\frac{\left(r^2 - r_h^2\right)^{1/2}}{r_h} \cosh\frac{r_h}{\ell^2}t + \frac{r}{r_h}\cosh\frac{r_h}{\ell}\phi\right)^{-\Delta},$$

$$(1.3.9)$$

where r_h is the horizon and will be very useful in the later chapters of this thesis.

1.3.3 Shock-waves

In this subsection we briefly examine shock waves in the BTZ geometry, using as reference [48, 49]. Understanding how shock waves work will be very useful for the purposes of this thesis. As mentioned in the introduction, in the traversable BTZ wormhole construction of [1] we have two negative energy shock waves propagating in the bulk. Starting from the unperturbed BTZ geometry, we insert a particle at the left boundary. The CFT state becomes

$$W(t_w)|TFD\rangle . \tag{1.3.10}$$

where t_w is the time we insert the particle at the left boundary. We assume that the energy of the particle is E, and that it is small compared to the mass of the black hole M.
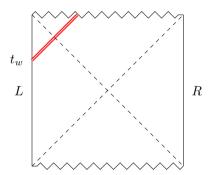
Figure 1.3: BTZ black hole geometry. We have inserted a particle on the left boundary. It propagates in the spacetime and eventually crosses the horizon and encounters the singularity.

Naively it seems like this cannot have a significant effect on the geometry. However, if we push the insertion far enough into the past, the particle will be boosted, in comparison to the original frame, and it will cross the the $t = 0$ slice with energy

$$E_p \sim \frac{E\ell}{r_h} e^{r_h t_w/\ell^2} , \tag{1.3.11}$$

where ℓ is the AdS radius and r_h the horizon radius. In this frame, the particle is actually a high energy shock wave that is going to have a non-trivial effect on the geometry. In order to find the new geometry we sew two BTZ geometries, one with mass M and one with $M + E$, along the null surface on which the shock is traveling, $V_w = e^{-r_h t_w/\ell^2}$.
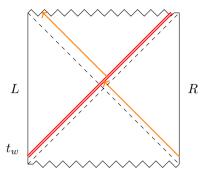
Figure 1.4: Penrose diagram of the perturbed BTZ black hole. The double red lines represent the shock wave. The orange line represents a signal that we send from the right boundary. Upon encountering the shock wave it shifts deeper in the black hole interior.

For E/M small, we find that the v coordinate gets shifted by an amount a

$$\tilde{V} = V + a, \quad a = \frac{E}{4M} e^{r_h t_w / \ell^2} \, . \tag{1.3.12}$$

The backreacted metric takes the following form

$$ds^2 = \frac{4\ell^2 \, dU \, dV + r_h^2 \left[1 - \left((U + a\theta(V)) \, V \right]^2 d\phi^2 \right.}{\left[1 + (U + a\theta(V)) \, V \right]^2} \, . \tag{1.3.13}$$

where $\theta(V)$ is the step function. If we send a signal from the right boundary towards the left boundary, it will suffer a time delay when it reaches the horizon $V = 0$, where the shock wave exists.

For the purpose of constructing a traversable wormhole, we need somehow to produce the "opposite" effect, namely, the signal should gain some time advance in order to avoid ending up at the singularity. If there was an operator that could create a negative energy shock wave instead of a positive one, the shift a would be negative. Then, the signal would eventually encounter the negative energy shock wave, shift towards the opposite direction and reappear on the left boundary.
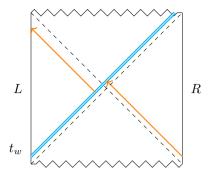
Figure 1.5: Negative shock wave in the BTZ geometry. The orange signal takes a time advance upon meeting with the shock wave and reappears on the left boundary.

In the next subsection we review how this was achieved by Gao, Jafferis and Wall in [1].

1.3.4 The Gao-Jafferis-Wall Wormhole

The first traversable wormhole in holography was constructed by Gao, Jafferis and Wall in [1]. They started from the unperturbed BTZ black hole geometry and coupled the two boundaries using a coupling term of the form

$$\delta S = -\int dt d\phi \; h(t,\phi)\mathcal{O}_R(t,\phi)\mathcal{O}_L(-t,\phi)\,, \qquad (1.3.14)$$

where $\mathcal{O}$ is a scalar primary operator with scaling dimension Δ, dual to a scalar field φ. The ultimate goal is to calculate the stress tensor due to the non-local coupling on the horizon $V = 0$ and see if it violates the averaged null energy condition (ANEC). After a number of tedious manipulations the authors find that the integrated stress tensor is

$$\int_{U_0}^{\infty} T_{UU}dU = -\frac{h\Gamma(2\Delta+1)^2}{2^{4\Delta}(2\Delta+1)\Gamma(\Delta)^2\Gamma(\Delta+1)^2\ell}\frac{{}_2F_1\left(\frac{1}{2}+\Delta,\frac{1}{2}-\Delta;\frac{3}{2}+\Delta;\frac{1}{1+U_0^2}\right)}{(1+U_0)^{\Delta+1/2}}\,, \tag{1.3.15}$$

where ℓ is the AdS radius. This quantity is always negative, which means that the ANEC is violated and the wormhole is rendered traversable. If we send a signal from the right boundary towards the left, upon meeting with the negative energy shock wave will gain a time advance and will reappear on the left boundary, as in Fig. 1.6.
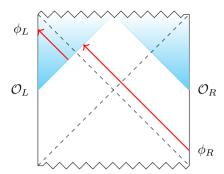
Figure 1.6: The red line represents the signal we send, from the right boundary. The blue regions represent the negative energy density. Upon collision with the negative energy the signal shifts and instead of ending up in the singularity it emerges on the left boundary. We must note that when we have even number of dimensions the negative energy is always localized on light cones (as we saw in 1+1 Minkowski spacetime), whereas in odd number of dimensions the negative energy is inside the light cones as well (as we see here, in case of the BTZ).

The opening of the wormhole (in other words, the time advance a lightray will gain) is equal to

$$\Delta V \sim \frac{hG_N}{\ell} \,, \tag{1.3.16}$$

where r_h is the black hole horizon radius, G_N is Newton's constant and V is the dimensionless Kruskal coordinate. ΔV is a very small number. Thus, this wormhole differs than the usual static type, such as the Morris-Thorne wormhole, that remain perpetually open. The GJW wormhole opens up for a small amount of time and then closes again. However, this is enough for highly boosted signals to traverse the wormhole.

Following GJW, an abundance of similar constructions appeared, including one version in two dimensions [2] and a rotating version in three dimensions [50], among many others [51–59]. We explore this setup in more detail in chapter 2.

1.4   The Black Hole information paradox

1.4.1   Black hole thermodynamics

For a long time, it was believed that nothing can escape a black hole. Classically, this is a true statement. This changed in the 70's, when Hawking performed his famous calculation [60], which showed that, quantumly, thermal radiation is

emitted from black holes with temperature

$$T = \frac{\kappa}{2\pi}\,,$$

$$(1.4.1)$$

where κ is the surface gravity. For a Schwarzschild black hole the surface gravity is $\kappa = \frac{1}{4G_N M}$. It is worth mentioning that Bekenstein was first to come up with the idea that black holes are thermal objects and have entropy [61]. Hawking believed that they did not and tried to prove him wrong, only to end up confirming Bekenstein's idea. This temperature (1.4.1) suggests that black holes might behave like a thermodynamic objects. A little earlier Bardeen, Carter and Hawking [62] had calculated the response of a rotating black hole to objects being thrown in it as

$$dM = \frac{\kappa}{8\pi G_N}dA + \Omega dJ\,,$$

$$(1.4.2)$$

where M, A, Ω and J are the mass, horizon area, angular velocity and the angular momentum of the black hole. This equation looks suspiciously similar to the first law of thermodynamics

$$dM = SdT + \text{work terms}\,,$$

$$(1.4.3)$$

and indeed if we assume that the black hole has temperature $T \propto \kappa$ and entropy $S \propto A$ then the two equations are identical. Classically of course, there is no reason to believe that this is anything more than a coincidence. However, when combined with Hawking's later calculation it confirms that black holes indeed emit radiation and have entropy

$$S_{BH} = \frac{A}{4G_N}\,.$$

$$(1.4.4)$$

Equation (1.4.4) is the well-known *Bekenstein-Hawking entropy* formula. We also call it the coarse-grained entropy of the black hole. The total entropy of the black hole is called the *generalized entropy* and it has the form [61]

$$S_{\text{gen}} = \frac{A}{4G_N} + S_{\text{out}}\,,$$

$$(1.4.5)$$

where S_{out} is the entropy of quantum fields outside of the horizon. It has been proved that it obeys the second law of thermodynamics [17]. In order to proceed in explaining the information paradox, it is crucial that we first discuss the notion of the von Neumann or otherwise, fine-grained entropy. It has the form

$$S_{vN} = -\operatorname{Tr}\rho \log \rho\,,$$

$$(1.4.6)$$

where ρ is the density matrix. The von Neumann entropy captures our ignorance about the state of the system. For pure states it is zero, which signifies that we know everything about the state.
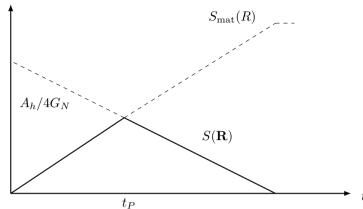
Figure 1.7: Page curve of the fine-grained entropy of an evaporating black hole.

1.4.2 The Page curve

The main issue that arises is the following. Assume we start with a black hole system in a pure state. At some point it starts evaporating. We usually think of this process as follows. Entangled Hawking pairs are created; one counterpart of each pair falls in the black hole and the other escapes in the ambient space. The outgoing pairs get collected at some far away part of spacetime, which we usually call a "bath".

We want to calculate the von Neumann entropy of the collected radiation. In the beginning of the evaporation process the entropy of the radiation is zero since there are no pairs in the bath. As the process starts, more and more outgoing pairs end up in bath and the von Neumann entropy increases. Based on Hawking's calculations [60, 63] it keeps on increasing and at some point surpasses the Bekenstein-Hawking entropy. This is the essence of the information paradox. In simple words, the entropy of the radiation becomes larger than what the black hole has room for. We would expect that if the process is unitary the entropy of the radiation would grow until it reaches the point where $S_{vN}=S_{BH}$ and then start decreasing until it vanishes.

This is what Page proposed in [64]. He showed that initially the fine-grained entropy grows, following the Hawking curve, but approximately halfway through the evaporation process, it starts decreasing and eventually vanishes, as in Fig 4.1, which is consistent with unitary evolution.

1.4.3   Holographic fine-grained entropy

We previously saw that in the semi-classical regime the total entropy of a black hole is given by (1.4.5). Interestingly, there exists a holographic version of the aforementioned formula. It was first conceived by Ryu and Takayanagi [65] and Hubeny, Rangamani, and Takayanagi [66]. It states that the entropy of a region R in the CFT has entropy proportional to a spacelike, codimension 2 extremal surface X such that $\partial X = \partial R$ and X is homologous to R

$$S(R) = \frac{A(X)}{4G_N} \, . \tag{1.4.7}$$

Faulkner, Lewkowycz and Maldacena [67] showed that when the quantum corrections are included, the formula for the entropy takes the form

$$S(R) = S_{gen}(X) = \frac{A(X)}{4G_N} + S_{\text{bulk}} \, , \tag{1.4.8}$$

where S_{bulk} is the entanglement entropy across X. Finally, Engelhardt and Wall [68] proposed that the correct formula that computes the fine grained entropy is

$$S(R) = \min_X \left\{ \text{ext}_X \left[\frac{A(X)}{4G_N} + S_{vN}(\Sigma_X) \right] \right\} \tag{1.4.9}$$

where Σ_X is the area bounded by X and $S_{vN}(\Sigma_X)$ is the fine grained entropy of the quantum fields on the area Σ_X. This formula means that in order to get the correct entropy for the region R we need to extremize and then minimize the generalized entropy.

1.4.4   Islands

In a series of breakthrough papers [4–9] the Page curve was recovered within semi-classical gravity. The authors achieved that after realizing that the fine-grained entropy of the radiation receives contributions from a disconnected region that lies behind the black hole horizon, namely, the island. The full entropy of the radiation is given by

$$S(\mathbf{R}) = \min_I \left\{ \text{ext}_I \left[\frac{A(\partial I)}{4G_N} + S_{\text{mat}}(R \cup I) \right] \right\} \, , \tag{1.4.10}$$

where $A(\partial I)$ is the area of the boundary of the island I, and $S_{\text{mat}}(R \cup I)$ is the renormalized entropy of the quantum fields on the union of the regions R and I. Initially, before the evaporation begins, no Hawking pairs are emitted and no islands exist. So, the exact entropy of the radiation is

$$S(\mathbf{R}) \approx S_{\text{mat}}(R) \, . \tag{1.4.11}$$

When the evaporation begins, Hawking partners start escaping from the black hole and (1.4.11) steadily grows. At some point of the evaporation, a non-trivial island appears behind the black hole horizon, extending almost through the whole black hole interior. Thus, the island includes most of the Hawking partners of the radiation that has escaped. So, the island purifies the radiation and the term $S_{\mathrm{mat}}(R \cup I)$ is approximately zero. The exact entropy of the radiation then becomes

$$S(\mathbf{R}) \approx \frac{A(\partial I)}{4G_N} \,. \tag{1.4.12}$$

As the evaporation procceds and the black hole horizon shrinks, (4.1.3) decreases and finally vanishes. Thus, the Page curve is followed and the black hole evaporation process is unitary (see Figure 1.7).

2 Traversable Wormholes in AdS and Bounds on Information Transfer

2.1 Introduction

Physicists and non-physicists have speculated about the possibility of connecting distant pieces of spacetime by creating a "shortcut" joining them [11]. A connection observers could travel through, called a traversable wormhole, remained in the realm of science fiction until a few years ago, when Gao, Jafferis and Wall (GJW) constructed traversable wormholes in the context of the AdS/CFT correspondence [69].

They began with an eternal AdS black hole, which contains an Einstein-Rosen bridge (wormhole) which is marginally non-traversable. This geometry is dual to two CFT's entangled in the thermofield double state [44]. As we will review in the next section, they added a coupling between the two CFTs. From the gravity perspective, this is a non-local coupling between the left and right asymptotic regions. This non-local coupling allows for negative null energy and makes the wormhole traversable.

The result of GJW provides a proof of existence for traversable wormholes in holography. Yet, the more fundamental question still remains to be answered: *what are the general rules for traversable wormholes?* In this paper we take a step towards answering this question by analyzing the amount of information that can be sent through GJW-type wormholes.

First, we clarify some aspects of the GJW wormhole geometry. We calculate the time that the wormhole is open, defined as the maximum proper time separation between the past and future event horizons, finding that this time is shorter than the Planck time. While this result might suggest that the GJW wormhole cannot be trusted, we explain why it can still be analyzed within the semiclassical regime despite apparent Planckian features.[1]

---

[1] We thank Daniel Jafferis for discussions on this point.

Next, we perform a bulk estimate of the amount of information that can be sent through the wormhole. We show that for the original GJW construction, in which the two CFT's are coupled by a single operator, the amount of information we can transfer through the wormhole is proportional to the number of thermal cells

$$N \sim \left(\frac{r_h}{\ell}\right)^{d-1} , \qquad (2.1.1)$$

in agreement with [50]. Here, r_h is the black hole radius, ℓ is the AdS radius and d are the boundary spacetime dimensions.

The procedure to send this number of messages is to use modes with low angular momentum, such that the signal varies on scales somewhat longer than the AdS length scale in the transverse directions. The message should be sent from the boundary long before the coupling between the two boundaries is turned on, so that it is very close to the horizon when it encounters the negative energy.

In order to derive the bound (2.1.1), we impose a number of consistency conditions to remain in a controlled regime. In particular, following [50], we impose the 'probe approximation': the message should backreact on the geometry by a small amount, so that the negative stress-energy tensor calculated in the absence of the signal is a good approximation. The probe approximation, in combination with our other conditions, allows us to do a well-controlled bulk analysis. However, as we discuss in more detail in the discussion section, it is not completely clear whether this condition must be imposed.

The capacity of the channel can be increased by including non-local couplings for a large number, K, of fields, as in [70]. In fact, many fields must contribute to the negative energy in order for the semiclassical description to be good. In particular, in order to talk about a single metric sourced by the expectation value of the stress tensor, the fluctuations in the stress tensor should be small compared to the mean. We will see that meeting this condition requires a large number K of coupled light fields.

The opening of the wormhole increases linearly in K, and so does the amount of information we can transfer. However, a black hole has finite entropy, so there should be an upper bound on K. We show that $K \lesssim \ell^{d-1}/G_N$ is needed for a self-consistent bulk solution, where G_N is the Newton constant. This bound can also be found by requiring that the UV cutoff of the theory is not lowered to the AdS scale.

The final result is that the amount of transferable information is bounded by of order the entropy of the black hole $N \lesssim S_{BH}$, as expected. In order to send this amount of information, we have to go beyond the s-channel and consider messages that are somewhat localized along the horizon. In particular we show that it is

inefficient to localize messages on sub-AdS scales in the transverse directions, but it is possible if we couple many fields K. This would be needed for the comfortable journey of a cat through the wormhole envisioned by Maldacena, Stanford, and Yang [70].

We show that this result for the amount of information transfer is in accordance with CFT expectations coming from quantum teleportation. From the quantum theory perspective, the GJW protocol should be seen as analogous to quantum teleportation [59, 70]. Indeed, the thermofield double state is a specific pure, entangled state of two copies of the CFT. Roughly, each thermal cell of the left CFT, with size β, is entangled with the corresponding thermal cell in the right CFT.

As in the standard qubit teleportation scenario, entanglement is not enough to send information from one copy to the other one: classical communication is also needed. Here, this is provided by the K couplings; these K couplings play the role of approximately K classical bits of information per thermal cell. Because the left-right coupling is local in space, it acts locally on the pairs of thermal cells. So at this rough level, the information transfer is simply standard quantum teleportation done on many qubits at once.

Note one miracle that has to occur: although the thermal cells have a pairwise entanglement of S_{cell}, separating this into S_{cell} EPR pairs would require solving a difficult problem at strong coupling. However, the K couplings between left and right simply couple primary operators on each side. The miracle is that this crude coupling is sufficient for the delicate task of quantum teleporting a large amount of information, as discussed in more detail in [71]. This miracle is the same miracle that allows for the preparation of the TFD state from a simple Hamiltonian [51, 72, 73].

The large value of K that maximizes the information transfer is of order the entropy of an AdS size black hole, $K \sim \ell^{d-1}/G_N$. For this value of K, the teleportation process uses up all of the quantum entanglement, destroying the black hole in the process.

Before continuing with our discussion, let us briefly comment on previous work related to traversable wormholes. It is by now well known that classical matter obeying the null energy condition, cannot support traversable wormholes – see, for instance, [74]. But this statement is no longer true if we include quantum corrections, leaving open the possibility that traversable wormholes are possible in the real world [?]. Earlier results on how to build traversables wormholes using exotic matter or higher curvature theories of gravity include, among others, [75–82]. In the context of AdS/CFT, the fact that entanglement is not enough to build a traversable wormhole in AdS, but one needs an explicit coupling between

the left and right asymptotic regions was already noted in [82, 83]. After GJW, traversable wormholes were further explored for the case of AdS$_2$ in [70], while recent attempts to construct eternal wormholes include [**?**, 51, 56, 84, 85]. The case of rotating wormholes in AdS was studied in [50]. Recently, the authors in [54] found bounds on the information that can be transferred in the GJW wormhole. We will comment on the differences of both approaches in the discussion section.

The rest of the paper is organized as follows. In section 2.2 we give a quick review of the GJW construction and we explore several interesting facts that have not yet been pointed out in previous literature. In section 2.3 we bound the amount of information that can be transmitted through the wormhole in the bulk and check that it agrees with the boundary calculation. We conclude in section 2.4 indicating some possible future directions.

2.2 Gao-Jafferis-Wall wormhole

In this section we review the traversable wormhole geometry constructed by Gao, Jafferis and Wall [69]. The main ingredient is a non-local coupling between the two asymptotic boundaries of a background BTZ black hole. This geometry contains an Einstein-Rosen bridge which is marginally non-traversable: photons falling along the horizon almost put in causal contact the two boundaries. The non-local coupling can generate a distribution of negative energy, which backreacts on the geometry such that these photons, if send early enough, can now fall from one boundary to the other. The wormhole becomes traversable.

The resulting geometry can be interpreted as the dual of the teleportation protocol [70]. The BTZ black hole is dual to two copies of a CFT entangled in a particular state, the thermofield double state (TFD) [44], which is defined by

$$|TFD\rangle \equiv \frac{1}{\sqrt{Z}} \sum_n e^{-\beta E_n/2} |n\rangle_L \otimes |n\rangle_R \,, \qquad (2.2.1)$$

where $|n\rangle_{L,R}$ are energy eigenstates of the left and right CFT's with energy E_n. This state is a pure entangled state from the perspective of the full system with the property that the reduced density matrix for each side is thermal with inverse temperature β. Details on how to create this state are given in [51, 72, 73]. The entanglement is the key resource for quantum teleportation, geometrically it *builds* the connected wormhole geometry [86]. However, it is not enough, the exchange of classical information is also needed. The non-local coupling takes care of this second passage [70], geometrically it makes the wormhole traversable.

We begin this section by recalling some basic properties of the unperturbed BTZ geometry.
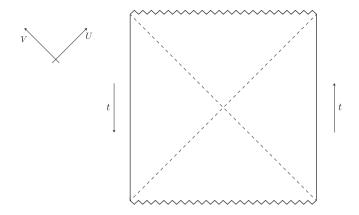
Figure 2.1: Penrose diagram for the BTZ black hole.

2.2.1 Unperturbed BTZ geometry

The metric of the uncharged, non-rotating BTZ black hole is given by [87, 88],

$$ds^2 = -\frac{r^2 - r_h^2}{\ell^2}dt^2 + \frac{\ell^2}{r^2 - r_h^2}dr^2 + r^2 d\phi^2, \tag{2.2.2}$$

where r_h is the horizon radius, ℓ is the radius of AdS and ϕ should be periodically identified $\phi \sim \phi + 2\pi$. The black hole mass and horizon radius are related by $r_h^2 = 8MG_N\ell^2$. The inverse temperature is given by $\beta = \frac{2\pi\ell^2}{r_h}$. G_N is Newton's constant, which, in three dimensions, is related to the Planck length by $\ell_P = 8\pi G_N$. We use the convention that time is flowing upwards at the right boundary and downwards at the left one.

For our purposes, it will be convenient to work in Kruskal coordinates,

$$\exp\left(2\frac{r_h t}{\ell^2}\right) = -\frac{U}{V}, \qquad \frac{r}{r_h} = \frac{1 - UV}{1 + UV}, \tag{2.2.3}$$

that cover the maximally extended two-sided geometry – see Fig. 2.1 – with the metric

$$ds^2 = \frac{-4\ell^2 dU dV + r_h^2 \left(1 - UV\right)^2 d\phi^2}{\left(1 + UV\right)^2}, \tag{2.2.4}$$

where $U > 0$ and $V < 0$ in the right wedge, $UV = -1$ at the boundaries and $UV = 1$ at the two singularities. The two horizons correspond to $U = 0$ and $V = 0$ and, as can be seen from the figure, are on the verge of causally connecting the two boundaries.

2.2.2 Adding a non-local interaction

The main novelty of the GJW construction is a non-local interaction between the two boundaries, introduced through a small deformation of the original CFT Hamiltonian

$$\delta H = -\ell \int d\phi \, h(t,\phi) \, \mathcal{O}_L(-t,\phi)\mathcal{O}_R(t,\phi) \,. \tag{2.2.5}$$

Here $\mathcal{O}_{L,R}$ are scalar primary operators with conformal weight Δ and $h(t,\phi)$ is the coupling constant. For the interaction to be relevant we need $\Delta < 1$. In principle, the coupling constant could have some explicit dependence on t or ϕ, but we will restrict to a constant coupling h turned on for some period of time

$$h(t,\phi) = \begin{cases} h\left(\frac{2\pi}{\beta}\right)^{2-2\Delta} & \text{if } t_0 \le t \le t_f \,, \\ 0 & \text{otherwise} \,. \end{cases} \tag{2.2.6}$$

Note that, as in GJW, the factors of β are chosen so that h is dimensionless. We will consider the perturbative problem with $h \ll 1$. As we explained above, a light ray falling along the horizon almost puts in causal contact the two boundaries. We want to show that the non-local coupling can be arranged in such a way that the backreacted null geodesic makes it from one boundary to the other. For simplicity we consider a radial geodesic, defined by $V = 0$.

First, we need to compute the expectation value of the stress-energy tensor along this geodesic. Since we will be interested in computing the shift in the V direction, we only need to find T_{UU}. The perturbation is spherically symmetric, hence T_{UU}, along $V = 0$, can only depend on U. Once T_{UU} is obtained, we compute the averaged null energy (ANE) by integrating it over the null ray,

$$\text{ANE}(h, U_0, U_f) \equiv \frac{h}{\ell} \mathcal{A}(U_0, U_f) \equiv \int_{U_0}^{\infty} \langle T_{UU} \rangle(U) \, dU \,, \tag{2.2.7}$$

where U_0 and U_f are the starting and ending times of the perturbation and, for later convenience, we have defined a dimensionless ANE, $\mathcal{A}$. Notice that in the last expression the dependance on the ending time of the perturbation U_f is implicit in the definition of the expectatiation value of T_{UU}.

This will be our main diagnosis of the wormhole traversability. As we will see later, a negative ANE "opens" the wormhole by a magnitude proportional to the amount of averaged negative energy. So in order to quantify how traversable the GJW wormhole is, it is important to understand what are the optimal configurations and how much negative energy can we obtain from those.

We compute the stress-energy tensor by point-splitting, hence we need to find the modified bulk-to-bulk two-point function in the presence of δH (2.2.5). As

usual in holography, the operators $\mathcal{O}_{L,R}$ are dual to a bulk scalar field φ with mass $m^2\ell^2 = \Delta(\Delta - 2)$. Working on the right wedge it is possible to compute the modified propagator with

$$
\begin{aligned}
G_h &\equiv \langle \varphi_R^H(t, r, \phi)\varphi_R^H(t', r', \phi')\rangle_h = \\
&= \langle u^{-1}(t, t_0)\varphi_R^I(t, r, \phi)u(t, t_0)u^{-1}(t', t_0)\varphi_R^I(t', r, \phi)u(t', t_0)\rangle_h \,.
\end{aligned}
\tag{2.2.8}
$$

Here the subscript R indicates that we are in the right wedge; the subscript h, that we are looking for the leading order correction in h; H and I indicate the Heisenberg and interaction fields respectively and $u(t, t_0) = \mathcal{T}\exp\left\{-i\int_{t_0}^{t} d\tilde{t}\, \delta H(\tilde{t})\right\}$ is the evolution operator in the interaction picture. The result to leading order in h is [69]

$$
G_h = 2\sin\pi\Delta \int dt_1 h(t_1) K_\Delta(t' + t_1 - i\beta/2) K_\Delta^r(t - t_1) + (t \leftrightarrow t')\,, \tag{2.2.9}
$$

where K_Δ and K_Δ^r are the bulk-to-boundary and the retarded bulk-to-boundary propagators. Notice that we are omitting the r, ϕ dependence for simplicity. The propagators are known analytically for the BTZ black hole[2] [46, 47]

$$
K_\Delta(t, r, \phi) = \left(\frac{r_h}{\ell^2}\right)^\Delta \frac{1}{2^{\Delta+1}\pi}\left(-\frac{\left(r^2 - r_h^2\right)^{1/2}}{r_h}\cosh\frac{r_h}{\ell^2}t + \frac{r}{r_h}\cosh\frac{r_h}{\ell}\phi\right)^{-\Delta}\,,
\tag{2.2.10}
$$

$$
K_\Delta^r(t, r, \phi) = |K_\Delta(t, r, \phi)|\theta(t)\theta\left(\frac{\left(r^2 - r_h^2\right)^{1/2}}{r_h}\cosh\frac{r_h}{\ell^2}t - \frac{r}{r_h}\cosh\frac{r_h}{\ell}\phi\right)\,,
\tag{2.2.11}
$$

where θ is the Heaviside step function. We then need to transform equation (2.2.9) into Kruskal coordinates and apply the point splitting formula to find the change in the expectation value of the stress tensor induced by the interaction at the horizon

$$
\langle T_{UU}\rangle(U) = \lim_{U'\to U}\partial_U\partial_{U'}G_h(U, U')\,. \tag{2.2.12}
$$

For details on how to obtain explicit expressions for the stress tensor, range of validity and integrability properties, we refer the courageous reader to [69]. For sources which are turned on at time t_0 and left on forever, the stress-energy tensor

---

[2]We suppress the sum over images in both propagators. When computing G_h we can include one of these sums by extending the domain of integration over ϕ from $[0, 2\pi]$ to the real line. We checked that the other sum gives contributions exponentially suppressed by $e^{-n\Delta r_h/\ell}$, where n is the index that runs over images.

is given by

$$\langle T_{UU} \rangle(U) = -\frac{h}{\ell} \frac{2^{\frac{1}{2}-2\Delta} \Delta \sin(\pi\Delta) \Gamma(1-\Delta)}{\pi^{3/2} \Gamma\left(\frac{3}{2}-\Delta\right)} \times$$

$$\times \lim_{U'\to U} \partial_U \int_{U_0}^{U} dU_1 \frac{F_1\left(\frac{1}{2}; \frac{1}{2}, \Delta+1; \frac{3}{2}-\Delta; \frac{U_1-U}{2U_1}, \frac{U_1-U}{U_1(1+U'U_1)}\right)}{U_1^{-\Delta+1/2}(U-U_1)^{\Delta-1/2}(1+U'U_1)^{\Delta+1}},$$

$$(2.2.13)$$

where F_1 is the Appell hypergeometric function. Now, to compute the ANE, we need to further integrate the above expression along U. Surprisingly, this can be done analytically [69]

$$\mathcal{A}^{\infty}(U_0, \Delta) \equiv \frac{\ell}{h} \mathrm{ANE}(h, U_0, \infty) =$$

$$= -\frac{\Gamma(2\Delta+1)^2}{2^{4\Delta}(2\Delta+1)\Gamma(\Delta)^2\Gamma(\Delta+1)^2} \frac{{}_2F_1\left(\Delta+\frac{1}{2}, \frac{1}{2}-\Delta; \Delta+\frac{3}{2}; \frac{1}{1+U_0^2}\right)}{(1+U_0^2)^{\Delta+\frac{1}{2}}}, \quad (2.2.14)$$

where now the ${}_2F_1$ is the ordinary hypergeometric function. It is instructive to plot the ANE to see how it depends on the different parameters involved. This is done in Fig. 2.2, where we plot the ANE as a function of Δ for different starting times U_0. As expected, the sooner we turn on the coupling the larger amount of negative energy we can get. The curve with $U_0 = 0$, *i.e.* $t_0 = -\infty$, gives an upper bound on the amount of negative energy we can get with this type of sources: $|\mathcal{A}^{\infty}(U_0, \Delta)| \lesssim 10^{-1}$. One might worry that if the source is turned on for such a long time we should take into consideration the backreaction of the negative energy on the geometry. However, one can check that the gravitational perturbation is small everywhere and so the linear order computation can be trusted.

The analytical expression (2.2.14) found by GJW is a remarkable result; however, it is somewhat impractical to deal with hypergeometric function. In particular in the next section we will need to quantify the backreaction of a message on the quantity of negative energy and it would be helpful to have at disposal a simpler expression for the ANE. In the following we provide such a simple analytic expression, valid for the case of instantaneous sources

$$h^{inst}(t, \phi) = h \left(\frac{2\pi}{\beta}\right)^{2-2\Delta} \delta\left(\frac{2\pi}{\beta}(t - t_0)\right). \quad (2.2.15)$$

This can be found by manipulating equation (2.2.14). First, we find an expression of the ANE for *smeared* interactions. This is a more physical scenario in which we turn on the sources only for a finite amount of time $\Delta U = U_f - U_0$. As before, we define a dimensionless ANE,

$$\mathcal{A}^s(U_0, U_f, \Delta) \equiv \frac{\ell}{h} \mathrm{ANE}(h, U_0, U_f), \quad (2.2.16)$$
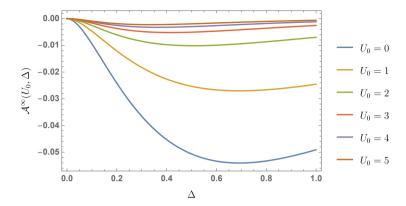
Figure 2.2: Dimensionless Averaged Null Energy as a function of Δ. The curves correspond to different starting time U_0, while the end point is always $U_f = +\infty$. The earlier we turn on the interaction the more negative energy we can obtain (note that $U_0 = 0$ corresponds to boundary time $t = -\infty$ and $U_0 = 1$ to $t = 0$).

where the subscript s stands for smeared. The ANE involves integrating over a whole null ray the stress-energy tensor, that by itself is an integral over the sources. Schematically, we can write this as

$$\mathcal{A}^s(U_0, U_f, \Delta) = \int_{U_0}^{\infty} dU \, \langle T_{UU} \rangle(U) \equiv \int_{U_0}^{\infty} dU \int_{U_0}^{U_f} dU_1 \, \tau(U, U_1) \qquad (2.2.17)$$

where we have defined a function $\tau(U, U_1)$ whose integral is the stress energy tensor. Notice that this quantity is allowed to have some discontinuities at the positions where the sources are turned on/off. We can rewrite $\mathcal{A}^s$ in terms of $\mathcal{A}^\infty$ as follows

$$\mathcal{A}^s(U_0, U_f, \Delta) = \int_{U_0}^{\infty} dU \left[\int_{U_0}^{\infty} dU_1 \, \tau(U, U_1) - \int_{U_f}^{\infty} dU_1 \, \tau(U, U_1) \right] =$$
$$= \left(\int_{U_0}^{\infty} dU \int_{U_0}^{\infty} dU_1 - \cancel{\int_{U_0}^{\infty} dU} \cancel{\int_{U_f}^{\infty} dU_1} - \int_{U_f}^{\infty} dU \int_{U_f}^{\infty} dU_1 \right) \tau(U, U_1) =$$
$$= \mathcal{A}^\infty(U_0, \Delta) - \mathcal{A}^\infty(U_f, \Delta) \,.$$
$$(2.2.18)$$

The integral in the second line vanishes because it adds up the energy generated along the null geodesic for $U < U_f$ by a source turned on only at U_f, *i.e.* the support of the first integral lies outside the lightcone of the second. Finally, we take the limit in which the coupling is turned on only for an instant of time and find a remarkably simple analytic expression. The dimensionless ANE in this case

is given by[3]

$$\mathcal{A}^{inst}(U_0, \Delta) = \lim_{U_f \to U_0} U_0 \frac{\mathcal{A}^s(U_0, U_f, \Delta)}{U_f - U_0} = -U_0\,\partial_{U_0}\mathcal{A}^\infty(U_0, \Delta)\,. \qquad (2.2.19)$$

It is straightforward to evaluate this expression: all the dependence on U_0, that before was encoded in the hypergeometric functions, now becomes simply

$$\mathcal{A}^{inst}(U_0, \Delta) = -\frac{\Gamma\left(\Delta + \frac{1}{2}\right)^2}{\pi\Gamma(\Delta)^2}\left(\frac{U_0}{1 + U_0^2}\right)^{2\Delta+1}\,. \qquad (2.2.20)$$

Notice that this expression might receive large correction from higher order terms in h, which should be cured by introducing a small smearing. Nonetheless, it provides a simple and helpful approximation to the smeared case. Also note that in this way of deriving equation (2.2.20), we did not need to directly integrate the stress-energy tensor for the instantaneous source, which was computed in [89], and has an apparent non-integrable divergence for $\Delta > 1/2$.

Plots of $\mathcal{A}^{inst}$ are shown in Fig. 2.3. Note that this expression has a few interesting properties. First, $\mathcal{A}^{inst}$ is symmetric under $U_0 \to U_0^{-1}$, which makes the time $U_0 = 1$ somewhat special. In fact, it is easy to show analytically that $U_0 = 1$ is a minimum of this function. It is also possible to note that the optimal weight, for $U_0 = 1$, is $\Delta \approx 0.9$. Finally, we observe that for δ-function source $|\mathcal{A}^{inst}(U_0, \Delta)| \lesssim 10^{-2}$. This means that turning on the non-local coupling for only an instant of time, at $U_0 = 1$, reduces the amount of negative energy by only an order of magnitude, as compared to $\mathcal{A}^\infty$.

Independently of the details of the interaction, we see that the averaged null energy of the Gao-Jafferis-Wall protocol is bounded, in absolute value, by $|h|/\ell$ times an order-one number. More precisely, we have

$$|\text{ANE}(h, U_0, U_f)| = \frac{|h|}{\ell}|\mathcal{A}| \lesssim \frac{|h|}{\ell}10^{-1}\,. \qquad (2.2.21)$$

Given that we are working perturbatively in h, we conclude that the ANE is generically very small in AdS units. This fact is worrisome because, as we show below, the amount of available negative energy determines the size of the wormhole opening.

Before continuing with our analysis let us clarify a point concerning the reference frame we have considered so far. We have worked in a frame in which $t_L = -t_R$, that we will call the *rest* frame. The BTZ geometry is invariant under boosts,

---

[3]The extra U_0 on the RHS comes from the fact that the source is a δ-function in time while for this limit we are taking a δ in the U-coordinate.

(a)

(b)
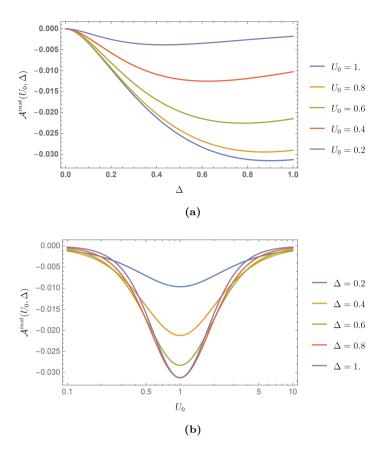
Figure 2.3: Averaged Null Energy for the case of instantaneous sources. In (a) we plot the ANE as a function of Δ for different U_0. The largest amount of ANE (in absolute value) is given by the curve with $U_0 = 1$. This corresponds to $t_L = t_R = 0$. Note that for this choice of times, the wormhole is shortest; therefore, it is not surprising that the effect of the non-local coupling is the largest. In (b), we plot the ANE as a function of U_0 for different Δ. The scale on the U_0 axis is logarithmic which makes evident that each curve has a minimum at $U_0 = 1$ and is symmetric under $U_0 \to U_0^{-1}$.

$\{U \to \lambda U, V \to \lambda^{-1} V\}$, which act on the asymptotic boundaries as time transla-tions $t_{L,R} \to t_{L,R} + \delta t$. Therefore, we can consider more general reference frames in which $t_L \neq -t_R$. We will call these, *boosted* frames. This is just a change of coordinates, so the bound on information transfer we are looking for should be independent of λ. However, the integrated null energy, and hence, the dimen-sionless coefficient $\mathcal{A}$ is not invariant under these boosts. In fact, an expression for $\mathcal{A}$ in generally boosted frames can be easily found, and in Schwarzschild-like

coordinates, is given by

$$\mathcal{A}_{\text{boosted}}^{inst}(t_R, t_L, \Delta) = -\exp\left(-\frac{\pi}{\beta}(t_L + t_R)\right) \frac{\Gamma\left(\Delta + \frac{1}{2}\right)^2}{\pi \Gamma(\Delta)^2} \left[\frac{1}{2}\cosh\left(\frac{\pi}{\beta}(t_R - t_L)\right)\right]^{-2\Delta-1} \quad (2.2.22)$$

The exponential on the r.h.s. corresponds to the boost factor λ we discussed above. Indeed, we see that in the boosted frames we can get much more negative energy than in the rest frame. In the next section we will explain why this, as expected, cannot enhance the amount of information we can transfer across the wormhole. In fact, for simplicity, we will keep working in the rest frame, eventually deriving a coordinate-independent expression for the opening of the wormhole – see equation (2.2.28).

2.2.3 Wormhole opening

We can relate the ANE to the opening size of the wormhole through the linearized Einstein equations. Let $g_{\mu\nu} = g_{\mu\nu}^{BTZ} + h_{\mu\nu}$, be the metric of the perturbed BTZ geometry, then in Kruskal coordinates, to leading order in $h_{\mu\nu}$ and at the horizon $V = 0$, the linearized Einstein equation reads [69]

$$\frac{1}{2}\left(\frac{Uh'_{UU}(U) + 2h_{UU}(U)}{\ell^2} - \frac{h''_{\phi\phi}(U)}{r_h^2}\right) = 8\pi G_N \langle T_{UU}\rangle, \quad (2.2.23)$$

where the primes denote derivative with respect to U. In fact, in order to use this equation, where the classical metric is sourced by the expectation value of the stress tensor, the fluctuations in the stress tensor should be small compared to its mean. As we discuss in more detail in section 2.3.1, this semiclassical condition is only met if a large number K of fields contributes to the negative energy. We do not include the factors of K for now, since we are reviewing the original construction, but will include them in our later analysis since they are essential for remaining in the semiclassical regime.

Integrating this equation, the total derivative terms do not contribute if the perturbation decays sufficiently fast at $U = \pm\infty$, which is the case unless the perturbation is turned on forever. We are left with

$$\frac{1}{2\ell^2}\int dU h_{UU}(U) = 8\pi G_N \int dU \langle T_{UU}\rangle. \quad (2.2.24)$$

A null ray traveling close to the horizon will suffer a shift in its $V-$coordinate, see Fig. 2.4a, due to the perturbation given by

$$\Delta V = \frac{1}{4\ell^2}\int dU h_{UU}. \quad (2.2.25)$$

Combining both equations together we obtain

$$\Delta V = 4\pi G_N \int dU \langle T_{UU} \rangle = 4\pi \frac{G_N h}{\ell} \mathcal{A}(U_0, U_f) \qquad (2.2.26)$$

where the dimensionless ANE, $\mathcal{A}$, is defined in (2.2.7). If $\Delta V < 0$, a null ray traveling close to the horizon and starting on one side of the black hole will end up traversing the wormhole and appear on the other side. Given the analysis in the previous subsection, it is clear that the non-local interaction can make ΔV negative by a proper choice of the sign of h. However, as explained above, $\mathcal{A}$ is frame dependent and so is ΔV. We can quantify the opening of the wormhole in a coordinate independent way by computing the proper time that the wormhole remains open. To do this, we zoom into the diamond region that appears between the future and the past horizon due to the backreaction of the negative energy, see Fig. 2.4b. Near the horizon, the metric is approximately $ds^2 \approx -4\ell^2 dU dV$. Consequently the proper time that separates the lower and upper vertices of the diamond region is

$$\Delta \tau \approx 2\ell\sqrt{\Delta V \Delta U}. \qquad (2.2.27)$$

In the rest frame the coupling is symmetric under $L \leftrightarrow R$, hence $\Delta V = \Delta U$ and the above relation reduces to $\Delta \tau \approx 2\ell \Delta V$. Combining everything, we have an upper bound on the proper time between the past and future event horizons,

$$\Delta \tau \approx 8\pi G_N h \mathcal{A} \lesssim G_N, \qquad (2.2.28)$$

where $\mathcal{A}$ is the one computed in the rest frame. In the boosted frames, the extra contributions coming from ΔU and ΔV will cancel perfectly, leaving the expression in the rest frame. We conclude that the time window that the wormhole remains open is indeed Planckian, independent of the chosen frame.

Since the time for which the wormhole is open is so small, one might worry that quantum gravity corrections are important and cannot be neglected. This is not the case. The diamond is just a - small - piece of the BTZ geometry, the invariant curvature is given by ℓ^{-2} and is well separated from the Planck scale. While passing through the wormhole a signal would just feel like traveling through empty flat spacetime. Nonetheless, we still need to make sure that the signal is localized to a Planck sized box to be certain that it will make it through the opening. This sounds like a difficult, even dangerous, task. In this case we don't need to worry about this issue because the mouth of the wormhole is located close to the horizon of a black hole. The gravitational blueshift makes sure that an ordinary message at infinity is boosted enough by the time it reaches the mouth of the wormhole to fit in such a Planck sized box. We just need to send the message from the boundary early enough. The same gravitational effect guarantees that we don't need to fine-tune the moment we send the message from the boundary up
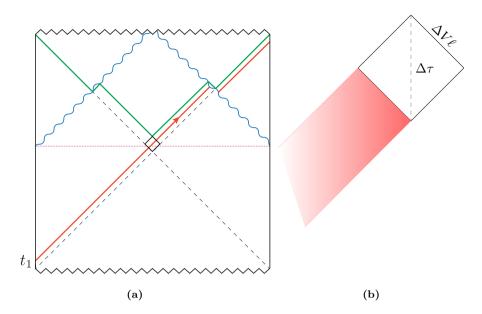
Figure 2.4: (a) The blue wavy lines represent the negative energy. The green line shows how the future horizon recedes due to the backreaction of the negative energy on the geometry. As the future horizon moves up, a diamond region is revealed in the middle of the diagram. The past horizon remains unaffected. The red line is the positive energy signal that we send through the wormhole. (b) Here, we have zoomed into the diamond region. The side of the diamond is equal to $\Delta V \ell$. $\Delta \tau$ is the amount of proper time that the wormhole remains open. The red region represents a signal that passes through the wormhole throat.

to a Planck-time precision, because an asymptotic observer sees the window open for an exponentially longer time. We conclude that, despite the smallness of the opening, it is kinematically possible to send a message through the wormhole.[4]

2.3 Bound on information transfer

In the previous section we have revised the construction of GJW. The non-local coupling between the two asymptotic boundaries is enough to open the wormhole for only a Planck-sized window of time. Nonetheless, we have argued that thanks to redshift this by itself is not an obstacle for a message traversing the wormhole. However, so far we have neglected the backreaction of the message on the geometry, staying in the so called *probe approximation*. Given that the message needs to be highly boosted to make it through the wormhole, one might worry that this is not

---

[4]We thank Daniel Jafferis for discussions on this point.

a valid approximation. In fact the signal might destroy the original traversable wormhole setup altogether. In this section we check that this is not the case. It is possible to send a large amount of information, while keeping under control the backreaction on the geometry.

For convenience we now summarize the main results that will be proven throughout the section. We begin by finding a simple condition on the total momentum that we can send through the wormhole before the probe approximation becomes unreliable. Because the signal is highly boosted by the time it reaches the horizon, it can be approximated by a shock wave and its stress energy tensor (in light-cone coordinates) is given by [90,91]

$$T_{VV} = \frac{p_V}{r_h} \delta(V) \,, \tag{2.3.1}$$

where p_V is the *total* momentum of the message. In the next subsection we show that the probe approximation is valid as long as[5]

$$\boxed{\text{probe approximation: } \frac{G_N \, p_V}{r_h} \ll 1 \,.} \tag{2.3.2}$$

This, combined with the requirement that each message we send is boosted enough to fit through the wormhole opening, is enough to constraint the amount of information we can transfer. We can estimate how much one signal needs to be boosted using the *uncertainty principle* [70].

First, we consider messages that are completely spread across the horizon, *i.e.* s-waves. We show that the amount of transferred information can be made large by increasing the radius of the black hole; however, it is always much smaller than the entropy of the black hole. To increase the number of bits that can be sent through the wormhole, for fixed r_h, we follow the approach of [70] and couple a large number K of fields. Combining the probe approximation with the uncertainty principle we obtain that the number N of bits that can go through the wormhole is given by

$$N \lesssim \frac{r_h}{\ell} K \,. \tag{2.3.3}$$

However, K cannot grow arbitrarily large. Treating the negative energy as a negative shock we find that the maximum number of coupled fields beyond which our construction becomes unreliable is

$$\boxed{\text{species bound: } K \lesssim \frac{\ell}{G_N} \,.} \tag{2.3.4}$$

---

[5]Note that this statement is coordinate dependent. We will also provide an equivalent statement in terms of the center-of-mass energy collision in equation (2.3.12).

We can reproduce this bound also by imposing that the renormalized UV cutoff, see [92, 93], is above the AdS scale. Combining both results, we obtain the final bound on the information that can be sent through the wormhole,

$$N \lesssim \frac{r_h}{G_N} \approx S_{BH} \,. \tag{2.3.5}$$

We check that this bound is consistent with the one we obtain by considering the boundary theory. Finally we consider signals that are localized in the transverse direction. We show that it is possible to localize messages on sub-AdS scales if we couple $K \gg 1$ fields. In the rest of the section we give details on how to derive these bounds.

Notice that the breakdown of the probe approximation does not necessarily imply that the wormhole closes. It only means that the GJW computation is not reliable anymore. One might wonder if by fully taking into account the backreaction, we might increase the amount of transferable information. The analysis of [50] suggests that this is not the case; however, we believe that this issue has not been settled yet. We will comment further on this in the discussion section.

2.3.1   S-wave channel

We want to bound the amount of information we can send through the wormhole. As we explained above, to do this we first need to understand how far we can trust the probe approximation. To begin with, we consider spherically symmetric messages. To estimate the effect of one such message on the amount of negative energy generated by the non-local coupling, we approximate the message as a positive energy shock, propagating along the horizon $V = 0$. At linear order we don't need to worry about the backreaction of the negative energy shock, the geometry is then simply given by [48]

$$\begin{aligned} ds^2 =& \frac{-4\ell^2 dU dV + r_h^2 (1 - (U + \Delta U \theta(V))V)^2 d\phi^2}{(1 + (U + \Delta U \theta(V))V)^2} \,, \\ =& \frac{-4\ell^2 d\tilde{U} dV + 4\ell^2 \Delta U \delta(V) dV^2 + r_h^2 (1 - \tilde{U} V)^2 d\phi^2}{(1 + \tilde{U} V)^2} \,, \end{aligned} \tag{2.3.6}$$

where in the second line we have used the discontinuous coordinate $\tilde{U} = U + \Delta U \theta(V)$. To compute the negative energy we need to know the propagator for the scalar field in this shockwave geometry. Away from $V = 0$ this is simply given by the BTZ propagator as the geometry is the one of the BTZ black hole. However, the shockwave induces a discontinuity across $V = 0$, one can check that it is enough to use the usual BTZ propagator but using the discontinuous coordinates,

$$K^{\mathrm{shock}}(U, V) = K^{\mathrm{BTZ}}(\tilde{U}, V) \,, \tag{2.3.7}$$
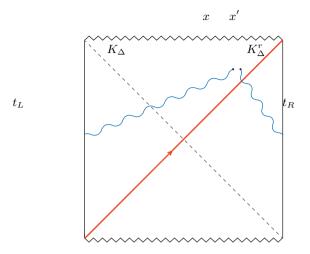
Figure 2.5: Schematically the ANE is given by the product of a boundary-to-bulk propagator coming from the left CFT and a retarded boundary-to-bulk propagator coming from the right one. Only the latter crosses the positive energy shock and undergoes a time delay.

where schematically K is a BTZ propagator. When computing the ANE we evaluate two BTZ boundary-to-bulk propagators. But note that only the one coming from the right boundary crosses the positive energy shock and undergoes a time delay. See Fig. 2.5. The effect of this delay is equivalent to shifting the insertion time of O_R in (2.2.5) by a quantity

$$\Delta t \approx \beta \frac{\Delta U}{U_0} \,, \tag{2.3.8}$$

where we have assumed that the shift is small. The rest of the ANE computation of GJW follows unchanged. The probe approximation is valid as long as the effect of the message on the geometry can be neglected, *i.e.* as long as $\Delta U \ll 1$. The time delay is related to the stress energy tensor generated by the message by [48, 91]

$$T_{VV} = \frac{\Delta U}{G_N} \delta(V) \,. \tag{2.3.9}$$

Comparing with (2.3.1) we can relate the time delay to the total momentum carried by the message

$$\Delta U = G_N \frac{p_V}{r_h} \ll 1 \,. \tag{2.3.10}$$

We will see below that this momentum needs to be large enough such that the message can fit through the wormhole. Notice that the momenta in Kruskal coordinates are dimensionless since they are the conjugate variables to the dimensionless U, V-coordinates. We can check that this condition is enough to ensure that

the negative energy is almost preserved by using our simple analytical expression (2.2.22), valid for the case of instantaneous sources. For simplicity we consider the optimal case in which $t_R - t_L = 0$. We can trust the probe approximation if

$$\left| \frac{\mathcal{A}(0, \Delta t) - \mathcal{A}(0, 0)}{\mathcal{A}(0, 0)} \right| \ll 1 \,. \tag{2.3.11}$$

It is easy to see that this condition reduces to (2.3.10).

It is also possible to express the constraint above in terms of coordinate-independent quantities. We approximate the interaction between the negative energy density and the signal as a collision between particles and assume that the scattering is dominated by gravitational interaction. Along the horizon of a BTZ black hole, gravitational interaction decays exponentially outside a region of size ℓ, see equation (2.3.43). This is expected since this region is a thermal cell on the horizon, *i.e.* it corresponds to a region of size β on the boundary. Therefore, we can split the collision in independent events, one per thermal cell. The probe approximation translates to the statement that the amplitude associated to each of these collision events should be small

$$G_N s_{cell} \ell \ll 1 \,. \tag{2.3.12}$$

Here $s_{cell} = p_V^{cell} q_U^{cell} / \ell^2$ is the center-of-mass energy squared of one of these collisions. In the rest frame, the momentum of the negative energy, per thermal cell, is given by $q_U^{cell} \approx 1$, p_V^{cell} is simply given by p_V divided by the number of thermal cells, r_h/ℓ. It is easy to see that with these identifications, equation (2.3.12) reproduces (2.3.2).

The probe approximation provides an upper bound on the momentum a particle traversing the wormhole can have. As pointed out in the previous section, this particle needs to be highly boosted to fit through the wormhole, so the momentum cannot be arbitrarily small. We can estimate the minimum required momentum using the uncertainty principle[6] [70]

$$p_V^{signal} \gtrsim \frac{1}{\Delta V} \approx \frac{\ell}{G_N h \mathcal{A}} \,, \tag{2.3.13}$$

where p_V^{signal} is the momentum of *one* signal. Now imagine sending N non-interacting signals. Then, $p_V = N p_V^{signal}$. Combining the uncertainty principle with the probe approximation condition (2.3.10), we find the following bound on the number of bits one can send through the wormhole,

$$N \lesssim h \mathcal{A} \frac{r_h}{\ell} \,. \tag{2.3.14}$$

---

[6]Notice that this momentum is superplanckian. This is not a problem, p_V^{signal} is a coordinate dependent quantity and can be larger than the cutoff of our theory.

Note that we can send a large number of bits through the wormhole if we consider large black holes with $r_h \gg \ell$. However, this number is still much less than the theoretical maximum, which should scale with the entropy of the black hole,

$$S_{BH} \approx \frac{r_h}{G_N} \gg \frac{r_h}{\ell} \,. \tag{2.3.15}$$

From now on, we set $h = \mathcal{A} = 1$, so our results are correct up to order-one (small) numbers that depend on the details of the non-local interactions. In [50], it was shown that one way of increasing N is to add rotation to the black hole. However, this is not enough to parametrically increase the amount of information transferred from order r_h/ℓ to the much larger r_h/G_N. An alternative way is to non-locally couple a large number of fields. This was done in the case of AdS_2 in [70]. Here we would like to analyze the consequences of this second approach in the case of AdS_3. Notice that if we interpret the non-local coupled fields as playing the role of the classical messages in the usual teleportation protocol, it is natural to consider many such fields to send more information.

Following [70], we consider a deformation of the theory in which we couple K fields

$$\delta H = -\sum_{i=1}^{K} \ell \int d\phi \, h(t, \phi) \, \mathcal{O}_R^i(t, \phi) \mathcal{O}_L^i(-t, \phi) \,. \tag{2.3.16}$$

Assuming that the non-locally coupled fields are not interacting, the negative energy scales linearly with K.

Large K also allows us to enter the semiclassical regime. In order to couple the metric to the expectation value of the stress tensor, we would like the fluctuations in the stress tensor to be small compared to its mean. The fluctuations in the stress tensor depend on the scale, increasing at short distances. We would at least like the fluctuations to be small compared to the mean at scales of order the AdS radius. In the presence of K light fields, the fluctuations in the stress tensor are of order

$$\langle (\Delta T_U{}^V)^2 \rangle \sim \frac{K}{\ell^6} \,, \tag{2.3.17}$$

where we have focussed on the crucial component of the stress tensor for our analysis, $T_U{}^V$. The mean value is[7]

$$\langle T_U{}^V \rangle \sim \frac{hK}{\ell^3} \,. \tag{2.3.18}$$

---

[7]Notice the different scaling in h between eq. (2.3.18) and eq. (2.3.17). The expectation value of $T_U{}^V$ is zero in the absence of non-local coupling and hence it is proportional to h. The fluctuation of $T_U{}^V$ instead is non-zero also in the absence of the non-local coupling, due to the quantum fluctuation of the fields, and hence, to leading order, it is independent of h.

Imposing that the fluctuations are small compared to the mean gives

$$h^2 K \gg 1 \,. \tag{2.3.19}$$

Since we require $h \ll 1$ in order to work to leading order in the source, we certainly need many fields,

$$K \gg \frac{1}{h^2} \gg 1 \,, \tag{2.3.20}$$

in order for the semiclassical description to be valid.

The opening of the wormhole is increased due to the increased negative energy,

$$\Delta V \approx \frac{K G_N}{\ell} \,. \tag{2.3.21}$$

As we have seen in section 2.2.2, the non-local coupling is most effective at $t = 0$ when the wormhole is shortest. For definiteness, we can then consider K instantaneous non-local couplings all turned on at $t = 0$. Turning on the coupling for a longer time would just modify the specific value of $\mathcal{A}$. The resulting picture is that of K superimposed negative energy shocks. Notice that the probe approximation condition (2.3.10) is not modified by the factor K. In the particle collision picture this means that we need to treat the collision between the N signals and the K shocks, in every thermal cell, as K independent processes. However, the presence of many fields does influence the uncertainty principle condition because the opening of the wormhole increases with the available amount of negative energy

$$p_V^{signal} \gtrsim \frac{1}{K} \frac{\ell}{G_N} \,. \tag{2.3.22}$$

Combining this condition with (2.3.10), we again find a bound on the number of particles that can traverse the wormhole,

$$N \lesssim K \frac{r_h}{\ell} \,. \tag{2.3.23}$$

This seem to suggest that we can send as much information as we want, if we allow K to be large enough. However, the black hole has finite entropy and cannot be used to extract infinite amount of entanglement, so we expect a restriction for large enough values of K. For example, it is known that the presence of many species lowers the cutoff of the theory [92,93]

$$\ell_{UV} \gtrsim K G_N \,. \tag{2.3.24}$$

The BTZ geometry cannot be treated as a semiclassical geometry when the UV cutoff becomes of the same order of the curvature scale, *i.e.* we should have $\ell_{UV} \ll \ell$. This leads to an upper bound on K,

$$K \lesssim \frac{\ell}{G_N} \,. \tag{2.3.25}$$

It turns out that this is already enough to make the bound on the number of particles consistent with the finiteness of the black hole entropy. For the maximum value of K, we thus obtain

$$N \lesssim \frac{r_h}{G_N} \approx S_{BH} \,. \tag{2.3.26}$$

Note that this requires the number of light operators in the CFT to be of order of the central charge c, and this is not the case in the usual known examples of AdS_3/CFT_2. Nevertheless, the GJW protocol seems to be robust enough that it will continue to make sense even in more exotic settings with a large number of light fields, where the UV cutoff of the field theory is not well-separated from the AdS scale, although the semiclassical bulk description will receive larger corrections.

2.3.2   A multiple shocks bound

In this section, we will build the bulk geometry by gluing together black hole patches with different masses. This will be due to the effect of the non-local interaction and the message that will be modelled by shockwaves. By restricting the masses of the different patches to be positive, we will obtain constraints on the amount of energy that can be carried by the shockwaves. The main objective is to justify the species bound in equation (2.3.25) from a bulk perspective.

Let's assume that the negative energy interaction between the two boundaries can be modeled in the bulk by the insertion of two negative-energy shockwaves at times $t_R = -t_L = t_0$. The message we would like to send through the wormhole can also be modeled as a shockwave, but now a positive-energy one. As shown in Fig. 2.6, for the sake of analyzing whether the geometry becomes traversable, it is possible to neglect the effect of the left negative shockwave and consider the collision between two spherical shells, one with positive and the other with negative energy. The positive shell has energy E_1 and the negative one $-E_2$. As shown in [49], this gravitational problem involving the collision of two shocks can be solved by gluing different black-hole geometries together. Note that in this section it will be more convenient to use Schwarzschild coordinates and energies, and to only translate the final results into the null coordinates we used in previous sections.

First, let us consider the simpler example where there is only one negative shockwave – see Fig.2.6a. It is easy to see that if the mass of the original black hole is M and the shock carries energy $-E_2$, then one should glue the geometry of a black hole with mass M in the past of the shock with another one with mass $M - E_2$ at the future of the shock.

The first bound comes from requiring that the mass of the second black holes

geometry remains positive, *i.e.,* $M - E_2 > 0$. The total energy E_2 of the negative shock is composed by the energy of the K species. In each thermal cell, the energy should be of order of the local temperature and given that there are r_h/ℓ thermal cells, the total energy is given by $E_2 = K\beta^{-1}\dfrac{r_h}{\ell} = \dfrac{K\,r_h^2}{\ell^3}$. Using that the mass of the BTZ blackhole is $M \approx r_h^2/(G_N\ell^2)$, it is immediate to note that

$$K \lesssim \frac{\ell}{G_N}\,, \tag{2.3.27}$$

that is exactly the species bound that appears in equation (2.3.25).

We can now add the positive energy shock, the message, and see if this setup provides additional constraints. In the case of two shocks colliding, the gluing gets more intricate as there are four different regions to consider. In [49], it was showed that it is enough to impose two gluing conditions in order to get a consistent answer: a continuity condition on the radius of the circle across the collision and a DTR regularity condition [91, 94]. These two conditions allow us to find the mass of the black-hole in the post collision regime, M_t. See Fig. 2.6b.

(a)   **(b)**
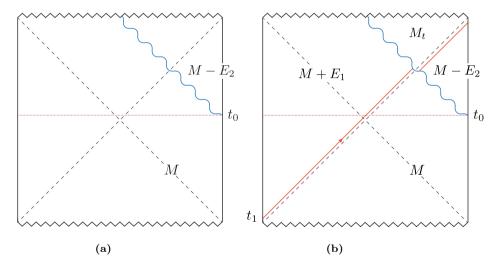
Figure 2.6: Penrose diagrams of the different shockwave geometries. In (a), we only consider the effect of a negative energy shock of energy $-E_2$ (blue curvy line) sent at t_0. In (b), we add the effect of a second shock with positive energy E_1 sent at t_1 from the left boundary (solid red line). The resulting geometry is formed by gluing four AdS black hole patches with different masses.

If we want to glue different metrics of the form $ds^2 = -f_i(r)dt^2 + f_i(r)^{-1}dr^2 +$

$r^2 d\phi^2$, from the DTR condition, we have that at the r-coordinate of collision r_c,

$$f_t(r_c) f_b(r_c) = f_l(r_c) f_r(r_c), \tag{2.3.28}$$

where t, b, l, r stand for the top, bottom, left and right regions respectively. The difference with [49] resides in that in our case one of the shocks carries negative energy (and is being sent at boundary time $t_0 \approx 0$). In this case, equation (2.3.28) becomes

$$\left(r_c^2 - 8G_N M \ell^2\right) \left(r_c^2 - 8G_N M_t \ell^2\right) = \left(r_c^2 - 8G_N(M + E_1)\ell^2\right) \left(r_c^2 - 8G_N(M - E_2)\ell^2\right).$$

This is sufficient to get M_t as a function of the initial data. Moreover, if we want to write it as a function of the boundary times at which the shocks are emitted, we can translate r_c in terms of the Kruskal coordinates. In the limit of small energies, $E_{1,2}/M \ll 1$, this can be done in any quadrant so for simplicity we consider the bottom one. In there, the horizon radius is the unperturbed one, given by $r_h^2 = 8G_N M \ell^2$. The U-coordinate of the negative shock wave is $U_- = e^{r_h t_0 / \ell^2}$ and the V-coordinate of the positive shock wave is $V_+ = e^{-r_h t_1 / \ell^2}$. So, from equation (2.2.3), the collision radius becomes

$$r_c = r_h \frac{1 - \exp\left(\frac{r_h}{\ell^2}(t_0 - t_1)\right)}{1 + \exp\left(\frac{r_h}{\ell^2}(t_0 - t_1)\right)}. \tag{2.3.29}$$

Plugging that back in equation (2.3.2) is enough to find the mass of the black hole in the top region,

$$M_t = M + E_1 - E_2 - \frac{E_1 E_2}{M} \cosh^2\left(\frac{r_h(t_0 - t_1)}{2\ell^2}\right). \tag{2.3.30}$$

Note that for $(t_0 - t_1)$ large enough, the last term grows exponentially leading to a negative mass in the upper region.[8] So, in the limit $E_{1,2}/M \ll 1$, imposing that M_t should be positive results in

$$M^2 \gtrsim E_1 E_2 \cosh^2\left(\frac{r_h(t_0 - t_1)}{2\ell^2}\right). \tag{2.3.31}$$

We are interested in the case where $t_0 \approx 0$. Using that $e^{\frac{2r_h t_1}{\ell^2}} = -\frac{U_+}{V_+}$, that $U_+ V_+ = -1$ on the boundary and that the shock with positive energy propagates close to the horizon $V_+ = 0$, we find that

$$M^2 \gtrsim \frac{E_1 E_2}{V_+} + \mathcal{O}(V_+). \tag{2.3.32}$$

---

[8]In fact, in three dimensions, this will happen even before the mass gets negative, as the BTZ black hole has a lower bound for its mass.

For comparison, it is convenient to express this bound in terms of the center-of-mass energy of the collision,

$$s = \frac{E_1 E_2}{V_+} \frac{\ell^2}{r_h^2} . \tag{2.3.33}$$

We obtain that

$$G_N \sqrt{s} \lesssim \frac{r_h}{\ell} \tag{2.3.34}$$

where we used the definition of the black hole mass $M \approx r_h^2 / G_N \ell^2$. Note that s here corresponds to the collision between all the N signals and the K negative shocks. To compare with the previous bounds, we translate this expression into light-cone coordinates, where the stress-energy tensor for the message is already given in eq. (2.3.1) and the one for the negative shocks has the generic form,

$$T_{UU} = \frac{q_U}{r_h} \delta(U - U_0) . \tag{2.3.35}$$

We have seen in the previous section that the magnitude of T_{UU} scales as ℓ^{-1}, see eq. (2.2.13). So, given, that the negative shock is composed by K signals, we expect $q_U = \frac{K r_h}{\ell}$. In light-cone coordinates, the center-of-mass energy squared is just

$$s = \frac{p_V q_U}{\ell^2}, \tag{2.3.36}$$

and so, eq. (2.3.34) becomes a bound on p_V,

$$p_V \lesssim \frac{r_h \ell}{G_N^2 K} \tag{2.3.37}$$

that, combined with the uncertainty principle, gives yet another bound on the number of signals that can go through the wormhole,

$$N \lesssim \frac{r_h}{G_N} . \tag{2.3.38}$$

Note that the final result is independent of K so it would seem to imply that we can saturate the entropy bound without the need to couple many fields. However, note that while it is true that by solving the junction condition we have solved the full nonlinear Einstein equations, the same is not true for the field theory computation. As we explained before, the amount of negative energy generally decrease when we take into account the backreaction of the signal. Therefore, when we go beyond the probe approximation, we cannot treat the negative energy shock as a particle with a well defined momentum, q_U, which is independent of the signal momentum. In other words our previous computation implicitly assumed the validity of the probe approximation and the final result is only valid when the probe approximation is satisfied.

2.3.3   Beyond spherical symmetry

So far we have bounded the amount on information we can transfer through the wormhole in the s-channel. We have seen that to send something through the wormhole we need $r_h \gg \ell$. However, it can be quite inconvenient to send signals spread over all the horizon. For example, a cat would have a hard time in such a delivery system. In this section we generalize our bound to signals that are localized to some region of size b along the horizon. We begin by rederiving the probe approximation condition (2.3.11) from a particle scattering perspective.

As before, we approximate the interaction between the signal and the negative energy as a gravitational scattering between particles. Following [90] the condition for the validity of the probe approximation is given by

$$S_{cl} = \frac{1}{2} \int d^3x \sqrt{-g} h_{UU} T^{UU} \ll 1 \,, \tag{2.3.39}$$

where S_{cl} is the gravitational action evaluated on the shockwave geometry. Here T^{UU} is the stress-energy tensor generated by the signal, and h_{UU} is the gravitational field generated by the negative energy. We approximate the stress energy tensors of the signal and the negative energy respectively with

$$T_{VV} = \frac{p_V}{r_h} \delta(V) t_V(\theta) \,; \quad T_{UU} = \frac{1}{\ell} \delta(U - U_0) \,. \tag{2.3.40}$$

The first expression is the usual stress tensor generated by an energy shock with momentum p_V, where the transverse profile function $t_V(\theta)$ is a function with support on an interval of size b/r_h and that integrates to 1. For our purpose, it will be enough to consider a step function. To define the second expression we have used that for the GJW construction the negative energy stress tensor scales like ℓ^{-1}, as shown in (2.2.13). The gravitational field obeys the following equation

$$\left(-\partial_\theta^2 + \frac{r_h^2}{\ell^2} \right) h_{UU} = G_N r_h^2 T_{UU} \,, \tag{2.3.41}$$

Since we are interested in the limit where $b \lesssim \ell \ll r_h$, we can approximate the horizon with an infinite line. This allows to avoid dealing with periodic boundary conditions and images. In other words let $x = \theta r_h / \ell$ we have

$$\left(-\partial_x^2 + 1 \right) h_{UU} = G_N \ell^2 T_{UU} \,, \tag{2.3.42}$$

where x takes values on the real line. The Green function for this equation is given by[9]

$$g(x - x') = \frac{1}{2} e^{-|x - x'|} \,. \tag{2.3.43}$$

---

[9]The correct expression on the circle is given by $g(\theta - \theta') = \frac{\ell}{2r_h} \sum_{n \in \mathcal{Z}} \exp\left\{ \left(-\frac{r_h}{\ell} |\theta - \theta' + 2\pi n| \right) \right\}$, we see that for $r_h \gg \ell$ we can neglect the images, *i.e.* the terms with $n \neq 0$.

Notice that this tells us that the gravitational interaction effectively shuts down when $\Delta\theta \approx \ell/r_h$, which is the angle corresponding to one thermal cell in the BTZ geometry. This means that, as we already pointed out earlier, the scattering between the messages and the negative energy shock naturally splits in r_h/ℓ independent shocks. In our case T_{UU} does not depend on θ and so,

$$h_{UU}(\theta) = G_N \ell^2 \int dx' g(x - x') T_{UU} \approx G_N \ell \delta(U) \,. \tag{2.3.44}$$

Finally, we find that the probe approximation is now given by

$$S_{cl} \approx \frac{G_N p_V}{\ell} \ll 1 \,. \tag{2.3.45}$$

Alternatively we can derive this expression by computing the time delay generated by the localized shock and impose that it is small. For the dependence on the transverse direction we take a simple step function

$$t_V(\theta) = \begin{cases} \dfrac{r_h}{b} & 0 < \theta < \dfrac{b}{r_h} \,, \\ 0 & \text{otherwise} \,. \end{cases} \tag{2.3.46}$$

The gravitational field generated by this shock is given by

$$h_{VV}(x) = \frac{G_N \ell^2 p_V}{b} \delta(V) \int_0^{b/\ell} dx' e^{-|x-x'|} \,. \tag{2.3.47}$$

The integral above can be easily evaluated

$$\int_0^{b/\ell} dx' e^{-|x-x'|} = \begin{cases} e^x - e^{x-b/\ell} & x < 0 \,, \\ 2 - e^{-x} - e^{x-b/\ell} & 0 \le x \le b/\ell \,, \\ e^{b/\ell-x} - e^{-x} & x > b/\ell \,. \end{cases} \tag{2.3.48}$$

Note that it is approximatively equal to b/ℓ in the interval $x \in [0, b/\ell]$, outside this interval is given approximatively by $b/\ell \, e^{-|x|}$. We see that this quantity is exponentially suppressed outside the thermal cell, *i.e.* for $|x| \gtrsim 1$. We conclude that

$$h_{VV}(\theta) \approx \begin{cases} G_N \ell p_V \delta(V) & \text{in the thermal cell} \,, \\ 0 & \text{otherwise} \,. \end{cases} \tag{2.3.49}$$

From this we can find the time delay given by the positive shock on the negative shock

$$\Delta U = \frac{1}{\ell^2} \int dV h_{VV} \approx \begin{cases} \dfrac{G_N p_V}{\ell} & \text{in the thermal cell} \,, \\ 0 & \text{otherwise.} \end{cases} \tag{2.3.50}$$

If we require $\Delta U \ll 1$ we recover (2.3.45).

Notice that, for a given value of momentum p_V, this is a more stringent requirement than the one we found for s-waves, (2.3.2). Indeed, as we localize the message on shorter scales the energy density corresponding to a given value of p_V increases, so it is natural that the probe approximation is harder to satisfy. However, the increased density ceases to play a role once we localize the signal on sub-AdS scales, *i.e.* inside a thermal cell. This can be explained by looking at the Green function (2.3.43). This is free of divergences in the $x \to x'$ limit. In fact, it is approximately constant over the whole thermal cell. This means that when we localize the message on sub-AdS scale, the gravitational field generated is smeared over the whole thermal cell and it is always approximatively given by $G_N \ell p_V$. This is true independently of the value of b. Notice that this is special to three dimensions. Later, we will see that in higher dimensions the situation is not as simple.

We would like now to proceed similarly to the previous subsection and bound p_V from below. However, there is a complication. To localize the message along the horizon we need to excite higher angular momentum modes. Compared to s-waves, these modes have a harder time crossing the wormhole. Even after having emerged from the horizon thanks to the negative energy shock, they still need to overcome the potential barrier of the black hole. This provides an extra lower bound on the momentum needed by the signal, which for high enough angular momenta overcomes the one provided by the uncertainty principle.

To find this new bound we consider the equation for spinning geodesics in the Schwarzschild metric. This can be obtained from the action

$$I = \frac{1}{2} \int d\lambda \, g_{\mu\nu} \frac{dx^\mu}{d\lambda} \frac{dx^\nu}{d\lambda} = \frac{1}{2} \int d\lambda \left(-f(r)\dot{t}^2 + \frac{\dot{r}^2}{f(r)} + r^2 \dot{\phi}^2 \right), \qquad (2.3.51)$$

where the dot represents derivatives with respect to λ. The symmetries of the geometry ensure that along geodesics the energy, $p_t = -f\dot{t} \equiv -E$, and the angular momentum, $p_\phi = r^2 \dot{\phi} \equiv L$, are conserved. We are interested in highly boosted particles, whose geodesics are approximately null. The equation can be obtained by simply imposing $ds^2 = 0$, which is equivalent to the equation of motion of a particle in a one dimensional potential

$$\dot{r}^2 + V(r) = E^2 \, ; \quad V(r) \equiv \frac{L^2}{\ell^2} \left(1 - \left(\frac{r_h}{r} \right)^2 \right) . \qquad (2.3.52)$$

It is easy to see that the geodesic reaches the boundary only if

$$E > \frac{L}{\ell} . \qquad (2.3.53)$$

To estimate the angular momentum needed localize the message to a region of size b consider a Gaussian wave-packet

$$f_V(\phi) \propto \exp\left(-\frac{(\phi - \phi_i)^2}{b/r_h}\right) .$$ (2.3.54)

Fourier transforming this expression it is easy to see that the needed angular momenta are those with $L \lesssim r_h/b$.

To compare this requirement with the uncertainty principle we first need to convert it to Kruskal coordinates. The momenta in Kruskal coordinates are given by

$$p_U = -\frac{E\ell^2}{2r_h U} + \frac{2Vr_h}{(1+UV)^2}\sqrt{\frac{E^2}{f^2} - \frac{L^2}{r^2 f}} ,$$

$$p_V = +\frac{E\ell^2}{2r_h V} + \frac{2Ur_h}{(1+UV)^2}\sqrt{\frac{E^2}{f^2} - \frac{L^2}{r^2 f}} .$$ (2.3.55)

To obtain this expression one first needs to find p_r by imposing $p^2 = 0$. We are interested in the limit where $U \approx 1$ and $V \approx \Delta V \ll 1$, for which we can approximate

$$f(U, V) = \frac{r_h^2}{\ell^2}\left(-\frac{4UV}{(1+UV)^2}\right) \approx -4\frac{r_h^2}{\ell^2}\Delta V .$$ (2.3.56)

Using this we see that $p_U \approx 0$ while the V component of the momentum is approximately given by

$$p_V \approx -\frac{E\ell^2}{r_h \Delta V} .$$ (2.3.57)

We conclude that the minimum required momentum needed to overcome the potential barrier is given by

$$p_V \gtrsim \frac{\ell}{b}\frac{1}{\Delta V} .$$ (2.3.58)

We see that for messages localized on scales smaller than a thermal cell this overcomes the uncertainty principle requirement (2.3.13). Combining this with the probe approximation bound (2.3.45) we find

$$N(b) \lesssim K\frac{b}{\ell}, \quad b \lesssim \ell .$$ (2.3.59)

This in particular means that to send one single message localized to a region of size $b \ll \ell$ we need to couple $K \approx \ell/b$. We see that while it becomes increasingly difficult to send messages localized on sub-AdS scales, it is still possible if we are willing to couple a large number of fields. If we set $N = 1$ in the above expression we can find the minimum allowed value of b for a given K

$$b(K) \gtrsim \frac{\ell}{K} .$$ (2.3.60)

However, as we increase K the cutoff of the theory gets lowered to $\ell_{UV} \approx KG_N$ and we should also impose that $b(K) > \ell_{UV}$. These two requirements coincide for $K_{min} \approx \sqrt{\ell/G_N}$, which leads to the following estimate for the minimum possible value of b

$$b_{min} \approx \sqrt{\ell G_N} \,. \tag{2.3.61}$$

Before concluding notice that in the opposite limit, $b \approx \ell$, the uncertainty principle and the potential barrier give the same bound and we find

$$N(b) \lesssim K \,, \quad b \gtrsim \ell \,. \tag{2.3.62}$$

This means that instead of sending Kr_h/ℓ s-waves we can also send messages localized in a thermal cell, sending K such messages per thermal cell.

2.3.4 Comparison to Quantum Information Bounds

In the previous sections, we have estimated the maximum information that can be sent through the wormhole with a bulk analysis. Here, we would like to briefly compare to a boundary analysis. A detailed boundary calculation is difficult because the theory is strongly coupled, but we can still place bounds on the amount of information transferred. As explained in [70], we can think of the procedure as quantum teleportation.[10] In standard quantum teleportation, if Alice and Bob share and EPR pair, they can use it as a resource to transfer a qubit. One qubit can be transferred at the cost of using up one entangled EPR pair and sending two bits of classical information. Here we think of the left-right coupling as playing the role of the classical communication, as explained in more detail in [70].

With these identifications, the amount of information sent is bounded by the decrease in entanglement entropy between the two CFT's,[11]

$$N \lesssim -\Delta S_{EE} \,. \tag{2.3.63}$$

We can compute the change in entropy from the change in energy induced by the non-local coupling

$$\Delta S_{EE} = \beta \Delta E \,. \tag{2.3.64}$$

This equation is valid because in the thermofield double the entanglement entropy between the two sides is equal to the thermal entropy. This statement is clear before acting with the coupling. After acting with the coupling, a bulk calculation tells us that the entanglement entropy is still equal to the thermal entropy, because

---

[10]We refer to quantum teleportation in a broad sense, without specializing to a particular quantum communication protocol. For a more detailed description of specific quantum communication protocols that might be dual to the traversable wormhole see [95].

[11]We thank David Berenstein for discussions on this point.

the bulk geometry is still an eternal AdS-Schwarzschild black hole. We do not have a direct CFT argument for this equality.

As mentioned above the boundary theory is strongly coupled, so computing ΔE directly on the boundary would be hard. The best we can do is to assume that the result of such a computation would match with the one we obtained with the bulk analysis. In other words we assume that the change in energy is given by one thermal quantum per coupling and per thermal cell,

$$\Delta E \approx -\frac{K\ell}{\beta^2}\,,\qquad(2.3.65)$$

where the number of thermal cells is given by ℓ/β. This is the only input we need from the bulk computation in this section. It would be interesting to check this, at least for some examples of weakly coupled boundary theories, see for example [96].

Combining the above equations we find

$$N \lesssim \frac{K\ell}{\beta}\,,\qquad(2.3.66)$$

which is K bits per thermal cell. This agrees with our bulk estimate found in equation (2.3.23) by requiring the bulk geometry to remain in the probe approximation. Clearly the entanglement entropy cannot decrease below zero, so an absolute bound is

$$N \lesssim S_{EE}\,.\qquad(2.3.67)$$

This absolute bound is saturated (up to order one prefactors) when we maximize the number of species providing the negative energy, as given in equation (2.3.26).

Notice that since we interpret the non-local coupled fields as playing the role of the classical messages in the usual teleportation protocol, it is natural to consider many such fields to send more information. However, from the CFT point of view it does not seem necessary that these are couplings between *different* fields, it might be possible to couple the same field but at different times. This seems to suggest that also in the bulk, if we were able to go beyond the probe approximation, we might be able to send order S_{BH} bits without coupling a parametrically large number of fields.

2.3.5   Generalization to $d+1$ dimensions

The picture we uncovered in the previous section is rather simple. Signals need to be highly boosted to fall through the wormhole, (2.3.13). Their backreaction on the geometry modifies the non-local coupling configuration, generally inducing a reduction of the negative energy. In other words, they close the wormhole.

We showed this at linear level, but the analysis of [50, 70] suggests that this is true also at nonlinear level. Certainly the negative energy is preserved if we can neglect the backreaction of the signal altogether, *i.e.* the probe approximation is valid, (2.3.2). The combination of this bound with the requirement that every signal is boosted enough constraints the amount of information that can be sent through the wormhole, see (2.3.23).

In this section we would like to understand how the bound on information transfer is modified in $d + 1$ dimensions. We expect the above picture to still be valid. Namely, the amount of information that can be transferred is bounded by a combination of the probe approximation and the uncertainty principle. Unfortunately, it is hard to carry out explicitly the calculation of GJW in higher dimensions, in particular we cannot find an expression for the negative energy. We will assume that the stress-energy tensor generated by the non-local coupling still scales with the AdS radius,

$$T_{UU} \propto \frac{K}{\ell^{d-1}} \,, \tag{2.3.68}$$

where we have already included K species.

To find the equivalent of the probe approximation bound (2.3.2) in $d+1$ dimensions, we again impose that the time delay generated by the positive energy shock is small, $\Delta U \ll 1$. The relation between the time delay and the stress energy tensor of the shock in general dimensions is still given by (2.3.9), where the Newton constant is now related to the Planck length by $8\pi G_N = \ell_P^{d-1}$. In terms of the total momentum carried by the signal the condition (2.3.2) becomes

$$\Delta U = \frac{G_N p_V}{r_h^{d-1}} \ll 1 \,. \tag{2.3.69}$$

We can again rewrite this condition in terms of coordinate independent quantities if we model the interaction between the signal and the negative energy as gravitational scattering. We showed that the gravitational interaction, close to the horizon of the BTZ black hole, is localized to a thermal cell of size ℓ and therefore, the collision could be split in independent events, K for each thermal cell. We demanded that each of these collision events was well described in the probe approximation, (2.3.12). In higher dimensions it is still true that the gravitational scattering is localized to a thermal cell. The limit on the validity of the probe approximation for gravitational scattering in $d + 1$ dimensions, see for example [97], is given by

$$G_N s_{cell} \frac{1}{\ell^{d-3}} \ll 1 \,, \tag{2.3.70}$$

Here we have set the impact parameter to be of order ℓ. To find s_{cell}, first notice that, as can be seen from (2.3.68), the negative energy particles still carry one unit

of momentum per thermal cell. To find the momentum carried by the positive energy shock per thermal cell, we simply divide the total momentum p_V by the number of thermal cells, r_h^{d-1}/ℓ^{d-1}. Under this identifications it easy to see that (2.3.70) agrees with (2.3.69).

The uncertainty principle condition carries on to higher dimension without modifications. However, the size of the wormhole opening is now given by

$$\Delta V = G_N \int T_{UU} \approx K \frac{G_N}{\ell^{d-1}} \,. \tag{2.3.71}$$

We can combine the uncertainty principle with the probe approximation requirement to bound the amount of information we can send through the wormhole. The computation is identical to the one above, the final result is

$$N \lesssim K \left(\frac{r_h}{\ell}\right)^{d-1} \,. \tag{2.3.72}$$

Similarly to the lower dimensional case the amount of information we can transfer scales with K and the number of thermal cells. We can find a bound on K recalling that in higher dimension the UV cutoff is renormalized as follows [92, 93]

$$\ell_{UV} \gtrsim (K G_N)^{\frac{1}{d-1}} \,. \tag{2.3.73}$$

Taking this into account we see that for the maximal value allowed, $K \approx \ell^{d-1}/G_N$, we find

$$N_{max} \approx \frac{r_h^{d-1}}{G_N} \approx S_{BH} \,. \tag{2.3.74}$$

This is the generalization to higher dimensions of our bound for information transfer in the s-wave channel. We see that in any dimensions, for the maximum value of K allowed by the species bound, we saturate the black-hole entropy.

We now turn to the case of localized messages presented above. For messages localized in regions larger than the AdS scale, everything works the same as in the three dimensional case. Instead of sending s-waves, we can send signals localized to thermal cells, K such signals per thermal cell. This is because, as pointed out above, the gravitational propagator in higher dimensions also decays exponentially outside the thermal cell. The behaviour at shorter distances, instead, is qualitatively different in higher dimensions. The propagator is not constant inside the thermal cell but acquires a singularity in the $x' \to x$ limit

$$g(x - x') \propto \frac{1}{|x - x'|^{d-3}} \,. \tag{2.3.75}$$

Here x_i are dimensionless coordinates defined similarly to (2.3.43). As a consequence the gravitational field generated by signals localized on sub-AdS scales is

not constant anymore inside the thermal cell and the analysis is not as simple. In particular, it might be possible to try and send many localized messages per thermal cell. We will not make this computation, but we simply imagine sending many localized messages superimposed at the center of the thermal cell. The time delay ΔU has now a non-trivial profile inside the thermal cell. For simplicity we impose that the maximum value of this delay inside the thermal cell is small. In principle we would need to solve

$$\left(-\partial_\Omega^2 + \frac{r_h^2}{\ell^2} \right) h_{VV} = G_N r_h^2 T_{VV} \,, \tag{2.3.76}$$

where ∂_Ω^2 is the Laplacian on the $(d-1)$-dimensional transverse sphere. Inside the thermal cell we can neglect the second term in the parenthesis and approximate the sphere with a plane. The equation reduces to the Poisson equation for a Newtonian potential in $d-1$ dimensions. For radii larger than the b/ℓ, the solution is simply given by[12]

$$h_{VV} \approx \frac{p_V \ell^{d-3}}{|x|^{d-3}} \delta(V) \,. \tag{2.3.77}$$

The maximum is given by $|x| = b/\ell$, which leads to

$$\Delta U \lesssim \frac{G_N}{\ell^2 b^{d-3}} p_V \ll 1 \,. \tag{2.3.78}$$

Similarly to the three dimensional case the signal needs to be boosted enough to overcome the angular momentum potential barrier, see (2.3.58). Combining these requirements we can find that the information transfer bound is given by[13]

$$N(b) \lesssim K \left(\frac{b}{\ell} \right)^{d-2} \,. \tag{2.3.79}$$

As compared to the three dimensional case it is indeed harder to send localized signals, for a given value of K. We can find the minimum value of b for a given K by setting $N = 1$ in the above equation

$$b(K) \gtrsim K^{\frac{-1}{d-2}} \ell \,. \tag{2.3.80}$$

As we increase the number of coupling we renormalize the UV cutoff of the theory, so we need also to check that b is larger than ℓ_{UV}. We have

$$b(K) \gtrsim K^{\frac{1}{d-1}} \ell_P \,. \tag{2.3.81}$$

---

[12]Notice that this equation is only valid for $d > 2$. Moreover, in the case $d = 3$ the polynomial reduces to a logarithm, $|x|^{3-d} \to \log|x|$.

[13]The correct result for $d = 3$ is $N(b) \lesssim K \frac{b}{\ell} \frac{1}{\log \ell/b}$

Combining these two bounds we find that the minimum possible value of b is given by[14]

$$b_{min} = \left(\frac{\ell}{\ell_P} \right)^{\frac{1}{d-2}} \ell_P \,. \tag{2.3.82}$$

We conclude that in high enough dimensions we can localize messages on scales smaller than what is possible in the three dimensional case. The reason is that even though it is harder to localize messages for a fixed value of K, in higher dimensions we can couple more fields before the UV cutoff reaches the AdS scale.

2.4   Discussion and future directions

In this work, we computed bounds on the amount of information that can be transferred in the traversable wormhole construction by Gao, Jafferis and Wall (and slight generalizations of it). This computation was motivated by some seemingly problematic features of the GJW wormhole. Namely, the perturbative nature of the non-local coupling opened the wormhole in the bulk only at a sub-Planckian scale, making it dubious whether large amounts of information could be actually transferred before closing the wormhole again. On the other hand, the wormhole is built perturbatively around the eternal blackhole geometry. This means that the entanglement entropy between the two boundaries is large and given by the black hole entropy. From the boundary perspective, and assuming this protocol is somehow dual to teleportation, this generates, in principle, a large amount of entropy available to teleport information from one side to the other. The question then becomes clear: is there a way we can use all that amount of entanglement entropy to maximize the information transfer through the wormhole?

In section 2.2, we studied in detail the construction of GJW, allowing for different types of non-local sources and computing the amount of negative energy generated by each of them. In particular, we found a simple analytic formula for the case where the sources are instantaneously turned on, avoiding much of the numerical computation that are usually done in the literature.

In section 2.3, we found that the amount of information transferred in the standard GJW wormhole is of order $\mathcal{O}(h\,r_h/\ell)$. Note that this, in general, is much smaller than the entanglement entropy, r_h/G_N.

Nevertheless, we found that large black holes can allow for more than one bit of information transfer. This contrast with previous results in the literature, in particular with [54], where it is claimed that the maximum amount of information that can be transferred is $\mathcal{O}(1)$. The difference lies in that their construction

---

[14]In the $d = 3$ this formula is correct up to logarithmic corrections.

only couples the s-wave between two boundaries, while the coupling we consider is local in space and therefore couples many angular modes. Coupling only the s-wave leads to a smaller amount of negative energy, allowing for at most one bit of information to be transmitted, as the authors find. Moreover the particular infinite boost limit that is taken in [54] does not seem physically well motivated: in the infinite boost limit, the collision between the negative energy and the signal will have an arbitrarily high center of mass energy and not be well-described in the semiclassical regime.

We also showed that it is possible to increase the amount of bits that can go from one boundary to the other by introducing a large number K of light fields coupled between the two boundaries. Using a combination of bounds coming from the uncertainty principle, the probe approximation and the existence of many species, we found that in principle it would be possible to send $N \approx S_{BH}$ bits of information. This is interesting, since it maximizes the amount of information that can be sent, at least from the boundary teleportation perspective.

The results on this paper rely on several assumptions and approximations of the traversable wormhole geometry. It will be interesting to further relax these assumptions and see whether it is possible to improve on our results. In the following, we comment on interesting possible future directions.

Beyond the probe approximation. Most of the results presented rely in the so-called probe approximation, assuming that the scattering processes between the shocks are small. This seems to be a strong restriction because it is only possible to send the maximum possible amount of information by allowing an extraordinarily large number K of light bulk fields, $K \approx \ell^{d-1}/G_N$. This large number of light fields lowers the UV cutoff of the bulk theory. Also, many holographic theories do not have a large number of light fields.

It would interesting to see if it is possible to saturate the amount of information transferred without the need of so many fields by going beyond the probe approximation. The calculation we presented in the multiple shocks section 2.3.2 is in this spirit, showing that independently of K, we get a bound on N coming from the gluing of the multiple shocks geometries.

One issue in going beyond the probe approximation is that the backreaction of the signal on the geometry means that we would have to re-compute the stress tensor coming from the coupled quantum fields, because we can no longer use the propagator in the BTZ background in calculating the stress tensor. This was explored in [50], where it was claimed that going beyond the probe approximation just reduces the amount of negative energy generated, and therefore does not allow for more information transfer.

We are not fully convinced by these results for the following reason. The effect of the backreaction is to create a time delay in the propagation across the signal. The new bulk-to-boundary propagator can be computed in the presence of the signal. Effectively, the signal induces a relative shift between the left and right boundary times. In the absence of the signal, the most effective boundary-boundary coupling occurs when the left and right boundary points are both halfway up the Penrose diagram, at $t_L = t_R = 0$, or at points related to this by symmetry. Upon introducing the signal, the shift means that the most effective coupling occurs when both points are in the lower half of the Penrose diagram. However, [50] does not consider allowing the coupled boundary points to be in this region. It would be very interesting (and probably not difficult for the authors of [50]) to extend their analysis into this regime.

If it is in fact possible, this would be rather surprising, given that from the teleportation picture it would seem that we would either need to couple a large number K of different fields, or we would need to keep the coupling turned on for a long time.

To summarize: in this paper we have calculated how much information can be sent while remaining in the probe regime, where the signal does not disturb the leading order calculation of the negative energy due to coupled quantum fields. These probe regime calculations and arguments are reliable. However, we do not have a persuasive bulk argument explaining why the information that can be sent is bounded by these probe regime calculations. It seems feasible to carry the analysis beyond the probe regime in the future.

Quantum metric fluctuations. Since the wormhole is open for such a short time, shorter than the Planck time, one might worry that quantum metric fluctuations will have a large correction on the transmission of a semiclassical message. We postpone a more complete discussion of these quantum fluctuations to future work. However, at least in 2+1 dimensions, we can argue that the quantum fluctuations will have a small effect. Quantum fluctuations include two effects: the thermofield double state includes a superposition of different black hole masses, and the black holes can be decorated by boundary gravitons.

Due the special properties of 2+1 dimensions, all of these metrics can be thought of as BTZ black holes, deformed arbitrarily close to the boundary by gravitons.[15] In analyzing the signal, these effects can all by combined into an uncertainty in the dimensionless time, t/β, that the signal is emitted from the left boundary or received by the right boundary. The effects of these perturbations are suppressed by powers of the gravitational coupling; we believe that the quantum uncertainty

---

[15]We thank Jan de Boer for discussion on this point.

is given by

$$\Delta(t/\beta) \approx \sqrt{\frac{G_N}{\ell}} \,.$$
(2.4.1)

Since we are interested in sending signals whose time duration is just a bit less than the thermal scale, these quantum corrections to the width of the signal are neglibible.

Beyond perturbative calculations. Many of the confusions that arise in the context of GJW are due to the perturbative nature of the non-local interaction. It would be interesting to find solutions at finite coupling and/or construct eternal wormholes in this context. In two bulk dimensions, it is possible to create an eternal wormhole [51], but the generalization to higher dimensions is not as straightforward –see, for instance [56].

Beyond three spacetime dimensions. The GJW construction relies heavily on the simplicity of the BTZ correlators. In section 2.3.5, we provide plausible generalizations to general dimensions of the bounds on information found on this work. It would be desirable to find a framework in higher dimensions where these claims could be checked by explicit calculations.

Beyond black hole horizons. A natural framework to study traversable wormholes are horizons in de Sitter spacetimes. Due to the nature of the cosmological horizon, the insertion of shockwaves naturally provides a mechanism for traversable wormholes. In the context of two dimensional gravity, it is possible to glue cosmological horizons in the IR, with an AdS boundary in the UV, and construct such shockwave solutions [98]. The nice feature about those solutions is that they do not need the insertion of non-local, negative energy couplings. It would be interesting to see whether they can be generalized to higher dimensions and compare the maximum bounds on information transferred in each case.

We hope to come back to some of these ideas in a future communication.

3   Eternal $AdS4$ Wormholes from Coupled CFT's

3.1   Introduction and Results

Wormholes have been a puzzling topic for physicists for a century. Many efforts have been made to build traversable wormholes using different kinds of fields and techniques, most of which require either the insertion of exotic matter [11, 76–79, 99, 100] or higher derivative theories [80–82, 101] which lack UV completions [102].

Recent work has shown how to build traversable wormholes in physically sensible theories. Gao, Jafferis, and Wall (GJW) [103] showed how to make asymptotically AdS black holes traversable for a short time by coupling the boundaries to each other. This approach has been extended in a number of other works since then [50, 53–55, 57, 59, 70, 85, 104–111]. The first eternal traversable wormhole was constructed by Maldacena and Qi [112] in asymptotically nearly-AdS$_2$ spacetime. More recently, Maldacena, Milekhin and Popov [3] found a long-lived $4D$ asymptotically flat traversable wormhole solution in the Standard Model (see also [113]).

In this paper, we make use of the ingredients developed by GJW and MMP in order to construct an eternal traversable wormhole in asymptotically AdS$_4$ spacetime. Our motivation is twofold. First, by constructing wormholes in asymptotically AdS spacetime, we can use AdS/CFT to learn more about them. Second, our wormhole solution can be used to learn more about CFT's. To this end, we identify a family of Hamiltonians consisting of two copies of a CFT coupled by simple, local interactions whose ground state is dual to the traversable wormhole.

This last point is significant for constructing traversable wormholes in a lab or on a quantum computer. Some very interesting ideas on how to do this are described in [71, 114, 115]. Given access to a holographic CFT, one simply needs to implement the coupling and allow the system to cool to its ground state, which is dual to a traversable wormhole.

Concretely, the bulk theory we consider is described in Section 3.2 and consists of

Einstein-Maxwell theory with negative cosmological constant, a $U(1)$ gauge field and massless Dirac fermions coupled to the gauge field. A particular solution is the magnetically charged Reissner-Nordström (RN) black hole. Due to the magnetic field, the charged fermions develop Landau levels. The lowest Landau level has exactly zero energy on the sphere, so we can think of them as effectively $2D$ fermionic degrees of freedom once we dimensionally reduce on the sphere.

The classical solution consists of two magnetically charged RN black holes connected through an Einstein-Rosen bridge which is non-traversable. The traversability of the wormhole is achieved by introducing a coupling between the two CFT's (labelled L, R) of the form

$$S_{\text{int}} = i \int d^3x \, h \left(\bar{\Psi}^R_- \Psi^L_+ + \bar{\Psi}^L_+ \Psi^R_- \right) \ . \tag{3.1.1}$$

Here Ψ^R is the bulk field at the right boundary that is dual to the charged fermions in the right CFT, and Ψ^L is defined analogously. Note that this is a local coupling involving a single, low dimension operator in each CFT; this contrasts with the beautiful construction of Maldacena and Qi [112] in the AdS$_2$ context, where a large number of operators must be coupled.

In Sections 3.2.3 and 3.2.4, we describe how this interaction has the effect of modifying the boundary conditions and the vacuum state. The stress tensor receives a quantum correction of the form

$$\langle T_{++}(x) \rangle = -\frac{1}{2\pi^3} \frac{q\lambda(h)}{R^2} \ , \tag{3.1.2}$$

where R is the sphere radius, q is the charge of the black hole, and λ is given by (3.2.33). For small coupling h, $\lambda(h) \approx h$, but our analysis remains valid for *finite h*. A priori it is not clear whether a self-consistent solution exists in which the negative null energy supports a traversable wormhole. Since it is only the quantum correction that has a chance of making the wormhole traversable, the quantum effects have a large backreaction on the metric.

Typically, this would constitute an intractable problem: we cannot calculate the quantum state, and hence the stress tensor, until we know the geometry, but on the other hand we cannot solve the Einstein equations to determine the geometry until we know the stress tensor. In this case, we are able to self-consistently solve the system because the stress tensor takes a particularly simple form, depending locally on the metric (up to an overall factor).

In Section 3.3, we discuss properties of both the linearized and non-linear solutions. The wormhole geometry has the following two regimes. The middle of the wormhole is nearly AdS$_2 \times \mathcal{S}^2$. As we move away from the middle of the wormhole, the geometry smoothly interpolates to the near-extremal region of two RN

black holes. Far away, the quantum contribution (3.1.2) becomes negligible and the geometry is that of two magnetically charged RN black holes (see Fig. 3.2).

As a consequence of the boundary perturbation, the mass of the wormhole is slightly *decreased* by a term proportional to the coupling

$$M = M_{\text{ext}} + \Delta M \ , \quad \text{with} \quad \Delta M \sim -\lambda^2(h) \ . \tag{3.1.3}$$

An infalling observer will experience that she is approaching a naked singularity from infinity. All of a sudden, deep in the throat region, the wormhole opens up and she comes out to the other side safely.

In Section 3.4.1, we identify a simple Hamiltonian whose ground state is dual to the wormhole. The procedure is to begin with two identical holographic CFT's, each with a global $U(1)$ symmetry, so that they are dual to Einstein-Maxwell theory at low energies. We then turn on a chemical potential for each CFT separately, and turn on a coupling of the form $\bar{\boldsymbol{\Psi}}^R \boldsymbol{\Psi}^L$ where the $\boldsymbol{\Psi}$ operators are dual to a bulk massless charged fermion.

Concretely, the Hamiltonian we analyze is

$$H = H_L + H_R + \mu(Q_L - Q_R) - \frac{ih}{\ell} \int d\Omega_2 \left(\bar{\boldsymbol{\Psi}}^R_- \boldsymbol{\Psi}^L_+ + \bar{\boldsymbol{\Psi}}^L_+ \boldsymbol{\Psi}^R_- \right) \ , \tag{3.1.4}$$

This Hamiltonian is similar to the construction of Cottrell et al [116]. The authors showed that the Hamiltonian in their case has the thermofield double state as its ground state. That construction, however, did not have a semiclassical gravity dual.

We show that the ground state of this theory is dual to our eternal traversable wormhole geometry for some range of the coupling h and chemical potential μ. We compare the wormhole to other geometries with the same boundary conditions, which may dominate the ensemble. In particular, we consider two disconnected black holes and empty AdS. We compute the ground state for different values of the parameters h and μ, and find that the wormhole is the ground state for $h > h_c$ and $\mu > \mu_c$, with the critical values given by

$$h_c = \frac{\bar{r}^2}{G_N q} \sqrt{\frac{2\pi}{3\mathcal{C}} \left(1 + \frac{2\bar{r}^2}{\ell^2} \right)} \ \text{ and } \ \mu_c = \sqrt{\pi} m_p \ , \tag{3.1.5}$$

with m_p the Planck mass. Interestingly, as the non-local coupling vanishes, there is a triple point located at $h = 0$, $\mu = \mu_c$ where the three phases meet. For values $h < 0$, the ground state is dominated by either empty AdS or the black hole phase.

The challenge of building a traversable wormhole is to have enough negative energy to allow defocusing of null geodesics, allowing the sphere to contract and

re-expand. Here we have added two ingredients so that the bulk dual remains semiclassical. First, the chemical potential makes the decoupled system closer to being traversable, since the near-horizon geometry for an extremal black hole is $AdS_2 \times S^2$. Because the size of the sphere is constant near the horizon, a small amount of negative energy will allow the sphere to re-expand, and render the wormhole traversable[1]. Second, by using bulk charged fermions in combination with a magnetically charged black hole, as was done in MMP [3], we enhance the negative energy due to the quantum effects. The key point is that a single 4d charged fermion acts like a large number q of 2d light charged fields due to the large degeneracy of lowest Landau levels.

Note: We understand that overlapping results will appear in [117]. We thank S. Banerjee for discussions. Also, [118] appeared very shortly before this work. There, asymptotically AdS$_4$ wormholes are also constructed, but with rather different ingredients. In addition, the solutions of [118] have different symmetries than our solution: they preserve the full Poincaré invariance in the boundary directions. It would be interesting to understand the relationship between the two constructions better. We thank M. Van Raamsdonk for discussions.

3.2 Massless fermions in AdS$_4$

We start this section by describing the particular theory of interest, as well as setting up the notation and conventions of spinors in curved space. Afterwards, we describe how the boundary conditions change once we couple the asymptotic boundaries. Finally, we compute the resulting stress tensor.

3.2.1 Dynamics

The theory consists of Einstein-Maxwell gravity with matter described by the action

$$S = \int d^4x \sqrt{g} \left(\frac{1}{16\pi G_N}(R - 2\Lambda) - \frac{1}{4g^2}F^2 + i\bar{\Psi}\slashed{D}\Psi \right) . \qquad (3.2.1)$$

In particular, we are considering a single massless Dirac fermion of charge one. In this section, we follow the approach and conventions of [3].

We consider g to be small, so that loop corrections are suppressed. A general class of spherically symmetric solutions with magnetic charge, denoted by the integer q, can be parametrized as follows

$$ds^2 = e^{2\sigma(x,t)}(-dt^2 + dx^2) + R^2(x) \, d\Omega_2^2 , \quad A = \frac{q}{2}\cos\theta d\phi . \qquad (3.2.2)$$

---

[1]We thank Daniel Jafferis for suggesting this approach.

Note that in this metric the range of x is compact and fixing this range can be seen as a gauge choice. For now we use $x \in [0, \frac{\pi}{2}]$. To have a well-defined representation of the Clifford algebra at each point of the spacetime we introduce the vierbein

$$e^1 = e^\sigma dt, \quad e^2 = e^\sigma dx, \quad e^3 = R d\theta, \quad e^4 = R \sin \theta d\phi . \tag{3.2.3}$$

and by solving

$$de^a + \omega^{ab} \wedge e^b = 0, \quad \omega^{ab} = -\omega^{ba} , \tag{3.2.4}$$

we compute the spin connection components

$$\omega^{12} = \sigma' dt + \dot\sigma dx, \quad \omega^{32} = R' e^{-\sigma} d\theta, \quad \omega^{42} = R' \sin \theta e^{-\sigma} d\phi, \quad \omega^{43} = \cos \theta d\phi . \tag{3.2.5}$$

Here a prime denotes a derivative with respect to x, while a dot denotes a derivative taken with respect to t. We use the following basis for the gamma matrices in flat space

$$\gamma^1 = i\sigma_x \otimes 1, \quad \gamma^2 = \sigma_y \otimes 1, \quad \gamma^3 = \sigma_z \otimes \sigma_x, \quad \gamma^4 = \sigma_z \otimes \sigma_y . \tag{3.2.6}$$

In this basis the Dirac operator has the form

$$
\begin{aligned}
\slashed{D} =& e^{-\sigma} \left[i\sigma_x \left(\partial_t + \frac{\dot\sigma}{2} \right) + \sigma_y \left(\partial_x + \frac{\sigma'}{2} + \frac{R'}{R} \right) \right] \otimes 1 \\
&+ \frac{\sigma_z}{R} \otimes \left[\sigma_y \frac{\partial_\phi - iA_\phi}{\sin \theta} + \sigma_x \left(\partial_\theta + \frac{1}{2} \cot \theta \right) \right] .
\end{aligned}
\tag{3.2.7}
$$

In the static case, the metric (3.2.2) has two Killing vectors ∂_t and ∂_ϕ. Introducing the following ansatz will allow us to decompose in Fourier modes on the sphere $\mathcal{S}^2$,

$$\Psi = \frac{e^{-\frac{\sigma}{2}}}{R} \sum_m \psi^m(t, x) \otimes \eta^m(\theta, \phi) . \tag{3.2.8}$$

Here ψ^m and η^m are bi-spinors. In the rest of the paper we will suppress the indices on ψ. In this ansatz the Dirac equation is given by

$$
\begin{aligned}
\frac{e^{-\frac{3}{2}\sigma}}{R} \left(i\sigma_x \partial_t + \sigma_y \partial_x \right) \psi \otimes \eta &= -\lambda , \\
\frac{e^{-\frac{\sigma}{2}}}{R^2} \sigma_z \psi \otimes \left(\sigma_y \frac{\partial_\phi - iA_\phi}{\sin(\theta)} + \sigma_x \left(\partial_\theta + \frac{1}{2} \cot(\theta) \right) \right) \eta &= \lambda .
\end{aligned}
\tag{3.2.9}
$$

Restricting to the lowest Landau level decouples the equations and admits solutions of the form

$$\psi_\pm = \sum_k \alpha_k^\pm e^{ik(t \mp x)} , \quad \eta_\pm^m = \left(\sin \frac{\theta}{2} \right)^{j_\pm \pm m} \left(\cos \frac{\theta}{2} \right)^{j_\pm \mp m} e^{im\phi}, \quad j_\pm = \frac{1}{2}(-1 \mp q) , \tag{3.2.10}$$

where $\psi_\pm$ are the components of ψ, and we choose $\sigma_z \eta_\pm = \pm \eta_\pm$ as the basis for η. If we take $q > 0$, the solution is

$$\eta_+ = 0, \quad \eta_- = \sum_m \mathcal{C}_m^j \eta_-^m, \quad -j \leq m \leq j \,, \tag{3.2.11}$$

where we define the quantum number $j := j_-$, so that in the lowest Landau level the degeneracy of the two-dimensional fields is q. The normalization constant is given by

$$(\mathcal{C}_m^j)^2 = \frac{1}{2} \frac{\Gamma(2 + 2j)}{\Gamma(1 + j - m)\Gamma(1 + j + m)} \,, \tag{3.2.12}$$

so that

$$\int d^2\Omega \; \bar{\eta}^{m_1} \eta^{m_2} = \delta_{m_1 m_2} \,. \tag{3.2.13}$$

3.2.2 Boundary conditions

According to the AdS/CFT dictionary, a bulk Dirac spinor of mass m is dual to a spin $1/2$ primary operator $\mathcal{O}$ of conformal dimension

$$\Delta_\pm = \frac{3}{2} \pm \sqrt{m^2 \ell^2} \,, \tag{3.2.14}$$

where ℓ is the AdS radius [119, 120]. The stability bound requires $m \geq 0$ [121]. When applying the correspondence, we should consider that the first order nature of the Dirac action goes hand in hand with the different dimensionality between the bulk and boundary spinors. The extrapolate dictionary instructs us to identify the two bulk chiral components with the same boundary field. In addition, when solving the Dirichlet boundary value problem, we should impose boundary conditions only on half of the spinor degrees of freedom. Our gamma matrix in the holographic radial direction satisfies $(\gamma^2)^2 = 1$ and $(\gamma^2)^\dagger = \gamma^2$. We can then decompose the bulk fermions onto the eigenspace of γ^2

$$\Psi_\pm := \mathcal{P}_\pm \Psi \,, \quad \mathcal{P}_\pm = \frac{1}{2}\left(1 \pm \gamma^2\right) \,, \tag{3.2.15}$$

and similarly for the Dirac conjugate. The orthogonal projection operator satisfies the two conditions $\mathcal{P}^2 = \mathcal{P}$ and $\mathcal{P}^\dagger = \mathcal{P}$. More explicitly

$$\begin{aligned}
\Psi_+ &:= \frac{1}{2}\frac{e^{-\frac{\sigma}{2}}}{R}\begin{pmatrix} \psi_+ - i\psi_- \\ i(\psi_+ - i\psi_-) \end{pmatrix} \otimes \begin{pmatrix} \eta_+ \\ \eta_- \end{pmatrix} \,, \\
\Psi_- &:= \frac{1}{2}\frac{e^{-\frac{\sigma}{2}}}{R}\begin{pmatrix} \psi_+ + i\psi_- \\ -i(\psi_+ + i\psi_-) \end{pmatrix} \otimes \begin{pmatrix} \eta_+ \\ \eta_- \end{pmatrix} \,.
\end{aligned} \tag{3.2.16}$$

The variation of the Dirac part of the action (3.2.1) with respect to $\Psi_\pm$ after integration by parts becomes

$$\Delta S_D = \text{bulk terms} + i \int_\partial d^3x \ \sqrt{\gamma} \left(\bar{\Psi}_- \delta \Psi_+ - \bar{\Psi}_+ \delta \Psi_- \right) \ , \tag{3.2.17}$$

where γ is the determinant of the induced metric at the boundary. The bulk terms are proportional to the equations of motion. In order to have a well-defined boundary value problem, we should include a boundary term of the form

$$S_\partial = i \int_\partial d^3x \sqrt{\gamma} \left(a_1 \bar{\Psi}_- \Psi_+ + a_2 \bar{\Psi}_+ \Psi_- \right) \ . \tag{3.2.18}$$

We can then either fix $\Psi_+ = 0$ or $\Psi_- = 0$ (and thus $\bar{\Psi}_+ = 0$ or $\bar{\Psi}_- = 0$) at the boundary depending on whether we set $(a_1 = -1, a_2 = 0)$ or $(a_1 = 0, a_2 = 1)$ respectively in the total variation of the action $\delta S_D + \delta S_\partial$.

In the massless case, both modes $\Psi_\pm$ are normalizable. We can then identify the asymptotic values

$$\Psi_\pm^0 := \lim_{x \to \frac{\pi}{2}} R(x)^{-\frac{3}{2}} \Psi_\pm \ , \tag{3.2.19}$$

with the normalizable part of the dual operator $\mathcal{O}$. After reducing on the $\mathcal{S}^2$ sphere, the effective $2D$ fermions obey reflective boundary conditions in both types of quantizations

$$\psi_+ = e^{i\alpha} \ \psi_- \ , \quad \text{with} \quad \alpha = \begin{cases} \frac{\pi}{2} \ , & \text{standard} \\ \frac{3\pi}{2} \ , & \text{alternate} \end{cases} \ , \tag{3.2.20}$$

which correspond to taking $\Psi_+^0 = 0$ or $\Psi_-^0 = 0$ respectively. Intuitively, they would not allow the charge and energy to leak out at the boundary. In fact, by using the conservation equations it is easy to see that at the boundary

$$\dot{E} = T_{12}\Big|_\partial = 0 \quad \text{and} \quad \dot{Q} = J_2\Big|_\partial = 0 \ , \tag{3.2.21}$$

where J_2 is the x component of the $U(1)$ current

$$J_2 = \psi^\dagger \sigma_z \psi \otimes \eta^\dagger \eta = \left(\psi_-^\dagger \psi_+ - \psi_+^\dagger \psi_- \right) \otimes \eta^\dagger \eta \ , \tag{3.2.22}$$

and T_{12} is the energy flux, which is given by the tx-component of the stress tensor

$$T_{12} = \frac{i}{2R^2} \left(\psi_+^\dagger (\partial_x - \partial_t)\psi_+ + \psi_-^\dagger (\partial_x + \partial_t)\psi_- - (\partial_x - \partial_t)\psi_+^\dagger \psi_+ - (\partial_x + \partial_t)\psi_-^\dagger \psi_- \right) \otimes \eta^\dagger \eta \ . \tag{3.2.23}$$

Now consider two decoupled and identical conformal theories with fermionic degrees of freedom. In principle, each one has its own bulk gravity dual. The boundary action then acquires the form[2]

$$S_\partial = i \int_\partial d^3x \sqrt{\gamma} \left(a_1 \bar{\Psi}^R_- \Psi^R_+ + a_2 \bar{\Psi}^R_+ \Psi^R_- + b_1 \bar{\Psi}^L_- \Psi^L_+ + b_2 \bar{\Psi}^L_+ \Psi^L_- \right) \ . \tag{3.2.24}$$

There are various options depending on what type of boundary sources we would like to keep turned-on. The guiding principle we will follow is CPT invariance. CPT-related boundary conditions imply a vanishing T_{++} component consistent with the fact that vacuum AdS$_2$ cannot support finite energy excitations [122]. For the purpose of this work, we choose the following CPT conjugate boundary conditions

$$\Psi^R_+ = 0 \ \xrightarrow{\ \text{CPT}\ } \ \bar{\Psi}^L_- = 0 \ , \tag{3.2.25}$$

which correspond to the coefficients $a_1 = -1$, $b_2 = 1$, and $a_2 = b_1 = 0$. The vanishing energy can also be understood as due to the conformal anomaly contribution present in the mapping between the energy of a CFT on the strip to AdS$_2$ [112].

3.2.3 Modified boundary conditions

We are interested in the case where the two bulk geometries are two magnetically charged RN black holes. Intuitively, we can think on them as being connected through an Einstein-Rosen bridge. A priori, however, it is not obvious how to connect both bulk geometries through the horizon. Moreover, in order to render the wormhole traversable, we need to establish a connection between the two asymptotic boundaries. We achieve that by using a non-local coupling of the form[3]

$$S_{\text{int}} = -i \int d^3x \sqrt{\gamma} \left(h_1 \bar{\Psi}^R_+ \Psi^L_- + h_2 \bar{\Psi}^L_- \Psi^R_+ + h_3 \bar{\Psi}^R_- \Psi^L_+ + h_4 \bar{\Psi}^L_+ \Psi^R_- \right) \ . \tag{3.2.26}$$

This term will provide us with the negative energy we need and will open up the wormhole. It is important to mention that if instead of fermions, we considered interacting scalar fields, similar to [103], the lowest Landau levels would have positive energy on the $\mathcal{S}^2$ sphere, making the problem of finding a traversable geometry much harder.

---

[2]Note that since we consider two copies of the theory we now have $x \in [-\frac{\pi}{2}, \frac{\pi}{2}]$, and we denote the left (right) boundary at $x = \mp \frac{\pi}{2}$ with L (R).

[3]In general, the coupling constants can be complex. However, they must satisfy $h_1 = h_2^*, h_3 = h_4^*$, in order for (3.2.26) to be real.

We are looking for an eternal traversable wormhole, so we let the coupling constants be turned on for all times. For the purposes of this work, we focus on the case where the coupling constants are real and $h_1 = h_2 = 0$[4]. The boundary conditions turn out to be

$$\Psi_+^R + h\Psi_+^L = 0, \quad \text{and} \quad \Psi_-^L + h\Psi_-^R = 0 \ , \tag{3.2.27}$$

where $h_3 = h_4 = -h$. Notice that the sources at the boundary are vanishing. In terms of the spinor components this implies the following boundary conditions

$$\psi_+^R - i\psi_-^R + h\psi_+^L - ih\psi_-^L = 0 \ , \quad \text{and} \quad \psi_+^L + i\psi_-^L + h\psi_+^R + ih\psi_-^R = 0 \ . \tag{3.2.28}$$

See Fig. 3.1 for an illustrations of the modified boundary conditions.

In order to obtain a solution to the equations of motion (3.2.9) with the boundary conditions (3.2.28), for the lowest Landau level, we use the following ansatz:

$$\psi_+ = \sum_k \frac{\alpha_k}{\sqrt{\pi}} e^{i\omega_k(t-x)} \quad \text{and} \quad \psi_- = \sum_k \frac{\beta_k}{\sqrt{\pi}} e^{i\omega_k(t+x)} \ . \tag{3.2.29}$$

Filling in this ansatz in to the boundary conditions (3.2.28) leads to the following constraint equations[5]

$$\begin{aligned}
(i^{3\omega_k} + hi^{\omega_k})\alpha_k + (i^{\omega_k+3} + hi^{3\omega_k+3})\beta_k &= 0 \ , \\
(i^{\omega_k} + hi^{3\omega_k})\alpha_k + (i^{3\omega_k+1} + hi^{\omega_k+1})\beta_k &= 0 \ ,
\end{aligned} \tag{3.2.30}$$

with solution

$$\omega_k = 2k - \frac{i}{\pi}\log\left(\frac{-2h \pm i|1-h^2|}{1+h^2}\right), \quad \beta_k = (-1)^{k+1}\alpha_k \ , \tag{3.2.31}$$

where $k \in \mathbb{Z}$. The solution can be written in the following form

$$\omega_k = \frac{2k+1}{2} + (-1)^k \frac{2}{\pi}\lambda(h) \ , \tag{3.2.32}$$

where λ is a function of h given by

$$\lambda(h) = \frac{1}{2}\arctan\left(\frac{2h}{|1-h^2|}\right) \ . \tag{3.2.33}$$

---

[4]It would be interesting to understand other combinations of the non-local couplings.

[5]Note that the equations are invariant under $h \mapsto \frac{1}{h}$ and $\beta_k \mapsto -\beta_k$, so the theory exhibits S-duality.
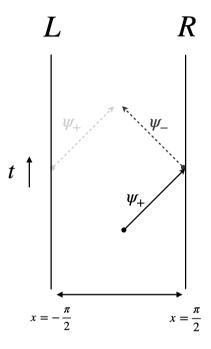
Figure 3.1: A right moving massless fermion, with amplitude $|\psi_+^R| = 1$, traveling on the strip hits the right boundary. The probability of the resulting left mover is equal to $\frac{(h^2-1)^2}{(h^2+1)^2}$, and the right mover emerging from the left boundary has amplitude $\frac{4h^2}{(h^2+1)^2}$.

3.2.4 Propagators and stress tensor

Using the solution (3.2.32), we write the fermionic fields as[6]

$$\psi_+ = \sum_k \frac{1}{\sqrt{\pi}} \alpha_k e^{i\omega_k(t-x)} , \quad \text{and} \quad \psi_- = \sum_k \frac{(-1)^{k+1}}{\sqrt{\pi}} \alpha_k e^{i\omega_k(t+x)} . \quad (3.2.34)$$

The modes α_k obey the following anti-commutation relations

$$\{\alpha_k, \alpha_j^\dagger\} = \delta_{k,j} , \quad \{\alpha_k, \alpha_j\} = 0 \quad \text{and} \quad \{\alpha_k^\dagger, \alpha_j^\dagger\} = 0 , \quad (3.2.35)$$

and the vacuum is defined as

$$\alpha_k|0\rangle = 0 \quad \forall \, k \in \mathbb{Z}_{<0}, \quad \text{and} \quad \alpha_k^\dagger|0\rangle = 0 \quad \forall \, k \in \mathbb{Z}_{\geq 0} . \quad (3.2.36)$$

Using equations (3.2.34)-(3.2.36) we calculate the propagators. We present one of them here and the rest can be found in the Appendix A

$$\langle \psi_+^\dagger(x_-)\psi_+(x_-') \rangle = \frac{1}{\pi} \frac{e^{\frac{i}{2}(x_-'-x_-)}}{1-e^{i(x_-'-x_-)}} + \frac{e^{\frac{i}{2}(x_-'-x_-)}}{1+e^{i(x_-'-x_-)}} \frac{2i\lambda(h)}{\pi^2}(x_-'-x_-) + \cdots . \quad (3.2.37)$$

We proceed by stating the relevant components of the stress tensor. Since (3.2.2) is spherically symmetric and does not depend on time, the only off-diagonal component of the stress tensor that could be nonzero is T_{12}. However, in Appendix B we show explicitly that T_{12} vanishes for our setup. Therefore, we only need the diagonal components of the stress tensor, which are given by

$$\begin{aligned} T_{11} &= \frac{i}{2R^2}\left(\psi_+^\dagger\partial_t\psi_+ + \psi_-^\dagger\partial_t\psi_- - \partial_t\psi_+^\dagger\psi_+ - \partial_t\psi_-^\dagger\psi_-\right)\eta^\dagger\eta , \\ T_{22} &= -\frac{i}{2R^2}\left(\psi_+^\dagger\partial_x\psi_+ - \psi_-^\dagger\partial_x\psi_- - \partial_x\psi_+^\dagger\psi_+ + \partial_x\psi_-^\dagger\psi_-\right)\eta^\dagger\eta , \\ T_{33} &= -\frac{ie^{-2\sigma}}{2}\frac{R'}{R}\psi^\dagger\sigma_z\psi\eta^\dagger\eta , \\ T_{44} &= -\frac{i\sin(\theta)}{2}\frac{e^{-2\sigma}}{R}R'\sin(\theta)e^{-\sigma}\psi^\dagger\sigma_z\psi\eta^\dagger\eta . \end{aligned} \quad (3.2.38)$$

In order to compute the quantum contribution to the components of the stress tensor due to the non-local coupling, we apply the point-splitting formula

$$\langle T_{\mu\nu} \rangle = \lim_{x' \to x} \frac{i\eta_{ab}}{2}\left(e^a_{(\mu}\gamma^b\nabla'_{\nu)} - \nabla_{(\mu}e^a_{\nu)}\gamma^b\right)\langle\bar{\Psi}(x)\Psi(x')\rangle . \quad (3.2.39)$$

---

[6]In the remainder of this work, we will use light-cone coordinates defined by $x_\pm = t \pm x$, whenever they are more convenient.

By using the propagators and after subtracting the vacuum contribution, we end up with the following finite result

$$\langle T^h_{\mu\nu} \rangle = -\frac{1}{2\pi^3} \frac{q\lambda(h)}{R^2} \text{diag}\,(1,1,0,0) \ , \tag{3.2.40}$$

where the factor q comes from the fact that in the lowest Landau level the degeneracy of the two-dimensional fields is q. The range for the compact radial coordinate ($\Delta x = \pi$) is present in the prefactor in the above expression. Picking a different gauge would result in a rescaling of the stress tensor. One can easily check that the stress tensor is conserved and traceless due to conformal symmetry. Details of the stress tensor calculation can be found in Appendix B.

3.3 Wormhole geometry

We start this section by describing the two different regimes of the wormhole geometry, after which we analytically solve the (linearized) Einstein equations in both regimes. We continue by showing that the solutions in the two regimes can be consistently patched together through a coordinate transformation in the overlapping region of validity. We end the section by solving the full, nonlinear Einstein equations numerically.

3.3.1 Two regimes

The next task is to solve the semi-classical Einstein equations to find a magnetically charged geometry sourced by (3.2.40)

$$G_{\mu\nu} + \Lambda g_{\mu\nu} = 8\pi G_N \langle T_{\mu\nu} \rangle \ . \tag{3.3.1}$$

As we approach the AdS$_4$ boundaries located at $r \to \pm\infty$, the electromagnetic contribution of the stress tensor dominates over the Casimir energy. Then, far away from the wormhole throat the solution should look like Reissner-Nordström AdS$_4$

$$ds^2 = -f(r)d\tau^2 + \frac{dr^2}{f(r)} + r^2 d\Omega_2^2 \ , \tag{3.3.2}$$

with emblackening factor

$$f(r) = 1 - \frac{2G_N M}{r} + \frac{r_e^2}{r^2} + \frac{r^2}{\ell^2}, \quad \text{and} \quad r_e^2 = \frac{\pi q^2 G_N}{g^2} \ . \tag{3.3.3}$$

Here M denotes the mass of the black hole, q is an integer and r_e^2 denotes the magnetic charge of the black hole. Close to extremality, the geometry develops

an infinitely long throat. The value of the extremal radius has the form

$$\partial_r f(r)\Big|_{r=\bar{r}} \overset{!}{=} 0 \quad \Rightarrow \quad \bar{r}^2 = \frac{\ell^2}{6}\left(-1+\sqrt{1+12\frac{r_e^2}{\ell^2}}\right) . \qquad (3.3.4)$$

Inverting this relation gives the charge of the black hole in terms of the extremal horizon radius and the AdS length

$$r_e^2 = \bar{r}^2\left(1+3\frac{\bar{r}^2}{\ell^2}\right) . \qquad (3.3.5)$$

In the range of masses that we are interested in, the quartic polynomial $f(r) = 0$ admits complex conjugate roots[7]. We choose to parametrize them by $r_{1,2} = \hat{r}(1 \pm i\epsilon)$ with $\epsilon > 0$ and $\hat{r} > 0$. We can analytically solve for the other two roots, r_3 and r_4, and the parameter $\hat{r}$ by matching the quadratic, cubic, quartic and constant contributions to $r^2 f(r)$. This parametrization is symmetric with respect to $\epsilon \mapsto -\epsilon$. Therefore, the expressions for $(r_3, r_4, \hat{r})$ will involve only even powers of ϵ. In the near extremal limit ($\epsilon \ll 1$), we then approximate f to order $\mathcal{O}(\epsilon^4)$ by

$$f(r) = \frac{1}{\ell^2}\left(\left(\frac{r-\hat{r}}{r}\right)^2 + \left(\frac{\hat{r}\epsilon}{r}\right)^2\right)(r-r_3)(r-r_4) , \qquad (3.3.6)$$

with

$$(r-r_3)(r-r_4) = \ell^2 + r^2 + 2r\bar{r} + 3\bar{r}^2 - \frac{\ell^2(r+4\bar{r})+2\bar{r}^2(r+6\bar{r})}{\ell^2+6\bar{r}^2}\bar{r}\epsilon^2 + \mathcal{O}(\epsilon^4) , \quad (3.3.7)$$

and

$$\hat{r} = \bar{r} + \epsilon^2 \frac{\bar{r}}{2\mathcal{C}(\bar{r})}\left(1+2\frac{\bar{r}^2}{\ell^2}\right) + \mathcal{O}(\epsilon^4) . \qquad (3.3.8)$$

Here $\mathcal{C}(r)$ is defined by

$$\mathcal{C}(r) = 6\left(\frac{r}{\ell}\right)^2 + 1 . \qquad (3.3.9)$$

In the region where $r - \bar{r} \ll \bar{r}$ and ϵ is small, we can approximate the metric (3.3.2) as

$$ds^2 = -\mathcal{C}(\bar{r})\left(\left(\frac{r-\bar{r}}{\bar{r}}\right)^2 + \epsilon^2\right)d\tau^2 + \frac{dr^2}{\mathcal{C}(\bar{r})\left(\left(\frac{r-\bar{r}}{\bar{r}}\right)^2 + \epsilon^2\right)} + \bar{r}^2 d\Omega_2^2 . \qquad (3.3.10)$$

By making the following identifications,

$$\rho = \frac{r-\bar{r}}{\epsilon\bar{r}} \quad \text{and} \quad t = \mathcal{C}(\bar{r})\frac{\tau\epsilon}{\bar{r}} , \qquad (3.3.11)$$

---

[7]As a function of r_e, the disciminant interpolates between $\Delta(r_e = 0) = -16G_N^2 M^2 \ell^8(\ell^2 + 27G_N^2 M^2)$ to infinity. In particular, $\Delta \approx 256\ell^6 r_e^6$ when $r_e \gg \ell$ and $\Delta \approx -16G_N \ell^{10} M^2$ when $r_e \ll \ell$. In both cases, there is at least one pair of complex conjugate roots.

the metric can be brought to global AdS$_2 \times \mathcal{S}^2$ form

$$ds^2 = \frac{\bar{r}^2}{\mathcal{C}(\bar{r})}\left(-(\rho^2 + 1)dt^2 + \frac{d\rho^2}{\rho^2 + 1}\right) + \bar{r}^2 d\Omega_2^2 \ . \qquad (3.3.12)$$

Following [3], we expect that in the wormhole region the solution is a slight per-turbation of the near extremal RN black hole. We make the following gauge choice for our ansatz geometry in the throat

$$ds^2 = \frac{\bar{r}^2}{\mathcal{C}(\bar{r})}\left(-(1 + \rho^2 + \gamma)dt^2 + \frac{d\rho^2}{1 + \rho^2 + \gamma}\right) + \bar{r}^2(1 + \psi)d\Omega_2^2 \ , \qquad (3.3.13)$$

where the functions $\psi(\rho)$ and $\gamma(\rho)$ are small fluctuations and $\bar{r}$ is given by (3.3.4). In these coordinates, the stress tensor contribution has the approximate form

$$\langle T_{\mu\nu}^h \rangle \approx -\frac{1}{2\pi^3}\frac{q\lambda(h)}{\bar{r}^2}\text{diag}\left(1, \frac{1}{(1 + \rho^2)^2}, 0, 0\right) \ . \qquad (3.3.14)$$

The linearized Esintein's equations in this geometry are given by

$$tt: \quad \frac{\zeta}{1 + \rho^2} + \psi(\rho) - \rho\psi'(\rho) - (1 + \rho^2)\psi''(\rho) = 0 \ , \qquad (3.3.15)$$

$$\rho\rho: \quad \frac{\zeta}{1 + \rho^2} - \psi(\rho) + \rho\psi'(\rho) = 0 \ , \qquad (3.3.16)$$

$$\theta\theta: \quad \frac{4}{\mathcal{C}(\bar{r})}\left(1 + 3\frac{\bar{r}^2}{\ell^2}\right)\psi(\rho) + \gamma''(\rho) + 2\rho\psi'(\rho) + (1 + \rho^2)\psi''(\rho) = 0 \ , \qquad (3.3.17)$$

$$\phi\phi: \quad \sin^2(\theta)\left(\frac{4}{\mathcal{C}(\bar{r})}\left(1 + 3\frac{\bar{r}^2}{\ell^2}\right)\psi(\rho) + \gamma''(\rho) + 2\rho\psi'(\rho) + (1 + \rho^2)\psi''(\rho)\right) = 0 \ , \qquad (3.3.18)$$

where ζ is a constant given by $\zeta = \frac{4G_N q\lambda(h)}{\pi^2 \bar{r}^2}$[8]. Note that the first two equations do not depend on γ. Therefore, we can find an expression for $\psi(\rho)$ by solving the first order equation (3.3.16). This results in

$$\psi(\rho) = \zeta(1 + \rho\arctan(\rho)) + c\rho \ , \qquad (3.3.19)$$

with c an integration constant. A simple check shows that (3.3.19) also solves the *tt* component of the Einstein equations (3.3.15). By using the solution for $\psi(\rho)$, we can now use the angular components of the Einstein equations to solve for $\gamma(\rho)$. It turns out that

$$\gamma(\rho) = -\frac{\zeta\left(1 + 4\frac{\bar{r}^2}{\ell^2}\right)}{\mathcal{C}(\bar{r})}\left(\rho^2 + \rho(3 + \rho^2)\arctan(\rho) - \log(1 + \rho^2)\right) + c_1 + \rho c_2 \ , \qquad (3.3.20)$$

---

[8]Note that we can write q in terms of $\bar{r}$. This results in $\zeta = \frac{4g\lambda(h)}{\pi^2\bar{r}}\sqrt{\frac{G_N\left(1 + 3\frac{\bar{r}^2}{\ell^2}\right)}{\pi}}$. From this we see that we can let ζ be small at finite h and independent of the ratio between $\bar{r}$ and ℓ.

solves (3.3.17) and (3.3.18). Integration constants can be set to zero by requiring that the geometry is invariant under $\rho \mapsto -\rho$ and by a redefinition of ρ and t.

In the next subsection, we show that there is an overlapping region between the two solutions deep in the RN-AdS throat and construct the full wormhole geometry.

3.3.2   Matching

Intuitively, once the non-local coupling h is turned on, the wormhole is formed and the throat acquires a certain finite length L which we will determine below. Outside this range, the linearized solution found in the previous section will not be valid anymore. In fact, both perturbations ψ and γ increase with the value of ρ, as we approach the wormhole mouth. More precisely, we expect the slightly deformed solution to be valid up to values of ρ for which the term $\zeta \rho^3$ is no longer subleading (since this is the leading order behaviour of γ). In the following, we consider ρ to be large, but $\zeta \rho$ small and fixed, and ζ small. We take the near-horizon limit of (3.3.6)

$$f(r) = \mathcal{C}(\bar{r})\epsilon^2 + \mathcal{C}(\bar{r}) \left(\frac{r-\bar{r}}{\bar{r}} \right)^2 - \mathcal{C}(\bar{r}) \left(\frac{r-\bar{r}}{\bar{r}} \right) \epsilon^2 - 2 \left(1 + 4\frac{\bar{r}^2}{\ell^2} \right) \left(\frac{r-\bar{r}}{\bar{r}} \right)^3 + \cdots ,$$
(3.3.21)

where we have expanded up to third order in ϵ and $\frac{r-\bar{r}}{\bar{r}}$ combined. As a first approximation let us set

$$\rho = \frac{L}{\bar{r}}\frac{r-\bar{r}}{\bar{r}}, \qquad t = \mathcal{C}(\bar{r})\frac{\tau}{L} .$$
(3.3.22)

In the limit

$$\rho \gg 1 , \quad \frac{L}{\bar{r}} \gg 1 , \quad \text{and} \quad \frac{r-\bar{r}}{\bar{r}} \ll 1 ,$$
(3.3.23)

equation (3.3.22) matches the order $\mathcal{O}(2)$ of the unperturbed ansatz geometry. Here L is an integration constant that denotes the rescaling between the t and τ coordinates. Furthermore, by considering the relation between ρ and r, one can see that L is a measure up to which we can trust the ansatz; so that ρ has a cutoff at $\rho \sim \frac{L}{\bar{r}}$. By comparing to the matching of the near-extremal Reissner-Nordström black hole given in (3.3.11), we see that L is connected to ϵ through[9]

$$L = \frac{\bar{r}}{\epsilon} .$$
(3.3.24)

By matching the angular coordinates we see that

$$r^2 = \bar{r}^2(1 + \psi(\rho)) \quad \rightarrow \quad \frac{r-\bar{r}}{\bar{r}} = \frac{\psi(\rho)}{2} + \mathcal{O}\left(\psi^2\right) = \frac{\pi\zeta}{4}\rho + \mathcal{O}\left(\zeta^2\right) , \quad (3.3.25)$$

---

[9]Recall that ϵ encodes how "far" from extremality the near-extremal black hole metric is.

where we have expanded $\sqrt{1 + \psi(\rho)}$, and in the third equality we used the expansion of $\psi(\rho)$ at large ρ. Using (3.3.22) and (3.3.25) we can find the value for L by examining

$$\rho dt = \mathcal{C}(\bar{r}) \frac{r - \bar{r}}{\bar{r}^2} d\tau \quad \Longrightarrow \quad L = \frac{d\tau}{dt} \mathcal{C}(\bar{r}) = \rho \bar{r} \frac{\bar{r}}{r - \bar{r}} = \frac{4\bar{r}}{\pi \zeta} . \tag{3.3.26}$$

One can easily see that with this value for L, (3.3.22) and (3.3.25) are consistent with one another. This also gives a relation between the non-local coupling constant h and ϵ. With (3.3.24) and (3.3.26) we see that

$$\epsilon^2 = \frac{\pi^2 \zeta^2}{16} = \frac{G_N g^2 \lambda^2(h)}{\pi^3 \bar{r}^2} \left(1 + 3 \frac{\bar{r}^2}{\ell^2} \right) = \frac{G_N^2 q^2 \lambda^2(h)}{\pi^2 \bar{r}^4} . \tag{3.3.27}$$

The matching of the time component of the geometry is discussed in Appendix C. In this appendix we show that the equations above give a consistent matching between the Reissner-Nordström geometry and the deformed $AdS_2 \times S^2$. A final comment we make concerning the matching is that the deformation γ gives a correction to the range of the radial coordinate, which in turn leads to a correction to the stress tensor. However, this correction is of order ζ, and therefore will not influence the matching[10]. The full wormhole geometry with the two regimes is schematically shown in Fig. 3.2.

An important fact to notice about the wormhole solution we find is that there are three independent parameters: the charge, the non-local coupling and the AdS length by which the solution is determined. As soon as these three parameters are fixed, there is a unique, static and spherically symmetric wormhole geometry that solves Einstein's equations. At radii below the cutoff the geometry is that of deformed $AdS_2 \times \mathcal{S}^2$. As ρ increases, the geometry smoothly interpolates to a near-extremal Reissner-Nordström black hole in AdS$_4$. This black hole is characterized by its charge r_e, while its mass is given by

$$M_{WH} = M_{\text{ext}} + \Delta M, \tag{3.3.28}$$

with

$$M_{\text{ext}} = \frac{\bar{r}}{G_N} + \frac{2\bar{r}^3}{G_N \ell^2}, \quad \text{and} \quad \Delta M = -\frac{\bar{r} \epsilon^2}{2 G_N} \mathcal{C}(\bar{r}) = -\frac{g^2 \lambda^2(h)}{2\pi^3 \bar{r}} \left(1 + 3 \frac{\bar{r}^2}{\ell^2} \right) \mathcal{C}(\bar{r}) , \tag{3.3.29}$$

where M_{ext} is the mass of an extremal black hole.

---

[10]The correction can be calculated by considering $\Delta x = \int_{-\infty}^{\infty} \frac{dy}{g_{yy}}$, with y the holographic coordinate, resulting in $\Delta x = \pi \left(1 + \zeta f(\bar{r}) \right)$, for some function f. Since we consider ζ to be small, the matching is consistent. If we had taken this correction into account the stress tensor would have been given by $\langle T_{\mu\nu}^h \rangle = \frac{1}{\Delta x} \frac{q \lambda(h)}{2\pi^2 R^2} \text{diag}\,(1, 1, 0, 0)$.
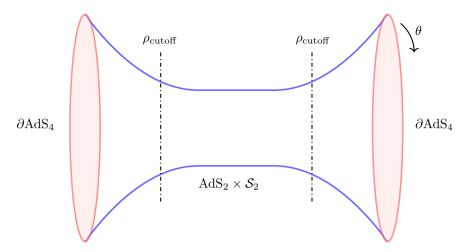
Figure 3.2: Wormhole geometry: In the throat region the metric has the AdS$_2$ $\times \mathcal{S}^2$ form (3.3.12) up to the cutoff located at $\rho \sim L/\bar{r}$. Around this point, where the limits (3.3.23) are satisfied, the geometry smoothly interpolates to near-extremal Reissner-Nordström black holes in AdS$_4$.

Since it is not very pleasant to have a factor of g in this formula, we use the definitions to rewrite this as

$$\Delta M = -\frac{G_N q^2 \lambda^2(h)}{2\pi^2 \bar{r}^3}\mathcal{C}\left(\bar{r}\right) \sim -\frac{q\lambda(h)\mathcal{C}\left(\bar{r}\right)}{\bar{r}}\zeta \ . \tag{3.3.30}$$

Therefore, the black hole is indeed near-extremal, with mass just below the extremal mass. Coming from infinity, as an observer approaches the wormhole mouth, the observer would experience getting closer and closer to a naked singularity. All of a sudden, the wormhole throat opens up and she traverses through the wormhole reaching the other side safely.

In the limit $\ell \gg r_e$, where the AdS radius is larger than the radii of the throats. The change in the mass due to the non-local coupling has the form

$$\Delta M = -\frac{G_N q^2 \lambda^2(h)}{2\pi^2 r_e^3} \ , \tag{3.3.31}$$

which has the same scaling as the binding energy, relative to the the energy of two disconnected extremal black holes, coming from the wormhole throat in the asymptotically flat case [3].

3.3.3   Non-linear solution

One might be concerned that the solution presented in the previous subsection only exists in the linearized analysis. We will proceed to find a similar solution to

the full Einstein's equations. The geometry ansatz we will consider is the following

$$ds^2 = \frac{\bar{r}^2}{\mathcal{C}(\bar{r})}\left(-f(\rho)dt^2 + \frac{d\rho^2}{f(\rho)}\right) + R^2(\rho)d\Omega_2^2 \,, \tag{3.3.32}$$

$\rho \in [0, \pm\infty)$, $t \in (-\infty, \infty)$ and we have assumed the extremal value for the radius in the overall factor. The non-zero components of the Einstein equations can be written as

$$tt: \quad \frac{3\bar{r}^2 f(\rho)}{\mathcal{C}(\bar{r})\ell^2} - \frac{\pi G_N q^2 \bar{r}^2 f(\rho)}{g^2 \mathcal{C}(\bar{r})R^4(\rho)} + \frac{4G_N q\lambda(h)}{\pi^2 R^2(\rho)} + \frac{\bar{r}^2 f(\rho)}{\mathcal{C}(\bar{r})R^2(\rho)}$$
$$- \frac{f(\rho)f'(\rho)R'(\rho)}{R(\rho)} - \frac{f^2(\rho)R'^2(\rho)}{R^2(\rho)} - \frac{2f^2(\rho)R''(\rho)}{R(\rho)} = 0 \,, \tag{3.3.33}$$

$$\rho\rho: \quad -\frac{3\bar{r}^2}{\mathcal{C}(\bar{r})\ell^2 f(\rho)} + \frac{\pi G_N q^2 \bar{r}^2}{g^2 \mathcal{C}(\bar{r})f(\rho)R^4(\rho)} + \frac{4G_N q\lambda(h)}{\pi^2 f^2(\rho)R^2(\rho)}$$
$$- \frac{\bar{r}^2}{\mathcal{C}(\bar{r})f(\rho)R^2(\rho)} + \frac{f'(\rho)R'(\rho)}{f(\rho)R(\rho)} + \frac{R'^2(\rho)}{R^2(\rho)} = 0 \,, \tag{3.3.34}$$

$$\theta\theta: \quad -\frac{\pi G_N q^2}{g^2 R^2(\rho)} - \frac{3R^2(\rho)}{\ell^2} + \frac{\mathcal{C}(\bar{r})R(\rho)f'(\rho)R'(\rho)}{\bar{r}^2}$$
$$+ \frac{\mathcal{C}(\bar{r})R^2(\rho)f''(\rho)}{2\bar{r}^2} + \frac{\mathcal{C}(\bar{r})f(\rho)R(\rho)R''(\rho)}{\bar{r}^2} = 0 \,, \tag{3.3.35}$$

$$\phi\phi: \quad \sin^2(\theta)\left(-\frac{\pi G_N q^2}{g^2 R^2(\rho)} - \frac{3R^2(\rho)}{\ell^2} + \frac{\mathcal{C}(\bar{r})R(\rho)f'(\rho)R'(\rho)}{\bar{r}^2}\right)$$
$$+ \sin^2(\theta)\left(\frac{\mathcal{C}(\bar{r})R^2(\rho)f''(\rho)}{2\bar{r}^2} + \frac{\mathcal{C}(\bar{r})f(\rho)R(\rho)R''(\rho)}{\bar{r}^2}\right) = 0 \,. \tag{3.3.36}$$

These differential equations depend on three independent physical parameters of the form

$$\frac{G_N q^2}{g^2 \ell^2}, \quad \frac{G_N q\lambda(h)}{\ell^2}, \quad \text{and} \quad \ell \,. \tag{3.3.37}$$

Since both functions f and R appear in the differential equations with two derivatives, there will be four integration constants. By requiring the solution to be symmetric around $\rho = 0$ we fix two of those. Requiring this $\mathbb{Z}_2$ symmetry is equivalent to setting $f'(0) = R'(0) = 0$. Furthermore we have the freedom to rescale the time coordinate. This allows us to pick $f(0) = 1$. Now the constraint equation (3.3.34) fixes $R(0)$ in terms of $f(0)$. By these choices all integration constants are then fixed. Also note that due to spherical symmetry whenever the $\theta\theta$ equation is solved, the $\phi\phi$ equation is automatically satisfied. With the integration constants as mentioned, we can now solve the tt and $\theta\theta$ equation numerically. The results of solving the non-linear Einstein equations are shown in Figures 3.3 and 3.4. In order to compare with the linearized results, we pick the integration constants so that the non-linear and linear solutions agree at $\rho = 0$. We should note however

that the non-linear solution makes sense for other parameter values and integration constants as well. We expect the linear and non-linear results to agree up to $|\rho| \sim \rho_{\text{cutoff}} = \frac{L}{r}$. As a final comment note that, as can be seen from Figure 3.3, for large ρ the numerical solution behaves as $R(\rho) \sim \left(\frac{L}{r}\right)^{-1} |\rho|$, which is precisely what we expect in light of equation (3.3.22) and by the fact that away from the wormhole we expect the $\mathcal{S}^2$ radius to be equal to r.

Figure 3.3: Solutions of $R(\rho)$ with parameters $\frac{G_N q^2}{g^2 \ell^2} = 0.01$, $\frac{G_N q \lambda(h)}{\ell^2} = 0.001$, and $\ell = 100$. The initial condition is $R(0) = 17$. For these parameters we expect agreement up to $\rho_{\text{cutoff}} = 7.2$. We see that for larger ρ the linear solution starts to deviate.

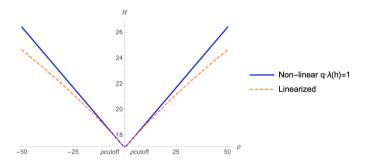**Figure 3.4:** Solutions of $f(\rho)$ with parameters $\frac{G_N q^2}{g^2 \ell^2} = 0.01$, $\frac{G_N q \lambda(h)}{\ell^2} = 0.001$, and $\ell = 100$. The initial condition is $R(0) = 17$. For these parameters we expect agreement up to $\rho_{\text{cutoff}} = 7.2$. We see that for larger $\r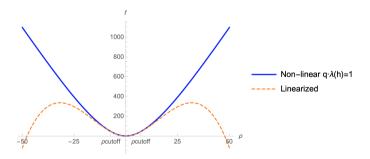ho$ the linear solution starts to deviate, and even becomes negative. Of course, in this region the RN AdS black hole dominates.

3.4   Thermodynamics

This section contains a calculation of the on-shell Hamiltonian of the wormhole solution. We propose a Hamiltonian and show that the wormhole solution is the ground state for a region of parameter space. Furthermore we give a qualitative discussion of the thermodynamic stability of the wormhole solution in the (grand) canonical ensemble.

3.4.1   Hamiltonian ground state

We expect the wormhole geometry presented in the previous section to be dual to the asymptotic field theories in some particular entangled state. In particular, it should be dual to the ground state of a certain local Hamiltonian whose ground state is approximately the thermofield double state with chemical potential [112, 116].

From the gravity point of view, given the set of boundary conditions, Einstein's equations fill in the bulk geometry smoothly. We will consider three solutions with the same boundary conditions at zero temperature: the wormhole, two disconnected black holes and empty AdS. Depending on the values of $\lambda(h)$ and μ, there is a dominant saddle. For concreteness we will focus on the symmetric case where the total magnetic charge is $Q := Q_R = -Q_L$ and the mass is $M := M_R = M_L$. Of course, less symmetric cases can also be considered but we believe they will not dramatically modify the presented results.

In a general covariant theory, the on-shell Hamiltonian can be computed as a boundary integral as follows

$$H[\zeta] = \int_{\partial\Sigma} d^2x \sqrt{\sigma} u^\alpha \zeta^\beta T_{\alpha\beta} \ , \quad T_{\alpha\beta} := \frac{2}{\sqrt{-\gamma}} \frac{\delta S}{\delta \gamma^{\alpha\beta}} \ , \tag{3.4.1}$$

where $T_{\alpha\beta}$ is the Brown-York stress tensor[11], u^α is the unit normal to a constant time hypersurface, ζ^β is the flow vector and $\sqrt{\sigma}$ is the volume element of the boundary at fixed time. The energy of a gravitational solution is associated to time-translation symmetry, *i.e.,* , to the Killing vector $\zeta = \partial_\tau$.

The wormhole solution presented in the last section is a solution to the action with interacting term

$$S_{\text{int}} = ih \int d^3x \sqrt{-\gamma} \left(\bar{\Psi}_-^R \Psi_+^L + \bar{\Psi}_+^L \Psi_-^R \right) \ . \tag{3.4.2}$$

---

[11]In order to avoid IR divergences in AdS, we need to include counterterms in the purely gravitational part of the action (3.2.1). In d=3, they result in a modified stress tensor $T_{\alpha\beta} = K_{\alpha\beta} - K\gamma_{\alpha\beta} - \frac{2}{\ell}\gamma_{\alpha\beta} - \ell G_{\alpha\beta}$, where $G_{\alpha\beta}$ is the Einstein tensor computed on the boundary induced metric $\gamma_{\alpha\beta}$ [123].

The interacting part of the boundary stress tensor then has the form

$$T_{\alpha\beta} := \frac{2}{\sqrt{-\gamma}} \frac{\delta S_{\text{int}}}{\delta \gamma^{\alpha\beta}} = ih\gamma_{\alpha\beta} \left(\bar{\Psi}^R_- \Psi^L_+ + \bar{\Psi}^L_+ \Psi^R_- \right) \ . \qquad (3.4.3)$$

The metric close to the AdS$_4$ boundary at $r \to \infty$ and the time-like unit vector are of the form

$$ds^2 = -f(r)d\tau^2 + \frac{dr^2}{f(r)} + r^2 d\Omega_2^2 \quad \text{and} \quad u = \sqrt{f} d\tau \ . \qquad (3.4.4)$$

The $\mathbb{Z}_2$ symmetry along the radial direction allows us to define a notion of gravitational energy by applying the formula (3.4.1) at the asymptotic AdS boundaries

$$H_{\text{int}} := H[\zeta^\tau] = -ihr^2 \sqrt{f} \int d^2\Omega \left(\bar{\Psi}^R_- \Psi^L_+ + \bar{\Psi}^L_+ \Psi^R_- \right) \ . \qquad (3.4.5)$$

At this point we need to evaluate the bulk spinors close to the asymptotic boundary. We can achieve this by evaluating the scaling factor close to the boundary[12]

$$\bar{\Psi}^R_- \Psi^L_+ = \frac{e^{-\sigma}}{R^2} \left[(\psi^R \otimes \eta)^\dagger \mathcal{P}_- \gamma^1 \mathcal{P}_+ \left(\psi^L \otimes \eta \right) \right] \qquad (3.4.6)$$

$$= \frac{\mathcal{C}(\bar{r})}{Lr^2\sqrt{f}} \left[(\psi^R \otimes \eta)^\dagger \mathcal{P}_- \gamma^1 \mathcal{P}_+ \left(\psi^L \otimes \eta \right) \right] \ ,$$

and a similar expression for $\bar{\Psi}^L_+ \Psi^R_-$. We then find

$$H_{\text{int}} = -ih\mathcal{C}(\bar{r})\frac{\epsilon}{\bar{r}} \int d^2\Omega \left[(\psi^R \otimes \eta)^\dagger \mathcal{P}_- \gamma^1 \mathcal{P}_+ \left(\psi^L \otimes \eta \right) + (\psi^L \otimes \eta)^\dagger \mathcal{P}_+ \gamma^1 \mathcal{P}_- \left(\psi^R \otimes \eta \right) \right] \ . \qquad (3.4.7)$$

We can compute the semi-classical interacting Hamiltonian in the state defined in (3.2.36) by computing the following expectation value

$$\langle H_{\text{int}} \rangle = -ih\mathcal{C}(\bar{r})\frac{\epsilon}{\bar{r}} \int d^2\Omega \left[\langle (\psi^R \otimes \eta)^\dagger \mathcal{P}_- \gamma^1 \mathcal{P}_+ \left(\psi^L \otimes \eta \right) \rangle + \langle (\psi^L \otimes \eta)^\dagger \mathcal{P}_+ \gamma^1 \mathcal{P}_- \left(\psi^R \otimes \eta \right) \rangle \right] \ . \qquad (3.4.8)$$

We can evaluate the boundary integral by taking first the angular spinors on-shell. The correlators involved in (3.4.8) can be computed perturbatively in the limit where $\lambda(h) \sim h$. They are explicitly given in Appendix D. Finally, we obtain the result[13]

$$\langle H_{\text{int}} \rangle = \mathcal{C}(\bar{r})\frac{\epsilon}{\bar{r}} \frac{2qh}{\pi} \left(-1 + \frac{4h}{\pi} \right) = 4\Delta M + \mathcal{O}\left(h^3 \right) \ , \qquad (3.4.9)$$

---

[12]In the RN background (3.4.4), far away from the horizon the metric is conformaly flat. The relation between the coordinates is $t = \frac{\tau}{L}\mathcal{C}(\bar{r})$, and $x = \int dr \frac{1}{L} \frac{1}{f(r)}\mathcal{C}(\bar{r})$, and the conformal factor equals $e^{2\sigma} = \left(\frac{L}{\mathcal{C}(\bar{r})} \right)^2 f$.

[13]Note that in the second equal sign we only take into account the terms up to order h^2, even though the expression in the middle contains a third order term. This is done to compare to the results of the previous section, which included terms up to second order.

with ΔM given by (3.3.29). In order to get the total wormhole energy, we need to add the energy asssociated to the non-interacting parts, *i.e.,* , of two near-extremal RN black holes

$$\langle H \rangle_{WH} = 2M_{WH} + 4\Delta M - 2\mu Q = 2M_{ext} + 6\Delta M - 2\mu Q \; , \tag{3.4.10}$$

where M_{ext} is the black hole extremal mass and Q the extremal charge. In this equation, we have taken into account the change in energy due to the chemical potential μ for the asymptotic charges. This is similar to the electric case [124].

Now that we understand the energy of the wormhole geometry, we would like to investigate whether it is the ground state of some Hamiltonian. We propose the following *local boundary Hamiltonian*

$$H = H_L + H_R - \frac{ih}{\ell} \int d\Omega_2 \left(\bar{\boldsymbol{\Psi}}_-^R \boldsymbol{\Psi}_+^L + \bar{\boldsymbol{\Psi}}_+^L \boldsymbol{\Psi}_-^R \right) + \mu(Q_L - Q_R) \; , \tag{3.4.11}$$

where H_L and H_R are the Hamiltonians associated to the boundary dual of the two identical original systems, and again we take into account the change in energy due to the chemical potential μ for the asymptotic charges. It is important to notice that equation (3.4.11) is an expression written purely in terms of boundary data. In particular, we have defined the boundary spinors, denoted as $\boldsymbol{\Psi}$, by removing the scaling factor defined in (3.2.19), so that

$$\Psi_{\pm} = R^{-\frac{3}{2}} \boldsymbol{\Psi}_{\pm} \; . \tag{3.4.12}$$

Note that the interacting term is inspired by (3.4.2), which in terms of the boundary data can be written as

$$S_{int} = \frac{ih}{\ell} \int d\tau d\Omega_2 \left(\bar{\boldsymbol{\Psi}}_-^R \boldsymbol{\Psi}_+^L + \bar{\boldsymbol{\Psi}}_+^L \boldsymbol{\Psi}_-^R \right). \tag{3.4.13}$$

The Hamiltonian determines the time-evolution with respect to the asymptotic time defined in (3.4.4). Note that the total charge of the field theories is conserved as a consequence of a global symmetry.

Next, we consider the expectation value of the Hamiltonian for the different phases. First of all note that the expectation value of (3.4.11) is precisely equal to (3.4.10) for the wormhole solution, since that is the primary reason for the definition of (3.4.11). Secondly, note that the empty AdS geometry has a vanishing Hamiltonian. Finally, we note that for the disconnected black holes, the interaction term of the Hamiltonian does not contribute to the energy. This can be seen from the fact that we can Wick rotate the RN black hole solution, after which the geometry is conformal to the disk. However, the conformal factor vanishes if the black hole

is extremal. Since the correlators on the disk must be finite, the total contribution of the interacting part of the Hamiltonian must indeed be equal to zero.

The difference between the wormhole and the extremal black holes phases is given by

$$\langle H \rangle_{2\text{BH}} - \langle H \rangle_{\text{WH}} > 0 \ . \tag{3.4.14}$$

It is easy to see that $\langle H \rangle_{2\text{BH}}$ has a minimum at the point

$$\bar{r} = \frac{\ell}{\sqrt{3\pi}} \sqrt{\frac{\mu^2}{m_p^2} - \pi} \ , \quad \text{for} \quad \frac{\mu^2}{m_p^2} > \pi \ , \tag{3.4.15}$$

for which $\langle H \rangle_{2\text{BH}} < \langle H \rangle_{\text{Vacuum}} = 0$ (see Figure 3.5). Then, *the wormhole phase (where it exists) dominates the ground state for values of the chemical potential* $\mu > \mu_c$. The complete phase diagram is shown in Figure 3.6. We see that the point $(h = 0, \mu = \mu_c)$ is actually a *triple point* where the three different phases meet. Intuitively, empty AdS is the dominant saddle for very small values of h, for which the wormhole has not been formed yet, and μ so that the charge contribution is negligible. For $h < 0$ and $\mu > \mu_c$, the black holes phase is the dominant saddle. Alternatively, for positive values of the coupling and $\mu > \mu_c$, the wormhole phase will be the ground state of (3.4.11).
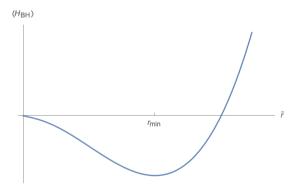
Figure 3.5: Expectation value of the Hamiltonian (3.4.11) in the two-disconnected black holes phase for different values of $\bar{r}$. The minimum is located at $r_{\min}$, which is given in (3.4.15).

3.4.2 Stability

We briefly discuss possible instabilities of the solution. When considering scalar fields in a Reissner-Nördstrom AdS background there are instabilities that lead to hairy black holes. These instabilities can be understood, for near-extremal
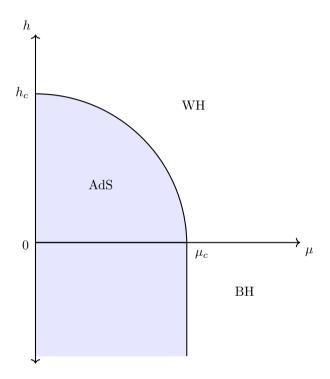
Figure 3.6: Diagram that shows the ground state of the Hamiltonian (3.4.11) for different values of h and μ. Empty AdS is the dominant contribution at the origin up to the critical values $h_c = \frac{\bar{r}^2}{G_N q} \sqrt{\frac{2\pi}{3C}} \left(1 + \frac{2\bar{r}^2}{\ell^2}\right)$ and $\mu_c = m_p \sqrt{\pi}$ where the wormhole phase becomes the ground state. The point $(h = 0, \mu = \mu_c)$ is a triple point where the three phases meet. For negative values of h, there is a competition between the empty AdS and the black holes phases. Note that depending on the mass of the monopoles in the theory there could be a region in the diagram where the ground state is AdS with monopoles.

black holes, as originating from the difference between the Breitenlöhner Freedman bounds for AdS$_2$ and AdS$_4$; fields that are allowed tachyons in the asymptotic AdS$_4$ spacetime lead to instabilities in the AdS$_2$ near-horizon region. Even though intuitively similar arguments would lead to fermionic instabilities, no evidence for the existence of fermionic hairy black holes has been found [125]. Since the argument crucially depends on the fact that there is an asymptotic AdS$_2$ geometry, we expect the same result to hold for the wormhole phase.

Besides investigating whether the wormhole solution is the ground state of the Hamiltonian (3.4.11), one could also wonder whether it is the thermodynamically favored phase in one of the standard thermodynamic ensembles. We must couple the two CFT's in order for a wormhole solution to exist; if signals can cross from one boundary to the other in the bulk, it must be possible to transfer information between the CFT's [108].

Before coupling the CFT's, each CFT has a global $U(1)$ symmetry with an associated charge conservation. After coupling the theories, charge can flow from one to the other, so only a single $U(1)$ survives. In our conventions, the conserved charge us $Q_L + Q_R$. In our conventions, the wormhole solution has $Q_L = -Q_R$. One can picture magnetic field lines threading the wormhole, so this convention is natural. Therefore, the conserved charge for the wormhole is $Q_L + Q_R = 0$. In the standard construction of thermodynamic ensembles, one can only turn on a chemical potential for this conserved charge. The term $\mu(Q_L - Q_R)$ appearing in our Hamiltonian looks like a chemical potential, but it is not really, because $Q_L - Q_R$ is not conserved: it does not commute with the interaction term in the Hamiltonian.

One can ask whether the wormhole dominates one of the standard thermodynamic ensembles at zero temperature; for example, consider the canonical ensemble. The different phases that should be compared are the following: empty AdS, two black holes, the wormhole solution.

The free energy is

$$F = E - TS \ , \tag{3.4.16}$$

in the canonical ensemble. At zero temperature, the wormhole phase will have free energy equal to $F = 2M_{WH}$, while empty AdS has a vanishing free energy. Therefore, empty AdS dominates the ensemble.

Finally, one could consider other ensembles in the hope of finding an ensemble in which the wormhole solution dominates. One candidate is the grand canonical ensemble, with potential given by

$$\Phi = E - TS - \mu Q. \tag{3.4.17}$$

However, the wormhole phase has a conserved charge $Q = Q_L + Q_R = 0$. Therefore, adding a term proportional to Q will not change the potential of the wormhole phase. Because of this it can never dominate the ensemble. The only thing that we have achieved by changing ensembles is that there can be even more phases with a lower potential than the wormhole. Note that it is not very clear how to interpret magnetic charges (and how to fix them) in the different ensembles. The electromagnetic duality suggests they should be treated in the same way as electric charges, but in the standard AdS/CFT context black holes with different electric charges are different states in the same theory, while black holes with different magnetic charges live in different theories. Presumably one can make a choice when imposing boundary conditions for the gauge field analogous to the standard vs alternate quantization for other light fields, and this choice determines whether electric or magnetic states live in the same theory. It would be interesting to understand this better, since our setup depends on the magnetic charges, but this subtlety is mostly orthogonal to our work here.

To summarize: the wormhole appears to be a stable solution that corresponds to the ground state of our Hamiltonian. However, it does not seem to arise as the dominant phase of one of the standard thermodynamic ensembles with chemical potential.

3.5   Discussion

We have found an eternal traversable wormhole in a four-dimensional AdS background. This geometry is a solution to the Einstein-Hilbert gravity action with negative cosmological constant, a $U(1)$ gauge field and massless fermions charged under the gauge field. To open up the wormhole we need negative energy, which we acquire by coupling the CFT's living on the two boundaries of the spacetime.

By calculating the backreaction of the negative energy on the geometry, we find a static traversable wormhole geometry with no horizons or singularities. This wormhole is dual to the ground state of a simple Hamiltonian for two coupled holographic CFT's. The parameters in the Hamiltonian are the chemical potential, the coupling strength, and the central charge. The wormhole dominates in some region of parameter space, while disconnected geometries dominate other regions.

Working in the semi-classical approximation, the authors of [108] proved that there are no traversable wormholes that preserve Poincaré invariance along the boundary field theory directions in more than two spacetime dimensions. The geometry found in this work evades this result because our solution is not Poincaré invariant.

There are a number of interesting future directions.

Traversable Wormholes in the lab; energy gap. One possible application of our results is to build traversable wormholes in the lab by implementing our interacting Hamiltonian and allowing the system to cool to the ground state. For this process to be efficient, it is important the energy gap between the ground state and the first excited state is not too small.

It would be interesting to carefully calculate the gap in this system. A rough estimate can be obtained by calculating the maximum redshift. Black holes have infinite redshift near the horizon and therefore support excitations with arbitrarily small energy in the semi-classical limit.

Looking back at our 'matching' section, we see that the black hole geometry is valid down to

$$r - \bar{r} \sim \epsilon L \sim \bar{r} \ . \tag{3.5.1}$$

At this location, the redshift is $f(r) \sim \mathcal{C}(\bar{r})$. Inside this matching radius, the geometry is $\mathrm{AdS}_2 \times S_2$. The relative redshift between the middle of the wormhole and the matching surface is

$$\frac{f_{\mathrm{match}}}{f_0} \sim \rho_{\mathrm{match}}^2 \sim \frac{1}{\epsilon^2} \ . \tag{3.5.2}$$

Combining these results, and restoring units using the AdS radius, our guess is

$$\mathrm{Gap} \sim \frac{\mathcal{C}(\bar{r})\epsilon^2}{\ell} \ . \tag{3.5.3}$$

This result looks concerningly small due to the ϵ^2; however, $\mathcal{C}(r) = 1 + 6\bar{r}^2/\ell^2$ is large for large black holes. We leave a fuller discussion and more reliable calculation for the future.

RG flow. Our bulk analysis is made convenient by the Weyl invariance of the massless fermions, which correspond to boundary operators of particular dimensions. If we think of the interaction term as an interaction in a single CFT, this term appears to be exactly marginal. It would be interesting to understand whether higher order corrections change the scaling dimension of this interaction, or more generally to understand the RG flow of our system.

Supersymmetry. Related to the RG flow, it would add a degree of theoretical control to realize the initial extremal black hole as a BPS state in a supersymmetric theory. Accomplishing this requires embedding our simple $U(1)$ theory in a theory with more conserved charges [126–129].

CFT state. In the related construction of Cottrell et al [116], the state of the dual CFT was identified with the thermofield double state, while the bulk geometry was not under semiclassical control. In this paper, we have constructed a controlled traversable wormhole, but have not calculated the quantum state of the CFT in boundary variables. One may expect that it is a thermofield double type state, but note that the wormhole is a zero temperature solution, so it cannot be exactly the TFD. On the other hand, the bulk geometry clearly looks like a slightly superextremal Reissner Nordstrom black hole away from the wormhole mouth, giving a clear hint regarding the CFT state.

Multi-mouth wormholes. In the present work, we focused on asymptotically AdS$_4$ two-mouth traversable wormhole geometries. It might be interesting to extend our results and explore in the future the possibility of fourth dimensional multi-mouth wormholes similar to those studied in [110, 111]. In particular, the results of this paper might be used to understand explicitly the role played by multiparty entanglement in the wormhole's traversability.

Information transfer. Moreover, it would be interesting to investigate the amount of information that can be sent through this type of wormhole, in a similar fashion as in [50, 55, 70].

Replica wormholes. Finally, it has been found that two dimensional eternal traversable wormhole geometries contribute to the fine-grained entropy in the context of islands in de Sitter spacetime [130] (see also [10, 131]). It would be interesting to understand whether more general set-ups in higher dimensions can be described with similar methods to those employed in this paper.

Appendices

A Propagators

In this appendix we present the results for the propagators. Below, we show the derivation of (3.2.37)

$$
\begin{aligned}
\langle \psi_+^\dagger(x_-)\psi_+(x'_-) \rangle &= \left\langle \sum_{k,j\in\mathbb{Z}} \frac{1}{\pi} \alpha_k^\dagger \alpha_j e^{i\omega_j x'_- - i\omega_k x_-} \right\rangle \\
&= \left\langle \sum_{k,j\in\mathbb{Z}_{\geq 0}} \frac{1}{\pi} \alpha_k^\dagger \alpha_j e^{i\omega_j x'_- - i\omega_k x_-} \right\rangle \\
&= \left\langle \sum_{k,j\in\mathbb{Z}_{\geq 0}} \frac{1}{\pi} (\delta_{k,j} - \alpha_j \alpha_k^\dagger) e^{i\omega_j x'_- - i\omega_k x_-} \right\rangle \\
&= \sum_{j\in\mathbb{Z}_{\geq 0}} \frac{1}{\pi} e^{i\omega_j(x'_- - x_-)} \\
&= \sum_{j\in\mathbb{Z}_{\geq 0}} \frac{1}{\pi} e^{i\left(\frac{2j+1}{2}\right)(x'_- - x_-)} \left(1 + (-1)^j \frac{2i\lambda(h)}{\pi}(x'_- - x_-) \right) + \mathcal{O}\left((x'_- - x_-)^2\right) \\
&= \frac{1}{\pi} \frac{e^{\frac{i}{2}(x'_- - x_-)}}{1 - e^{i(x'_- - x_-)}} + \frac{e^{\frac{i}{2}(x'_- - x_-)}}{1 + e^{i(x'_- - x_-)}} \frac{2i\lambda(h)}{\pi^2}(x'_- - x_-) + \mathcal{O}\left((x'_- - x_-)^2\right) \;.
\end{aligned}
$$
$$\text{(A.1)}$$

The rest of the propagators can be derived in a similar fashion. We present the results

$$
\langle \psi_-^\dagger(x_+)\psi_-(x'_+) \rangle = \frac{1}{\pi} \frac{e^{\frac{i}{2}(x'_+ - x_+)}}{1 - e^{i(x'_+ - x_+)}} + \frac{e^{\frac{i}{2}(x'_+ - x_+)}}{1 + e^{i(x'_+ - x_+)}} \frac{2i\lambda(h)}{\pi^2}(x'_+ - x_+) + \mathcal{O}\left((x'_- - x_-)^2\right) \;,
$$
$$\text{(A.2)}$$

$$
\langle \psi_+^\dagger(x_-)\psi_-(x'_+) \rangle = -\frac{1}{\pi} \frac{e^{\frac{i}{2}(x'_+ - x_-)}}{1 + e^{i(x'_+ - x_-)}} - \frac{e^{\frac{i}{2}(x'_+ - x_-)}}{1 - e^{i(x'_+ - x_-)}} \frac{2i\lambda(h)}{\pi^2}(x'_+ - x_-) + \mathcal{O}\left((x'_- - x_-)^2\right) \;,
$$
$$\text{(A.3)}$$

and

$$
\langle \psi_-(x_+)\psi_+(x'_-) \rangle = \langle \psi_-(x_+)\psi_-(x'_+) \rangle = \langle \psi_+(x_-)\psi_+(x'_-) \rangle = 0 \;. \qquad \text{(A.4)}
$$

B Stress tensor

In this appendix we show the calculation of the stress tensor. First of all note that we can average over the angular directions by taking the spherical components

on-shell in equation (3.2.38). Since the spherical components are normalized such that $\int d^2\Omega \; \bar{\eta}^m \eta^n = \delta_{m,n}$, averaging over the angular directions results in a factor of $\frac{1}{4\pi}$. Using this and point-splitting, the first line of (3.2.38) becomes

$$
\begin{aligned}
\langle T_{11} \rangle &= \lim_{\substack{t' \to t \\ x' \to x}} \frac{1}{4\pi} \sum_{m,n} \int d^2\Omega \frac{i}{2R^2} \left(\partial_t' - \partial_t \right) \left(\langle \psi_+^{m\dagger}(x_-) \psi_+^n(x_-') \rangle + \langle \psi_-^{m\dagger}(x_+) \psi_-^n(x_+') \rangle \right) \eta^{m\dagger} \eta^n \\
&= \lim_{\substack{t' \to t \\ x' \to x}} \frac{qi}{8\pi R^2} \left(\partial_t' - \partial_t \right) \left(\langle \psi_+^{\dagger}(x_-) \psi_+(x_-') \rangle + \langle \psi_-^{\dagger}(x_+) \psi_-(x_+') \rangle \right) .
\end{aligned}
\tag{B.1}
$$

The renormalized $\langle T_{11} \rangle$ is found by subtracting the $h = 0$ contribution from the $h \neq 0$ expression as follows

$$
\begin{aligned}
\langle T_{11} \rangle &= \langle T_{11}^{h \neq 0} \rangle - \langle T_{11}^{h=0} \rangle \\
&= \lim_{\substack{t' \to t \\ x' \to x}} \frac{qi}{8\pi R^2} \left(\partial_t' - \partial_t \right) \left(\frac{e^{\frac{i}{2}(x_-' - x_-)}}{1 + e^{i(x_-' - x_-)}} \frac{2i\lambda(h)}{\pi^2} (x_-' - x_-) + \frac{e^{\frac{i}{2}(x_+' - x_+)}}{1 + e^{i(x_+' - x_+)}} \frac{2i\lambda(h)}{\pi^2}(x_+' - x_+) \right) \\
&= \lim_{\substack{t' \to t \\ x' \to x}} \frac{qi}{8\pi R^2} \left(\frac{4i\lambda(h)}{\pi^2} + \frac{3i\lambda(h)}{2\pi^2} \left((t' - t)^2 + (x' - x)^2 \right) \right) \\
&= -\frac{q\lambda(h)}{2\pi^3 R^2} ,
\end{aligned}
\tag{B.2}
$$

where we have omitted combined factors of $(t' - t)$ and $(x' - x)$ to higher orders. Similarly, we find that the rest of the renormalized components of the stress tensor are given by

$$
\langle T_{22} \rangle = -\frac{q\lambda(h)}{2\pi^3 R^2}, \quad \text{and} \quad \langle T_{33} \rangle = \langle T_{44} \rangle = 0 .
\tag{B.3}
$$

It is easy to see that this contribution to the stress tensor is traceless

$$
\langle T_\mu{}^\mu \rangle = g^{\mu\nu} \langle T_{\mu\nu} \rangle = e^{-2\sigma} \left(\frac{q\lambda(h)}{2\pi^3 R^2} - \frac{q\lambda(h)}{2\pi^3 R^2} \right) = 0 .
\tag{B.4}
$$

We can also check that the stress tensor is conserved. We will need the following components of $\nabla_\mu \langle T_{\rho\nu} \rangle$

$$\nabla_x \langle T_{xx} \rangle = \partial_x \langle T_{xx} \rangle - \Gamma^\rho_{xx} \langle T_{\rho x} \rangle - \Gamma^\rho_{xx} \langle T_{x\rho} \rangle$$
$$= \frac{q\lambda(h)R'}{\pi^3 R^3} + \frac{q\lambda(h)\sigma'}{\pi^3 R^2},$$
$$\nabla_t \langle T_{tx} \rangle = \partial_t \langle T_{tx} \rangle - \Gamma^\rho_{tt} \langle T_{\rho x} \rangle - \Gamma^\rho_{tx} \langle T_{x\rho} \rangle$$
$$= \frac{q\lambda(h)\sigma'}{\pi^3 R^2},$$
$$\nabla_\theta \langle T_{\theta x} \rangle = \partial_\theta \langle T_{\theta x} \rangle - \Gamma^\rho_{\theta\theta} \langle T_{\rho x} \rangle - \Gamma^\rho_{\theta x} \langle T_{x\rho} \rangle$$
$$= -\frac{q\lambda(h)R'e^{-2\sigma}}{2\pi^3 R},$$
$$\nabla_\phi \langle T_{\phi x} \rangle = \partial_\phi \langle T_{\phi x} \rangle - \Gamma^\rho_{\phi\phi} \langle T_{\rho x} \rangle - \Gamma^\rho_{\phi x} \langle T_{x\rho} \rangle$$
$$= -\frac{q\lambda(h)R'e^{-2\sigma}\sin^2(\theta)}{2\pi^3 R},$$

so that

$$\nabla_\mu \langle T^\mu_{\ \nu} \rangle = g^{\mu\rho} \nabla_\mu \langle T_{\rho\nu} \rangle$$
$$= g^{xx} \nabla_x \langle T_{xx} \rangle + g^{tt} \nabla_t \langle T_{tx} \rangle + g^{\theta\theta} \nabla_\theta \langle T_{\theta x} \rangle + g^{\phi\phi} \nabla_\phi \langle T_{\phi x} \rangle$$
$$= e^{-2\sigma} \left(\frac{q\lambda(h)R'}{\pi^3 R^3} + \frac{q\lambda(h)h\sigma'}{\pi^3 R^2} \right) \tag{B.5}$$
$$- e^{-2\sigma} \frac{q\lambda(h)\sigma'}{\pi^3 R^2} - \frac{1}{R^2} \frac{q\lambda(h)R'e^{-2\sigma}}{2\pi^3 R} - \frac{1}{R^2 \sin^2(\theta)} \frac{q\lambda(h)R'e^{-2\sigma}\sin^2(\theta)}{2\pi^3 R}$$
$$= 0. \tag{B.6}$$

As a final check one can show that the t, x component of the stress tensor is indeed equal to zero. First note that T_{12} is equal to

$$T_{12} = \frac{i}{2R^2} \left(\psi_+^\dagger \partial_- \psi_+ - \psi_-^\dagger \partial_+ \psi_- - \partial_- \psi_+^\dagger \psi_+ + \partial_+ \psi_-^\dagger \psi_- \right) \otimes \eta^\dagger \eta. \tag{B.7}$$

Using point-splitting this becomes

$$\langle T_{12} \rangle = \lim_{\substack{t'\to t \\ x'\to x}} \frac{1}{4\pi} \sum_{m,n} \int d^2\Omega \frac{i}{2R^2} \Big(\partial'_- \langle \psi_+^{m\dagger}(x_-)\psi_+^n(x'_-) \rangle - \partial_- \langle \psi_+^{m\dagger}(x_-)\psi_+^n(x'_-) \rangle$$
$$- \partial'_+ \langle \psi_-^{m\dagger}(x_+)\psi_-^n(x'_+) \rangle - \partial_+ \langle \psi_-^{m\dagger}(x_+)\psi_-^n(x'_+) \rangle \Big) \eta^{m\dagger}\eta^n$$
$$= \lim_{\substack{t'\to t \\ x'\to x}} \frac{qi}{8\pi R^2} \Big(\partial'_- \langle \psi_+^\dagger(x_-)\psi_+(x'_-) \rangle - \partial_- \langle \psi_+^\dagger(x_-)\psi_+(x'_-) \rangle$$
$$- \partial'_+ \langle \psi_-^\dagger(x_+)\psi_-(x'_+) \rangle - \partial_+ \langle \psi_-^\dagger(x_+)\psi_-(x'_+) \rangle \Big), \tag{B.8}$$

and we see that

$$
\begin{aligned}
\langle T_{12} \rangle =& \langle T_{12}^{h \neq 0} \rangle - \langle T_{12}^{h=0} \rangle \\
=& \lim_{\substack{t' \to t \\ x' \to x}} \frac{qi}{8\pi R^2} \Bigg(\partial'_- \frac{e^{\frac{i}{2}(x'_- - x_-)}}{1 + e^{i(x'_- - x_-)}} \frac{2\lambda(h)i}{\pi^2} (x'_- - x_-) - \partial_- \frac{e^{\frac{i}{2}(x'_- - x_-)}}{1 + e^{i(x'_- - x_-)}} \frac{2\lambda(h)i}{\pi^2} (x'_- - x_-) \\
& - \partial'_+ \frac{e^{\frac{i}{2}(x'_+ - x_+)}}{1 + e^{i(x'_+ - x_+)}} \frac{2\lambda(h)i}{\pi^2} (x'_+ - x_+) - \partial_+ \frac{e^{\frac{i}{2}(x'_+ - x_+)}}{1 + e^{i(x'_+ - x_+)}} \frac{2\lambda(h)i}{\pi^2} (x'_+ - x_+) \Bigg) \\
& + \mathcal{O}\left((x'_- - x_-)^2\right) + \mathcal{O}\left((x'_+ - x_+)^2\right) \\
=& 0 \,.
\end{aligned}
\tag{B.9}
$$

C Matching

Let us turn to the time component of the metrics. At large ρ we can expand $\gamma(\rho)$ in the following way

$$
\gamma(\rho) = \frac{\zeta}{\mathcal{C}(\bar{r})} \left(1 + 4\frac{\bar{r}^2}{\ell^2} \right) \left(-\frac{\pi}{2}\rho^3 - \frac{3\pi}{2}\rho + 2\log(\rho) \right) + \cdots \,.
\tag{C.1}
$$

In order to match the cubic term in ρ to the $\left(\frac{r-\bar{r}}{\bar{r}}\right)^3$ term in (3.3.21) we will consider the following limit. We consider ρ to be large, but $\zeta\rho$ small and fixed. In this limit ψ is still given by (3.3.25). Furthermore, from (3.3.27) we see that we should consider ϵ to be of order ζ. This limit corresponds to expanding f at small $\frac{r-\bar{r}}{\bar{r}}$, but even smaller $\zeta \propto \epsilon$. More precisely, compared to (3.3.21) we still expand in $\frac{r-\bar{r}}{\bar{r}}$ up to third order. However, we only consider ϵ up to zeroth order

$$
f(r) = \mathcal{C}(\bar{r}) \left(\frac{r - \bar{r}}{\bar{r}} \right)^2 - 2 \left(1 + 4\frac{\bar{r}^2}{\ell^2} \right) \left(\frac{r - \bar{r}}{\bar{r}} \right)^3 + \mathcal{O}\left(\left(\frac{r - \bar{r}}{\bar{r}} \right)^4 \right) \,.
\tag{C.2}
$$

We should now match the expansion (C.2) to the following expression, where we will assume to be in the limit discussed above

$$
\begin{aligned}
\frac{\bar{r}^2}{\mathcal{C}(\bar{r})} (1 + \rho^2 + \gamma(\rho)) \frac{dt^2}{d\tau^2} &= \mathcal{C}(\bar{r}) \left(\rho^2 - \frac{\pi}{2}\rho^3 \frac{\zeta}{\mathcal{C}(\bar{r})} \left(1 + 4\frac{\bar{r}^2}{\ell^2} \right) \right) \frac{1}{\rho^2} \left(\frac{r - \bar{r}}{\bar{r}} \right)^2 \\
&= \mathcal{C}(\bar{r}) \left(\frac{r - \bar{r}}{\bar{r}} \right)^2 - \frac{\pi}{2}\rho \left(\frac{r - \bar{r}}{\bar{r}} \right)^2 \zeta \left(1 + 4\frac{\bar{r}^2}{\ell^2} \right) \\
&= \mathcal{C}(\bar{r}) \left(\frac{r - \bar{r}}{\bar{r}} \right)^2 - 2 \left(1 + 4\frac{\bar{r}^2}{\ell^2} \right) \left(\frac{r - \bar{r}}{\bar{r}} \right)^3 ,
\end{aligned}
\tag{C.3}
$$

where in the third line we used (3.3.25). We see that we recover (C.2) up to third order.

D   Correlators in $\langle H_{\text{int}}\rangle$

In this appendix, we show explicitly the equal-time correlators involved in the computation of the semi-classical interacting Hamiltonian in terms of the $2D$ propagators presented in Appendix A. Note that in Appendix A, the propagators are expanded in $x - x'$, while here we need the location of the fields to approach opposing boundaries. However, the expressions obtained are still valid if we take h small, and expand in h instead. The equal-time correletors present in the Hamiltonian are given by[14]

$$
\begin{aligned}
\langle H_{\text{int}}\rangle \supset{}& -ih\mathcal{C}(\bar{r})\frac{\epsilon}{\bar{r}}\int d^2\Omega\langle\bar{\Psi}^R_-\Psi^L_+\rangle \\
={}& -\frac{ih\epsilon}{2\bar{r}}\mathcal{C}(\bar{r})\int d^2\Omega\left(\langle-\psi^{R\dagger}_+\psi^L_+\rangle + i\langle\psi^{R\dagger}_+\psi^L_-\rangle + i\langle\psi^{R\dagger}_-\psi^L_+\rangle + \langle\psi^{R\dagger}_-\psi^L_-\rangle\right)\eta^\dagger_-\eta_- \\
={}& \frac{qh\epsilon}{\pi\bar{r}}\mathcal{C}(\bar{r})\left(-1 + \frac{4h}{\pi}\right) + \mathcal{O}\left(h^4\right)\ ,
\end{aligned}
\tag{D.1}
$$

and

$$
\begin{aligned}
\langle H_{\text{int}}\rangle \supset{}& -ih\mathcal{C}(\bar{r})\frac{\epsilon}{\bar{r}}\int d^2\Omega\langle\bar{\Psi}^L_+\Psi^R_-\rangle \\
={}& -\frac{ih\epsilon}{2\bar{r}}\mathcal{C}(\bar{r})\int d^2\Omega\left(\langle\psi^{L\dagger}_+\psi^R_+\rangle + i\langle\psi^{L\dagger}_+\psi^R_-\rangle + i\langle\psi^{L\dagger}_-\psi^R_+\rangle - \langle\psi^{L\dagger}_-\psi^R_-\rangle\right)\eta^\dagger_-\eta_- \\
={}& \frac{qh\epsilon}{\pi\bar{r}}\mathcal{C}(\bar{r})\left(-1 + \frac{4h}{\pi}\right) + \mathcal{O}\left(h^4\right)\ .
\end{aligned}
\tag{D.2}
$$

---

[14]Note that we include higher orders than we need for the computation in the main text.

4 Islands in FRW Cosmologies

4.1 Introduction

One of the long-standing puzzles in modern physics is the black hole information paradox. Its essence can be captured by examining the entropy of the sub-systems of an evaporating black hole. In Hawking's seminal calculation [60, 63], the fine-grained entropy of the radiation seemingly exceeds the Bekenstein-Hawking entropy of the black hole. This signifies information loss. In a unitary process, a pure state evolves into a pure state. Page showed [64] that initially the fine-grained entropy grows, following the Hawking curve, but approximately halfway through the evaporation process, it starts decreasing and eventually vanishes, which is consistent with unitary evolution. In a series of breakthrough papers [4–9], it was shown that the Page curve can be recovered within semiclassical gravity. The key to this advance was realizing that the fine-grained entropy of the radiation receives contributions from a disconnected region that lies in the gravitating system, namely, the island. The exact entropy of the radiation is given by the island formula

$$S(\mathbf{R}) = \min_I \left\{ \operatorname*{ext}_I \left[\frac{A(\partial I)}{4 G_N} + S_{\text{mat}}(R \cup I) \right] \right\}, \qquad (4.1.1)$$

where $A(\partial I)$ is the area of the boundary of the island I, and $S_{\text{mat}}(R \cup I)$ is the renormalized entropy of the quantum fields on the union of the regions R and I. Before the evaporation begins, there are not any non-trivial islands and no Hawking pairs have been emitted. So, initially, the exact entropy of the radiation is

$$S(\mathbf{R}) \approx S_{\text{mat}}(R). \qquad (4.1.2)$$

When the process starts, more and more Hawking partners escape from the black hole and (4.1.2) steadily grows. As the evaporation proceeds, a non-trivial island appears in the interior of the black hole. Its boundary is very close to the black hole horizon. Since it extends almost through the whole black hole interior, it contains most of the partners of the Hawking radiation that have escaped from
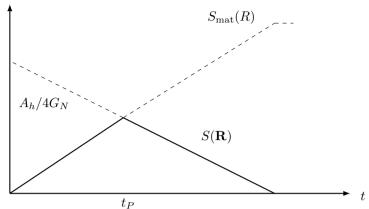
Figure 4.1: Page curve of the fine-grained entropy of an evaporating black hole.

the black hole. The partners contained in the island region purify the ones of the black hole, so the term $S_{\mathrm{mat}}(R \cup I)$ in (4.1.1) vanishes and the exact entropy of the radiation becomes

$$S(\mathbf{R}) \approx \frac{A(\partial I)}{4G_N} \, . \tag{4.1.3}$$

As the black hole horizon shrinks, (4.1.3) decreases and finally vanishes. Thus, the Page curve is followed and the black hole evaporation process is unitary (see Figure 4.1). Remarkably, the island formula (4.1.1) has been derived using the Euclidean path integral by applying the gravitational replica trick [132] (See [9] for a review). It was shown that after the Page time replica wormholes become dominant [7, 8]. The island formula (4.1.1) is a generalization of Ryu-Takayanagi formula [65–68, 133, 134] which has been extensively studied in the literature [135–149].

It is worth emphasizing once more that in [7, 8] the Page curve was recovered in the context of semiclassical gravity. This leads one to ask whether islands exist in cosmological spacetimes, where we do not have AdS/CFT duality [37] to assist us. Moreover, since our universe has positive cosmological constant, it is natural to wonder whether or not we might be living in an island.

The first cosmological islands were found in [150]. The authors considered a setup where a radiation-dominated, flat Friedmann-Robertson-Walker (FRW) spacetime is entangled with a non-gravitating auxiliary system. They examined the cases with zero, positive and negative cosmological constant and concluded that islands appear only in the last case. The way they achieved this was by introducing three conditions that aid the search for islands. The beauty of these conditions is that they are independent of the radiation region R. Once a non-trivial island region is found, it is natural to wonder where the information of the degrees of freedom in I

is encoded. One possible way to answer this question is by introducing an auxiliary system that purifies the state of the system in I, for example preparing the whole state in a thermofield double like state. This process is however non-unique.

In this paper, we build upon the work of [150]. We extend their analysis to FRW universes with non-zero spatial curvature. We consider a state that is approximately thermal with inverse temperature β. We use the island conditions proposed in [150] along with an extra set of conditions that ensure our candidate islands are in the semiclassical regime. In regions of spacetime where all of the above are satisfied we conclude that islands can exist. Our main results are summarized below.

Summary of results: As was mentioned before, we study FRW cosmologies that are supported by radiation in a thermal state, cosmological constant and non-zero spatial curvature. In closed universes, with any type of cosmological constant, there is always an island that is the whole Cauchy slice. Additionally, when $\Lambda < 0$, for any spatial curvature, we find that there is a different type of candidate island region. These universes are recollapsing and have a time-symmetric slice. For $k > 0$ and $\Lambda < 0$, we find that there is a candidate island region in the middle of the Penrose diagram around the time-symmetric slice. This region is shown in Figure 4.9. For $k < 0$ and $\Lambda < 0$, we have a similar situation, i.e. a candidate island region around the time-symmetric slice, only this time it starts at a finite value of the radial coordinate and extends to infinity, as shown in Figure 4.12. This island is similar to the one found in [150] for $k = 0$ and $\Lambda < 0$. We conclude that the main element that allows for the existence of candidate island regions is a negative cosmological constant.

For the purpose of this study, we use both analytical and numerical methods. In order to have analytic control of the solution to the Friedmann equation, in all the universes that it is possible, we focus on the time-symmetric slice, where $a'(\eta)|_{\eta=\eta_0} = 0$. We study the solution, $a(\eta)|_{\eta=\eta_0} = a_0$, at the low and high temperature limits and find that for $\Lambda < 0$ islands appear only in the latter case, as the former is always in the non-semiclassical regime. In the high temperature limit, we see that a_0 does not have contributions from the curvature, i.e., to leading order it coincides with the solution of the flat radiation-dominated FRW universe evaluated at its time-symmetric slice. Hence, we conclude that at the turnaround time, in the high temperature limit, the spatial curvature is negligible. In order to support and complement our analytic calculations, we also "scan" the whole spacetime for candidate island regions numerically and provide multiple figures that show where the existence of islands is possible.

Outline: This paper is organized as follows. We begin in Section 4.2 by intro-

ducing the setup and general framework. In Section 4.3 we review the analysis of the radiation-dominated, flat FRW universes done in [150]. In Sections 4.4 and 4.5, we explore the possibility of islands in radiation-dominated FRW cosmologies with positive and negative curvature respectively. Finally, in Section 4.6 we briefly summarize our results and discuss future directions.

Note added: While finishing this work, the paper [151] appeared on the arXiv which has some overlap with our results.

4.2 General framework

We are interested in finding candidate island regions in four dimensional FRW cosmologies. The metric in conformal coordinates is given by

$$ds^2 = a^2(\eta) \left(-d\eta^2 + d\chi^2 + S_k^2(\chi)d\Omega_2^2\right) \ , \quad S_k(\chi) := \begin{cases} R_0 \sinh(\chi/R_0) \ , & k = -1 \\ \chi \ , & k = 0 \ , \\ R_0 \sin(\chi/R_0) \ , & k = 1 \end{cases}$$

$$(4.2.1)$$

for open, flat, and closed universes, respectively. Here, R_0 is a fixed length scale and $a(\eta)$ is the scale factor. We assume that the state of the system is approximately thermal

$$\rho \approx \frac{1}{Z} e^{-\beta H} \ , \tag{4.2.2}$$

where $\beta = \beta_0 a(\eta)$ is the inverse temperature at conformal time η, and β_0 refers to the temperature in Minkowski spacetime. Given a subregion I on a particular Cauchy slice at time $\eta = \eta_0$, the matter entropy of the bulk fields enclosed in it is given by the thermal entropy

$$S_{\text{mat}}(I) = s_{\text{th}}\widetilde{V}(I) \ , \tag{4.2.3}$$

where s_{th} is the thermal entropy density, and $\widetilde{V}(I)$ is the comoving volume enclosed by I. For the metric (4.2.1), the comoving volume is

$$\widetilde{V}(I) = 4\pi \int\limits_0^{\chi_I} d\chi \ S_k^2(\chi) \ . \tag{4.2.4}$$

We define the region G as the complement of region I in the gravitating system such that they share the same boundary, $\partial I = \partial G$. The entropy of matter fields enclosed by G is also extensive and is simply

$$S_{\text{mat}}(G) = s_{\text{th}} \left(\widetilde{V}_{\text{total}} - \widetilde{V}(I)\right) \ , \tag{4.2.5}$$

where $\widetilde{V}_{\text{total}}$ is the total volume enclosing both regions G and I. We consider FRW cosmologies supported by radiation, spatial curvature, and cosmological constant. The radiation and entropy densities have the form

$$\rho_{\text{rad}} = \frac{c_{\text{th}} T_0^4}{a(\eta)^4} \quad \text{and} \quad s_{\text{th}} = \frac{3}{4} c_{\text{th}} T_0^3 \; , \tag{4.2.6}$$

respectively. Here, c_{th} is proportional to the number of degrees of freedom and T_0 is the temperature in Minkowski spacetime. The scale factor $a(\eta)$ is the solution to the Friedmann equation[1]

$$\frac{1}{a(\eta)^2} \left(\frac{a'(\eta)}{a(\eta)} \right)^2 = \frac{8\pi G_N}{3} \frac{c_{\text{th}} T_0^4}{a(\eta)^4} - \frac{k}{a(\eta)^2 R_0^2} + \frac{\Lambda}{3} \; . \tag{4.2.7}$$

We will apply the necessary island conditions for the existence of islands [150]. The explicit form of these three conditions in spacetimes arising from (4.2.1) are as follows

- The Bekenstein bound is violated:

$$\widehat{S}_{\text{mat}}(I) \gtrsim \frac{A(\partial I)}{4 G_N} \; , \tag{4.2.8}$$

  where $\widehat{S}_{\text{mat}}$ is the finite part of the matter entropy and the wiggly inequality means that the subleading terms compared to right hand side are ignored. The derivation of this condition needs a careful treatment of UV divergences of the matter entropy [150]. In our case, the thermal entropy (4.2.3) represents the extensive part of $\widehat{S}_{\text{mat}}(I)$ and is finite.

- I is a quantum normal region:

$$(\pm \partial_\eta + \partial_\chi) \, S_{\text{gen}}(I) \geq 0 \; . \tag{4.2.9}$$

- G is a quantum normal region:

$$(\pm \partial_\eta - \partial_\chi) \, S_{\text{gen}}(G) \geq 0 \; . \tag{4.2.10}$$

Notice that in both conditions, we are using the null directions to deform the surfaces ∂I and ∂G with respect to the region I. For a closed universe, for example, the entire Cauchy slice always satisfies these three conditions.

Once an overlapping region is found in a FRW cosmology, we still need to be sure that they live in the semiclassical regime. In order to do so, we use the following semiclassical conditions:

---

[1]For the case of a negative cosmological constant, we will define a positive $\Lambda_0 > 0$ such that $\Lambda = -\Lambda_0$.

- The proper time to the singularity requires

$$\Delta\tau = \int\limits_0^\eta d\eta \; a(\eta) \gg l_P \; . \qquad (4.2.11)$$

- The thermal length scale should satisfy

$$\beta \gg l_P \; , \quad i.e., \quad \frac{a(\eta)}{T_0} \gg l_P \; . \qquad (4.2.12)$$

- The energy density should satisfy

$$\rho_{\text{rad}} = \frac{c_{\text{th}}T_0^4}{a(\eta)^4} \ll M_P^4 \; . \qquad (4.2.13)$$

- The size of the S^2 obeys

$$a(\eta)S_k(\chi) \gg l_P \; . \qquad (4.2.14)$$

- The curvature radius requires

$$a(\eta)R_0 \gg l_P \; . \qquad (4.2.15)$$

Let us emphasize that the island conditions together with the semiclassical conditions give a strong indication that an island exists in a given spacetime without making any reference to the radiation region R.

Consider the case when we find a candidate island region I, *i.e.,* , a region in spacetime that fulfills the above criteria. A natural question to ask is in which auxiliary system, R, is this region encoded? Following [150], one possible way to answer this question is by purifying the original thermal state with a second copy of Minkowski space and preparing the whole system in the thermofield double state (TFD) using the Euclidean path integral

$$|\beta_0\rangle = \frac{1}{\sqrt{Z}} \sum_n e^{-\beta_0 E_n} |n\rangle_1^* |n\rangle_2 \; . \qquad (4.2.16)$$

This is of course a non-unique procedure. In this paper, we are agnostic about the radiation region R and focus more on the question of whether islands can exist in FRW cosmologies.

4.3   Flat slicing

In this section, we review the results of [150] for FRW cosmologies with flat slicing.

A   Zero cosmological constant

We first consider the case where the vacuum energy density is zero. The solution of the Friedmann equation (4.2.7) has the simple form. It is given by

$$a(\eta) = \sqrt{\frac{8\pi G_N c_{\text{th}} T_0^4}{3}} \eta \ . \tag{4.3.1}$$

Island conditions

For a spherical region I located at χ_I at time η_I, the Bekenstein bound is violated for

$$\frac{\chi_I}{\eta_I} \gtrsim \frac{3\pi}{2} T_0 \eta_I \ . \tag{4.3.2}$$

In order for region I to be quantum normal, the ingoing condition is true for values

$$\frac{\chi_I}{\eta_I} \geq \begin{cases} \frac{\pi T_0 \eta_I}{\pi T_0 \eta_I - 1} \ , & \pi T_0 \eta > 1 \\ 0 \ , & \pi T_0 \eta < 1 \ , \end{cases} \tag{4.3.3}$$

while the outgoing condition is always satisfied. The third condition implies that the outward part is true for

$$\frac{\chi_I}{\eta_I} \geq \frac{\pi T_0 \eta_I}{\pi T_0 \eta_I + 1} \ , \tag{4.3.4}$$

whereas the ingoing, for $\pi T_0 \eta < 1$, is satisfied when

$$\frac{\chi_I}{\eta_I} \geq \frac{\pi T_0 \eta_I}{1 - \pi T_0 \eta_I} \ . \tag{4.3.5}$$

There is an overlapping region where the three conditions are fulfilled for values of conformal time such that

$$T_0 \eta_I < \frac{1}{\pi} \ . \tag{4.3.6}$$

Semiclassical regime

Using the proper time condition (4.2.11), we find that we are in the semiclassical regime when

$$T_0 \eta_I \gg \frac{1}{c_{\text{th}}^{1/4}} \ , \tag{4.3.7}$$

which is in conflict with (4.3.6).

Conclusion

There is an overlapping region where all three island conditions are simultaneously satisfied and it is shown in teal in Figure 4.2. However, this region is outside of the semiclassical regime of validity. We conclude that we do not have islands in this universe.
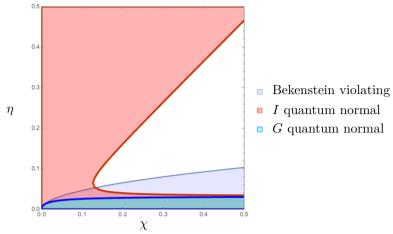
Figure 4.2: Regions where the three island conditions are satisfied. We chose the numeric values $k = 0$, $\Lambda = 0$, $c_{th} = 1$, $T_0 = 10$, and $G_N = 0.01$. There is an overlapping region close to $\eta \approx 0$. However, this region is outside of the semiclassical regime as it violates the proper time condition (4.2.11).

B Positive cosmological constant

We proceed by turning on the cosmological constant and checking the three conditions. The Bekenstein bound is violated when

$$\chi_I \gtrsim \frac{3a(\eta)^2}{4G s_{\text{th}}} \ . \tag{4.3.1}$$

The region I should be quantum normal. The outgoing condition is always satisfied while the ingoing condition requires

$$\chi_I \leq a(\eta)/a'(\eta). \tag{4.3.2}$$

The G quantum normal condition implies

$$a(\eta)(\pm a'(\eta)\chi_I - a(\eta)) + 2G_N s_{\text{th}}\chi_I \geq 0 \ . \tag{4.3.3}$$

Similarly as before, the overlap occurs outside of the semiclassical region. This part of the geometry is depicted in teal in Figure 4.3.

C Negative cosmological constant

Finally, we consider the case with negative cosmological constant. There is a recollapsing FRW universe as a solution to the Friedmann equation (4.2.7). Importantly, a new ingredient of this cosmology is the existence of a time-symmetric
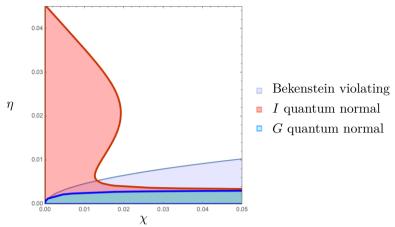
Figure 4.3: Regions where the three island conditions are satisfied. We chose the numeric values $k = 0$, $c_{th} = 1$, $T_0 = 100$, and $\Lambda_0 G_N = 0.01$. There is an overlapping region close to $\eta \approx 0$ where the proper time condition (4.2.11) is not satisfied.

slice. By solving (4.2.7) at the time $\eta = \eta_0$ such that $a'(\eta_0) = 0$, we get

$$a_0 = \left(\frac{8\pi G_N c_{\text{th}} T_0^4}{\Lambda_0} \right)^{\frac{1}{4}} . \tag{4.3.1}$$

Island conditions

At this particular time the Bekenstein bound is violated for values

$$\chi_I \gtrsim \frac{9}{4T_0} \left(\frac{\pi}{2c_{\text{th}} \Lambda_0 G_N} \right)^{1/2} . \tag{4.3.2}$$

The ingoing and outgoing quantum normal conditions for region I are reduced to one condition

$$\partial_\chi S_{\text{gen}}(I) \geq 0 , \tag{4.3.3}$$

which is always satisfied in this case. Similarly, the G quantum normal condition becomes

$$-\partial_\chi S_{\text{gen}}(G) \geq 0 \implies \chi_I \geq \frac{3}{2T_0} \left(\frac{\pi}{2c_{\text{th}} \Lambda_0 G_N} \right)^{1/2} , \tag{4.3.4}$$

which is approximately the same result as the one we get from the first condition. Hence, there is triple overlap when (4.3.2) is fulfilled.

Semiclassical regime

We still have to check that these regions, along the time-symmetric slice, are in the semiclassical regime. The thermal length (4.2.12) and energy density (4.2.13)
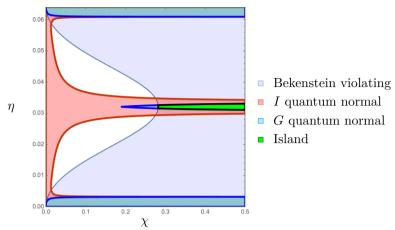
Figure 4.4: Regions where the three island conditions are satisfied. We chose the numeric values, $k = 0$, $c_{\text{th}} = 1$, $T_0 = 10$, and $\Lambda G_N = -0.01$. We see that all conditions are simultaneously satisfied starting from the value $\chi_I = 3a_0^2/4G_N s_{\text{th}}$. The island region is depicted in green. There are also overlapping regions at times where the solution $a(\eta)$ recollapses. However, they lie outside the semiclassical regime of validity given by the proper time condition (4.2.11).

conditions imply $\Lambda_0 G_N \ll 1$. From (4.2.14), the size of the region has to be

$$T_0 \chi_I \gg \left(\frac{\Lambda_0 G_N}{c_{\text{th}}} \right)^{1/4} , \tag{4.3.5}$$

which is a less restrictive condition than (4.3.2). The curvature radius condition (4.2.15) gives

$$T_0 R_0 \gg \left(\frac{\Lambda_0 G_N}{c_{\text{th}}} \right)^{1/4} . \tag{4.3.6}$$

All of the semiclassical conditions are satisfied and compatible with the island conditions in the overlapping region (4.3.2).

Conclusion

We conclude that there is an island region in the semiclassical regime for values that satisfy (4.3.2). This region is shown in green in Figure 4.4 together with the island conditions in the whole spacetime.

4.4 Positive curvature

A Zero cosmological constant

We first consider the case where the vacuum energy density is vanishing and the FRW cosmology is supported by radiation and positive curvature. Without loss of generality, we can fix $k = 1$. In these coordinates, $\chi \in [0, \pi R_0]$ is one of the angles that parametrize the $\mathcal{S}^3$. Solving (4.2.7), gives a scaling factor of the form

$$a(\eta) = \left(\frac{8\pi G_N R_0^2 c_{\mathrm{th}} T_0^4}{3} \right)^{1/2} \sin \left(\frac{\eta}{R_0} \right) . \tag{4.4.1}$$

Island conditions

In order to look for island regions in this cosmology, we impose the three conditions to the region I located at $\chi = \chi_I$ and $\eta = \eta_I$. The Bekenstein bound has the form

$$2\chi_I - R_0 \sin \left(\frac{2\chi_I}{R_0} \right) \gtrsim \frac{a(\eta_I)^2}{s_{\mathrm{th}} G_N} \sin^2 \left(\frac{\chi_I}{R_0} \right) . \tag{4.4.2}$$

In this equation we are basically comparing the comoving volume of the $\mathcal{S}^3$, with the area term $A(\partial I)/4G_N$. A natural place to look for island regions is the point where the volume is maximum and the area is very small. In fact, the $\mathcal{S}^3$ acquires its maximum size at $\chi_I = \pi R_0$. Close to this particular value (4.4.2) becomes

$$\delta^2 \lesssim \frac{R_0}{T_0} \frac{1}{\sin \left(\frac{\eta_I}{R_0} \right)^2} , \quad \delta := \pi R_0 - \chi_I . \tag{4.4.3}$$

Going to small times, $\eta_I/R_0 \ll 1$, so that the area term shrinks, we get

$$\left(\frac{\delta}{R_0} \right)^2 \lesssim \frac{R_0}{T_0 \eta_I^2} . \tag{4.4.4}$$

Imposing that I and G should be quantum normal results in

$$T_0 \eta_I \leq \frac{1}{\pi} . \tag{4.4.5}$$

This region, however, is non-semiclassical. We can see this by computing the proper time to the singularity and the thermal length. Both (4.2.11) and (4.2.12) are valid when

$$T_0 \eta_I \gg 1 , \tag{4.4.6}$$

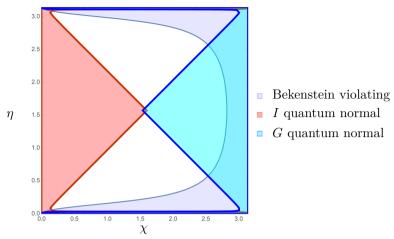which is clearly in conflict with (4.4.5).

Figure 4.5: Regions where the three conditions are satisfied. We chose the numeric values $k = 1$, $\Lambda = 0$, $c_{th} = 1$ and $R_0 T_0 = 10$ and $G_N = 0.01$. There are overlapping regions close to the singularities, which are outside the semiclassical regime given by the proper time condition (4.2.11).

Therefore, there are no island regions close to the singularities located at $\eta_I \approx 0$ and $\eta_I \approx \pi$, and the place where the area term shrinks $\chi_I \approx \pi R_0$. We now proceed to analyze the time-symmetric slice. At $\eta_I = \pi R_0/2$, the scale factor is

$$a_0 = \sqrt{\frac{8\pi c_{\text{th}} G_N}{3}} R_0 T_0^2 \ . \tag{4.4.7}$$

Let us examine again the region close to $\chi_I = \pi R_0$. Expanding (4.4.2), we obtain

$$\left(\frac{\delta}{R_0}\right)^2 \lesssim \frac{1}{R_0 T_0} \ . \tag{4.4.8}$$

For I to be quantum normal, we have

$$\frac{\delta}{R_0} \geq \pi R_0 T_0 \ , \tag{4.4.9}$$

while the condition for region G is always satisfied. We see that the three conditions are simultaneously true in the regime where $R_0 T_0 < 1$.

Semiclassical regime

The semiclassical conditions for the thermal length (4.2.12) and the energy density (4.2.13) are satisfied for large values of the temperature

$$R_0 T_0 \gg 1 \ . \tag{4.4.10}$$

In this limit, the island conditions do not overlap and therefore there is no finite-size island at the time-symmetric slice. In Figure 4.5, we show the regions where the three conditions are valid in the semiclassical regime. As the temperature decreases into non-semiclassical values, the Bekenstein violating region progressively covers half of the spacetime, creating a triple overlap in the middle of the Penrose diagram. Moreover, there are overlapping regions close to the singularities outside the scope of the semiclassical analysis.

Conclusion

The only possible island is the the entire Cauchy slice.

B   Positive cosmological constant

As a warm-up example, we first neglect the density of radiation. This cosmology then corresponds to the thermal state in de Sitter space. Here, it is convenient to translate everything to the de Sitter radius ℓ_{dS}. In four dimensions, we have

$$\ell_{\mathrm{dS}} = \sqrt{\frac{3}{\Lambda_0}} \; . \tag{4.4.1}$$

The Friedmann equation (4.2.7) reads

$$\frac{1}{a(\eta)^2} \left(\frac{a'(\eta)}{a(\eta)} \right)^2 + \frac{1}{a(\eta)^2 \ell_{\mathrm{dS}}^2} - \frac{\Lambda_0}{3} = 0 \; , \tag{4.4.2}$$

and the solution is found to be

$$a(\eta) = \frac{1}{\cos\left(\frac{\eta}{\ell_{\mathrm{dS}}} \right)} \; . \tag{4.4.3}$$

Island conditions

We now check the three necessary conditions. We restrict to the time-symmetric slice, where $a_0 = 1$. Here, the entropy density has the form $s_{\mathrm{th}} = 1/\ell_{\mathrm{dS}}^3$. The Bekenstein bound then is

$$\frac{\pi}{G_N} \sin^2 \left(\frac{\chi_I}{\ell_{\mathrm{dS}}} \right) \lesssim \frac{1}{\ell_{\mathrm{dS}}^3} \left(2\chi_I - \ell_{\mathrm{dS}} \sin \left(\frac{2\chi_I}{\ell_{\mathrm{dS}}} \right) \right) \; . \tag{4.4.4}$$

We notice that the first condition is satisfied at $\chi_I = \pi R_0$. If we expand close to that point, (4.4.4) gives

$$\delta^2 \lesssim G_N \; , \quad \delta := \pi R_0 - \chi_I \; . \tag{4.4.5}$$
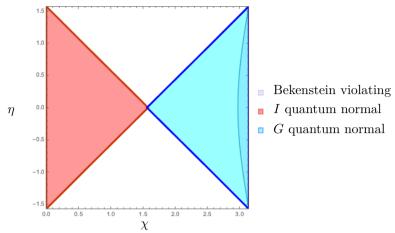
Figure 4.6: Regions where the three conditions are satisfied. The numeric values are chosen to be $k = 1$, $c_{th} = 1$, $\Lambda_0 G_N = 0.01$. There are no non-trivial island regions in thermal dS_4.

This means that in order to satisfy the first island condition we have to go to the distance that is smaller than l_P away from $\chi_I = \pi R_0$. Therefore, there are no islands smaller than the full Cauchy slice in the thermal dS_4. However, for completeness we continue the analysis. We consider the second condition which leads to

$$\delta \geq \frac{\ell_{dS}^3}{G_N} \ .$$

(4.4.6)

The third condition is always satisfied. In Figure 4.6, we show the three islands conditions in the semiclassical regime. We see that there are no overlapping regions.

Conclusion

The only possible island is the entire Cauchy slice.

Adding radiation

We now add radiation. We focus on the time-symmetric slice where (4.2.7) takes the form

$$-\frac{8\pi G_N c_{\text{th}} T_0^4}{3a(\eta_0)^4} + \frac{1}{a(\eta_0)^2 R_0^2} - \frac{\Lambda_0}{3} = 0 \ .$$

(4.4.7)

By solving (4.4.7) we obtain

$$a_0 = \sqrt{\frac{3 \pm \sqrt{9 - 32\pi c_{\text{th}}\Lambda_0 G_N R_0^4 T_0^4}}{2R_0^2\Lambda_0}} \ .$$

(4.4.8)

In order for this cosmology to have a time-symmetric solution, the following bound must be satisfied

$$c_{\text{th}}\Lambda_0 G_N (R_0 T_0)^4 \leq \frac{9}{32\pi} \ . \tag{4.4.9}$$

It is obvious that it is not possible to go to the high temperature limit since that would lead to a negative argument under the root in (4.4.8). So, we focus on the low temperature limit.

Low temperatures

In the low temperature limit,

$$R_0 T_0 \ll \frac{1}{(\Lambda_0 G_N)^{1/4}} \ , \tag{4.4.10}$$

there are two possible values for the scale factor, *i.e.,* , $a_0 \approx 1/R_0\sqrt{\Lambda_0}$ and $a_0 \approx c_{\text{th}}G_N^{1/2} R_0 T_0^2$. The latter is Planckian, so we do not explore this case further. The former represents the limit where the radiation becomes almost negligible and we check the island conditions below.

Island conditions

For scale factor equal to $a_0 \approx 1/R_0\sqrt{\Lambda_0}$, we look for island regions other than the full Cauchy slice close to $\chi = \pi R_0$. As we explained before, in a closed universe, this is the region where the probability of violating the Bekenstein bound is the highest, since that is where the volume has its maximum value and the area its minimum. The Bekenstein bound close to $\chi_I = \pi R_0$ leads to

$$\left(\frac{\delta}{R_0}\right)^2 \lesssim \frac{8\pi}{9} c_{\text{th}} (R_0 T_0)^3 \Lambda_0 G_N \ . \tag{4.4.11}$$

Next, we consider the quantum normal condition for region I, which gives

$$\frac{\delta}{R_0} \geq \frac{1}{c_{\text{th}}(R_0 T_0)^3 \Lambda_0 G_N} \ . \tag{4.4.12}$$

The third condition is always satisfied. Consequently, there is triple overlap when

$$R_0 T_0 \gtrsim \frac{1}{(c_{\text{th}}\Lambda_0 G_N)^{1/3}} \ . \tag{4.4.13}$$

However, (4.4.13) together with (4.4.10) imply $\Lambda_0 G_N \gg 1$. The overlapping region is therefore outside the semiclassical regime.

Semiclassical regime

For semiclassical spacetimes, we know that $\Lambda_0 G_N \ll 1$, as can be easily seen from (4.2.15). In Figure 4.7, we show three island conditions in the semiclassical limit. We see that for the two physical roots in (4.4.8) the island conditions are never simultaneously satisfied.
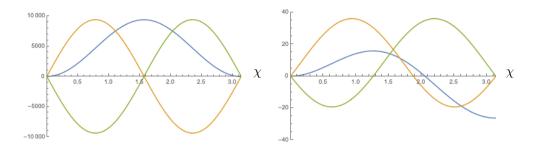
Figure 4.7: Three island conditions in the semiclassical regime for the two physical roots in (4.4.8). The Bekenstein condition, $A(\partial I)/4G_N - s_{\text{th}} \widetilde{V}(I)$, is shown in blue, I quantum normal condition in yellow and G quantum normal condition in green. We chose the numeric values $k = 1$, $c_{\text{th}} = 1$, $R_0 T_0 = 1$, and $\Lambda_0 G_N = 0.001$. (Left) The Bekenstein bound is never satisfied, as $A(\partial I)/4G_N - s_{\text{th}} \widetilde{V}(I)$ is always positive. (Right) Bekenstein and G conditions are both satisfied close to $\chi \approx \pi R$. In all cases, the I and G quantum normal conditions are mutually exclusive. The three islands conditions are never satisfied.

Conclusion

The only possible island is the entire Cauchy slice.

C   Negative cosmological constant

We now turn to the case where $\Lambda = -\Lambda_0$, with $\Lambda_0 > 0$. At the time-symmetric slice (4.2.7) reduces to

$$-\frac{8\pi G_N c_{\text{th}} T_0^4}{3a(\eta_0)^4} + \frac{1}{a(\eta_0)^2 R_0^2} + \frac{\Lambda_0}{3} = 0 \ . \tag{4.4.1}$$

At this time, the scale factor acquires the value

$$a_0 = \frac{1}{R_0 \sqrt{2\Lambda_0}} \sqrt{-3 + \sqrt{9 + 32\pi c_{\text{th}} G_N R_0^4 T_0^4 \Lambda_0}} \ . \tag{4.4.2}$$

In the small temperature limit, $R_0 T_0 \ll 1/(\Lambda_0 G_N)^{1/4}$, (4.4.2) takes the form

$$a_0 \approx \sqrt{\frac{8\pi c_{th} G_N}{3}} R_0 T_0^2 \ . \tag{4.4.3}$$

This is effectively the limit where the vacuum energy density is negligible and coincides with the analysis in Section A where there are no island regions.
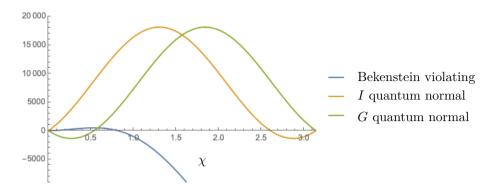
Figure 4.8: Three island conditions in the semiclassical regime along the time-symmetric slice. We use the scale factor (4.4.5). The Bekenstein condition shown is $A(\partial I)/4G_N - s_{th}\widetilde{V}(I)$, which is satisfied when this quantity is negative. We chose the numeric values $k = 1$, $c_{\text{th}} = 1$, $R_0 T_0 = 10$, and $\Lambda_0 G_N = 0.1$. The three islands conditions are satisfied in the overlapping region 2δ around the value $\chi_I = \pi R_0/2$.

High temperatures

We now analyze the high temperature limit

$$R_0 T_0 \gg 1/(\Lambda_0 G_N)^{1/4} \ . \tag{4.4.4}$$

Here, (4.4.2) becomes

$$a_0 \approx \left(\frac{8\pi c_{\text{th}} G_N T_0^4}{\Lambda_0} \right)^{1/4} \ . \tag{4.4.5}$$

Importantly, in this limit the curvature contribution is negligible since the scale factor coincides with (4.3.1). Naively, one might think that the best place to look for islands is where the volume is maximal as in the spatially flat case. However, for a closed universe, regions close to $\chi_I = \pi R_0/2$ are in fact anti-normal.

Island conditions

It turns out that the best place to look for islands is at the middle of the $\mathcal{S}^3$ in the direction of χ, *i.e.,* , $\chi_I = \pi R_0/2$. Let us first take values of χ_I such that $0 < \pi/2 - \chi_I/R_0 \ll 1$. For high temperatures, the Bekenstein bound reduces to the condition

$$\frac{\delta}{R_0} \lesssim \frac{\pi}{4} - \frac{3}{8} \frac{1}{\sqrt{\pi c_{\text{th}} \Lambda_0 G_N}} \frac{1}{R_0 T_0} \ , \quad \delta := \frac{\pi R_0}{2} - \chi_I \ . \tag{4.4.6}$$

The G quantum normal condition to first order implies

$$\frac{\delta}{R_0} \leq \frac{2}{3} \sqrt{\frac{2c_{\text{th}} \Lambda_0 G_N}{\pi}} R_0 T_0 \ , \tag{4.4.7}$$

while the condition for I quantum normal is always satisfied. We see that both (4.4.6) and (4.4.7) are satisfied when

$$R_0 T_0 > \frac{1}{\sqrt{c_{\text{th}} \Lambda_0 G_N}} \ . \tag{4.4.8}$$

This regime of parameters, where the three island conditions are satisfied, is consistent with the high temperature limit (4.4.4).

Semiclassical regime

We proceed to determine if the overlapping region is in the semiclassical regime. The condition for the proper time (4.2.11) is valid for times $T_0 \eta_I \gg (G_N \Lambda_0)^{1/4}$. The conditions (4.2.12) and (4.2.13) are satisfied when $\Lambda_0 G_N \ll 1$. The curvature condition (4.2.15) implies $R_0 T_0 \gg (G_N \Lambda_0)^{1/4}$. Finally, the sphere size condition (4.2.14), to leading order in the separation δ, has the following form

$$R_0 T_0 \gg \left(\frac{\Lambda_0 G_N}{8\pi c_{\text{th}}} \right)^{1/4} + \frac{1}{2} \left(\frac{\Lambda_0 G_N}{8\pi c_{\text{th}}} \right)^{1/4} \left(\frac{\delta}{R_0} \right)^2 + \dots \ . \tag{4.4.9}$$

We see that all these conditions are compatible with (4.4.8) in the high temperature limit (4.4.4). We present the three island conditions in Figure 4.8 for the time-symmetric slice.

Conclusion

There is a semi-classical region at the time-symmetric slice and around the half-sphere point, $\chi_I = \pi R_0 / 2$, where the three island conditions are satisfied. Therefore, an island region appears when (4.4.8) is satisfied together with $R_0 T_0 \gg 1$ and $\Lambda_0 G_N \ll 1$. A similar analysis follows for the values $\pi/2 - \chi_I / R_0 < 0$. In fact, there is a symmetric island region with respect to the half-sphere location. These regions are depicted in Figure 4.9.

4.5   Negative curvature

A   Zero or positive cosmological constant

These types of universes do not admit recollapsing solutions where $a'(\eta)|_{\eta = \eta_0} = 0$. Both of them expand forever.

B   Negative cosmological constant

We take the values $k = -1$ and $\Lambda = -\Lambda_0$. When we focus on the time-symmetric slice, (4.2.7) simplifies to

$$-\frac{8\pi G_N \epsilon_0}{3 a(\eta_0)^4} - \frac{1}{a(\eta_0)^2 R_0^2} + \frac{\Lambda_0}{3} = 0 \ . \tag{4.5.1}$$
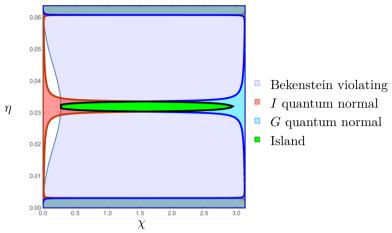
Figure 4.9: Regions where the three island conditions are satisfied in the semiclassical regime for a closed FRW cosmology. We chose the numeric values $k = 1$, $c_{\text{th}} = 1$ and $R_0 T_0 = 100$ and $\Lambda_0 G_N = 0.01$. There is an island region along the time-symmetric slice and around $\chi_I = \pi R_0/2$. There are also overlapping regions at times where the solution $a(\eta)$ recollapses. However, they lie outside the semiclassical regime.

Then the scale factor is

$$a_0 = \frac{1}{R_0 \sqrt{2\Lambda_0}} \sqrt{3 + \sqrt{9 + 32\pi c_{\text{th}} \Lambda_0 G_N R^4 T_0^4}} \ . \qquad (4.5.2)$$

Low temperatures

First, in the low temperature limit $R_0 T_0 \ll 1/\left(c_{\text{th}} G_N \Lambda_0\right)^{1/4}$, (4.5.2) becomes

$$a_0 \approx \frac{1}{R_0} \sqrt{\frac{3}{\Lambda_0}} \ . \qquad (4.5.3)$$

We do not expect to find islands in this case, as this limit corresponds to having almost no radiation. In fact, when we analytically check the first condition, we end up in contradictions. Using (4.5.3) for large values of $\chi/R_0 \gg 1$, we find that in order to violate the Bekenstein bound, we need

$$R_0 T_0 \gtrsim \frac{1}{(c_{\text{th}} G_N \Lambda_0)^{1/3}} \ , \qquad (4.5.4)$$

which is very large in the semiclassical regime. However, our initial assumption was that the temperature is very low. Similarly, for small values of $\chi_I/R \ll 1$, we find that the same condition (4.2.8) requires

$$\frac{\chi_I}{R_0} \gtrsim \frac{1}{(R_0 T_0)^3 G \Lambda_0} \ , \qquad (4.5.5)$$
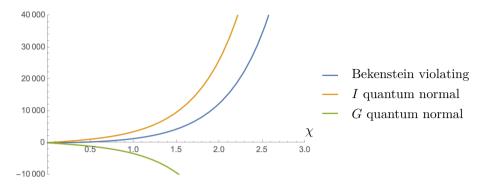
111

Figure 4.10: Three island conditions in the semiclassical regime along the time-symmetric slice in the low temperature limit. We use the scale factor in (4.5.3). The Bekenstein condition shown is given by $A(\partial I)/4G_N - s_{\mathrm{th}}\widetilde{V}(I)$, which is satisfied when this quantity is negative. We chose the numeric values $k = -1$, $c_{th} = 1$, $R_0 T_0 = 1$, and $\Lambda_0 G_N = 0.01$. The I quantum normal condition is always valid. The G condition is never satisfed. The Bekenstein bound is never violated.

which together with the small temperature limit imply that $\chi_I/R_0 \gg 1/(c_{\mathrm{th}}G_N\Lambda_0)^{1/4}$ outside of the regime of validity. Hence, the first condition is never satisfied and consequently it is not possible to have islands. In Figure 4.10, we show the three conditions in the small temperature limit.

High temperatures

We now look at the high temperature limit $R_0 T_0 \gg 1/\left(c_{\mathrm{th}}G_N\Lambda_0\right)^{1/4}$. Here, (4.5.2) takes the form

$$a_0 = \left(\frac{8\pi G_N c_{th} T_0^4}{\Lambda_0}\right)^{1/4}, \tag{4.5.6}$$

which corresponds to having negligible curvature at the turnaround time.

Island conditions

For small $\chi_I/R_0 \ll 1$, we find for the Bekenstein bound

$$\frac{\chi_I}{R_0} \gtrsim \frac{9}{4R_0 T_0}\left(\frac{\pi}{2c_{\mathrm{th}}\Lambda_0 G_N}\right)^{1/2}. \tag{4.5.7}$$

For large $\chi_I/R_0 \gg 1$, we get

$$R_0 T_0 \gtrsim \frac{3}{2}\left(\frac{\pi}{2c_{\mathrm{th}}G_N\Lambda_0}\right)^{1/2}. \tag{4.5.8}$$

The second condition that requires I to be quantum normal is always satisfied at the time-symmetric slice, and the third results to the same inequalities up to small
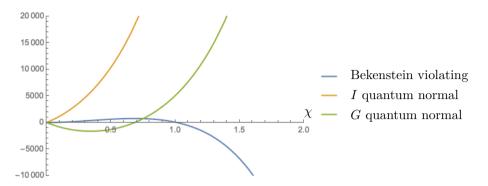
Figure 4.11: Three island conditions in the semiclassical regime along the time-symmetric slice in the high temperature limit. We use the scale factor in (4.5.6). The Bekenstein condition shown is given by $A(\partial I)/4G_N - s_{\text{th}}\widetilde{V}(I)$, which is satisfied when this quantity is negative. We chose the numeric values $k = -1$, $c_{\text{th}} = 1$, $R_0T_0 = 10$, and $\Lambda_0 G_N = 0.1$. The I quantum normal condition is always valid. The three island conditions are satisfied for values in (4.5.7).

order one numbers as the first condition. Therefore, there is an overlapping region when (4.5.7) is valid.

Semiclassical regime

We also check that the semiclassical conditions at the time-symmetric slice are satisfied. The conditions for the thermal length (4.2.12) and energy density (4.2.13) are obeyed for $G_N\Lambda_0 \ll 1$, which are true for reasonable spacetimes. Moreover, we require that the size of the $\mathcal{S}^2$ sphere is bigger than the Planck length. For large $\chi/R_0 \gg 1$ the condition is automatically satisfied. For small $\chi/R_0 \ll 1$, we have

$$\frac{\chi}{R_0} \gg \frac{1}{R_0T_0}\left(\frac{G_N\Lambda_0}{c_{\text{th}}}\right)^{1/4}, \tag{4.5.9}$$

which is compatible with (4.5.7). Finally, we check the radius of curvature condition (4.2.15)

$$R_0T_0 \gg \left(\frac{G_N\Lambda_0}{c_{\text{th}}}\right)^{1/4}, \tag{4.5.10}$$

which is again compatible with (4.5.8). Therefore, when we combine all the conditions, we get an elongated teardrop region, (4.5.7). In Figure 4.11, we show three island conditions in the semiclassical limit.
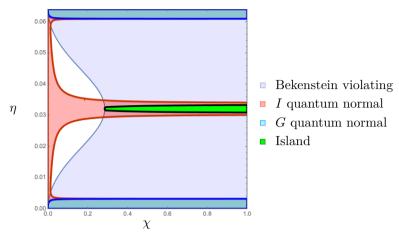
Figure 4.12: Regions where the three island conditions are satisfied in the semiclassical regime for an open FRW cosmology. We chose the numeric values $k = -1$, $c_{\text{th}} = 1$, $R_0 T_0 = 100$, and $\Lambda_0 G_N = 0.01$. There is an island region along the time-symmetric slice that extends to infinity. There are also overlapping regions at times where the solution $a(\eta)$ recollapses. However, they lie outside the semiclassical regime.

Conclusion

There is a semiclassical region at the time-symmetric slice where the three island conditions are satisfied. Therefore, the existence of islands is possible for the values in (4.5.8) together with $R_0 T_0 \gg 1$, and $\Lambda_0 G_N \ll 1$. This region is shown in green in Figure 4.12.

4.6 Discussion

In this paper, we studied the possible existence of islands in FRW cosmologies supported by radiation, curvature, and cosmological constant. To this end, we applied the three necessary conditions to subregions of the spacetime I and G, together with the semiclassical conditions introduced in Section 4.2. We found that the key element for the existence of non-trivial islands is a negative cosmological constant. In the case of a closed universe, there is an island region around the half-sphere point located at $\chi_I = \pi R_0/2$. This island is finite in size and is qualitatively different from the island found in [150]. For open universes, an island region shows up for large enough radius and extends all the way to infinity. By studying the spacetime at the time-symmetric slice, we provided analytic evidence for the existence of these islands in the high temperature limit where the spatial curvature is negligible. We also performed a numerical analysis in the entire spacetime.

It turns out that having an FRW cosmology with a time-symmetric slice is not sufficient for the existence of islands smaller than the whole Cauchy slice. For example, closed de Sitter and a recollapsing universe with $\Lambda = 0$ and closed slicing have time-symmetric slices, but the only possible island is the full Cauchy slice.

The analysis carried out in this paper is valid for more general class of cosmologies. We expect to find islands in cosmologies with $\Lambda < 0$ for which the effective potential $V_{\text{eff}}(a)$ vanishes at the turning point $a'(\eta) = 0$. For example, we expect that adding ordinary matter would not change the conclusions of this paper.

There are a few exciting avenues of research related to our work that are worth exploring. Since currently our universe is undergoing another period of inflation, it would be interesting to study if islands are relevant in the context of inflation. This can be modeled by bubbles of false vacuum where an inflating region forms behind the horizon [152–154]. It is worth understanding whether inflating regions are encoded in non-gravitating systems and if their formation is allowed in our universe. Additionally, it would also be interesting to understand the implications of our work in the case of eternally inflating multiverse studied in [155] where islands have been shown to appear in collapsing AdS bubbles. Furthermore, islands in Jackiw–Teitelboim de Sitter multiverse have been studied in [156] where they appeared in the crunching regions. Another direction of inquiry would be to explore the existence of islands in more general cosmologies in the spirit of [156].

5 Conclusions

In this thesis we focused on holographic wormholes and islands (see section 1.1 for a summary of the results). Research focused both on islands and wormholes has increased our understanding about gravity and its connection to quantum information.

In the two initial island papers Almheiri, Engelhardt, Marolf and Maxfield and independently Penington managed to recover the Page curve of an evaporating black hole within semiclassical gravity [4, 5]. An abundance of papers has appeared since [6–10, 136, 143, 145, 145, 148, 151, 155, 156, 156–178, 178–183], others applying the island formula in different dimensions, in other spacetimes than AdS and a number raising some concerns [139, 184, 185]. One very interesting aspect of the island formula is that it allows us to compute the full quantum gravitational entropy of the radiation within semiclassical gravity. This indicates that semiclassical gravity "knows" more than we previously thought. Moreover, we learned that information is not lost, but it is actually encoded in the radiation. However, the mechanism of how exactly this happens is still unclear. By understanding how this works we might be able to indirectly learn more about the interior of the black hole. Although we have not managed to understand the complete picture yet, there are new intuitions and lessons that we have learned along the way.

On the wormhole front, Gao, Jafferis and Wall managed to make a holographic traversable wormhole through which we can send information [1], an accomplishment in itself. Since then, numerous papers have used the non-local coupling conceived in [1] in order to create and study traversable wormholes in higher or lower dimensions [50–55, 57, 59, 70, 85, 104–111, 186–189]. One of the most interesting aspects of this type of wormhole is that it can be seen as the dual of quantum teleportation on the boundary side. The two entangled black holes play the role of the entangled pair in the quantum teleportation scenario and the coupling between the two sides represents the classical channel through which the two sides commu-

nicate[1]. Since the wormhole is rendered traversable, we do expect that things will go through. From the wormhole perspective the signal has a relatively smooth journey from one side to the other. From the dual description this is surprising as quantum teleportation is a highly quantum process where the teleported qubit undergoes a "violent" procedure after the classical information is received.

However, the question of whether or not wormholes exist in nature is still unanswered. There are two main avenues when it comes to discovering and probing wormholes. The first one is observationally. It has been proposed that in order to understand whether an object is a wormhole we need to observe properties such as gravitational lensing [190–197], the "shadow" [198–205], the trajectories of stars orbiting the mouths [206–215], the spectra of accretion disks [216–224] and the trajectories of stars orbiting the (potential) mouths [225–233]. The lists of references are by no means exhaustive. In all of these cases, a lot of theoretical work has been done in order to find out the unique signature of wormholes in contrast to black holes. As most wormholes solutions are black hole mimickers it is not easy task. For an instructive review of the aforementioned methods we recommend [234], and references therein. Another approach that is hoped to give results is gravitational wave tests. Already in LIGO many gravitational wave signals from the merging of black holes have been detected, and LISA is under way. There have been studies that identify the differences between a black hole merger and a wormhole merger [226, 235], which can be used as templates in the search for wormholes.

The second option in order to probe wormholes is in the lab. One way we could do this is if we built two entangled CFTs with a holographic dual, then applied the non-local coupling of GJW to obtain a traversable wormhole. Even though there are studies that tell us how to build the thermofield double state [72], preparing two strongly coupled CFTs with a gravity dual in a lab is certainly not easy. However, a simplified version of this set-up might be possible [71, 236, 237].

In a recent paper [238] that attracted a lot of attention, the authors claim that they have managed to observe traversable wormhole dynamics on a quantum computer. The setup included two systems of entangled particles that act as the mouths of the wormhole. Each contained seven qubits. Then an eighth qubit (which is entangled with another external qubit) is swapped with on of the seven qubits of one side and its information is scattered among the other qubits. This is equivalent to inserting a particle in one of the mouths of the wormhole. Then, the two systems are coupled using a coupling term of the type $e^{i\mu V}$, similar to the GJW one. This

---

[1]Generically, the channel is quantum, but to circumvent that we can measure the operator $\mathcal{O}_L$, for example and transfer the classical information of the outcome to the right. More detail on how this works can be found in [2]

is supposed to have the effect of opening the dual wormhole. The result is that the transferred qubit appears on the other side, and remains entangled with its partner that lives on the other side, outside of the first mouth.

Of course this study is interesting because it opens up the way in making even more complicated and nuanced experiments on quantum computers in order to understand wormholes. It is important though to note, that despite the confusion in the press, a physical wormhole was not constructed. The goal was to observe the dynamics via a dual "baby" SYK model. However, many researchers have been skeptical about the interpretation of the results. From the fact that the number of qubits is too small to have an interesting gravity dual to more specific technical issues [239, 240]. Nevertheless is it a step towards the right direction and it might serve as a blueprint for future experiments on quantum computers.

Even though as we discussed wormholes have still not been observed in nature, we remain hopeful that in the future they will be.

Bibliography

[1] P. Gao, D. L. Jafferis, and A. C. Wall, "Traversable wormholes via a double trace deformation," *Journal of High Energy Physics*, vol. 2017, no. 12, p. 151, 2017.

[2] J. Maldacena, D. Stanford, and Z. Yang, "Diving into traversable wormholes," *Fortschritte der Physik*, vol. 65, no. 5, 2017.

[3] J. Maldacena, A. Milekhin, and F. Popov, "Traversable wormholes in four dimensions," 2018.

[4] A. Almheiri, N. Engelhardt, D. Marolf, and H. Maxfield, "The entropy of bulk quantum fields and the entanglement wedge of an evaporating black hole," *JHEP*, vol. 12, p. 063, 2019.

[5] G. Penington, "Entanglement Wedge Reconstruction and the Information Paradox," *JHEP*, vol. 09, p. 002, 2020.

[6] A. Almheiri, R. Mahajan, J. Maldacena, and Y. Zhao, "The Page curve of Hawking radiation from semiclassical geometry," *JHEP*, vol. 03, p. 149, 2020.

[7] A. Almheiri, T. Hartman, J. Maldacena, E. Shaghoulian, and A. Tajdini, "Replica Wormholes and the Entropy of Hawking Radiation," *JHEP*, vol. 05, p. 013, 2020.

[8] G. Penington, S. H. Shenker, D. Stanford, and Z. Yang, "Replica wormholes and the black hole interior," 11 2019.

[9] A. Almheiri, T. Hartman, J. Maldacena, E. Shaghoulian, and A. Tajdini, "The entropy of Hawking radiation," *Rev. Mod. Phys.*, vol. 93, no. 3, p. 035002, 2021.

[10] T. Hartman, Y. Jiang, and E. Shaghoulian, "Islands in cosmology," *JHEP*, vol. 11, p. 111, 2020.

[11] M. S. Morris and K. S. Thorne, "Wormholes in space-time and their use for interstellar travel: A tool for teaching general relativity," *Am. J. Phys.*, vol. 56, pp. 395–412, 1988.

[12] S. Carroll, *Spacetime and geometry : an introduction to general relativity / Sean Carroll.* San Francisco, CA [etc.: Addison Wesley, 2004.

[13] H. Epstein, V. Glaser, and A. Jaffe, "Nonpositivity of energy density in Quantized field theories," *Nuovo Cim.*, vol. 36, p. 1016, 1965.

[14] F. J. Tipler, "Energy conditions and spacetime singularities," *Physical Review D*, vol. 17, no. 10, p. 2521, 1978.

[15] L. H. Ford and T. A. Roman, "Averaged energy conditions and quantum inequalities," *Phys. Rev. D*, vol. 51, pp. 4277–4286, 1995.

[16] C. J. Fewster, K. D. Olum, and M. J. Pfenning, "Averaged null energy condition in spacetimes with boundaries," *Phys. Rev. D*, vol. 75, p. 025007, 2007.

[17] A. C. Wall, "A proof of the generalized second law for rapidly changing fields and arbitrary horizon slices," *Phys. Rev. D*, vol. 85, p. 104049, 2012. [Erratum: Phys.Rev.D 87, 069904 (2013)].

[18] W. R. Kelly and A. C. Wall, "Holographic proof of the averaged null energy condition," *Phys. Rev. D*, vol. 90, no. 10, p. 106003, 2014. [Erratum: Phys.Rev.D 91, 069902 (2015)].

[19] T. Faulkner, R. G. Leigh, O. Parrikar, and H. Wang, "Modular Hamiltonians for Deformed Half-Spaces and the Averaged Null Energy Condition," *JHEP*, vol. 09, p. 038, 2016.

[20] L. H. Ford, "Quantum coherence effects and the second law of thermodynamics," *Proceedings of the Royal Society of London. Series A, Mathematical and Physical Sciences (1934-1990)*, vol. 364, pp. 227–236, December 1978.

[21] S. K. Lamoreaux, "Demonstration of the Casimir force in the 0.6 to 6 micrometers range," *Phys. Rev. Lett.*, vol. 78, pp. 5–8, 1997. [Erratum: Phys.Rev.Lett. 81, 5475–5476 (1998)].

[22] U. Mohideen and A. Roy, "Precision measurement of the Casimir force from 0.1 to 0.9 micrometers," *Phys. Rev. Lett.*, vol. 81, pp. 4549–4552, 1998.

[23] G. Bressi, G. Carugno, R. Onofrio, and G. Ruoso, "Measurement of the Casimir force between parallel metallic surfaces," *Phys. Rev. Lett.*, vol. 88, p. 041804, 2002.

[24] H. B. G. Casimir, "On the Attraction Between Two Perfectly Conducting Plates," *Indag. Math.*, vol. 10, pp. 261–263, 1948.

[25] H. B. G. Casimir and D. Polder, "The Influence of retardation on the London-van der Waals forces," *Phys. Rev.*, vol. 73, pp. 360–372, 1948.

[26] M. Bordag, G. L. Klimchitskaya, U. Mohideen, and V. M. Mostepanenko, *Advances in the Casimir effect*, vol. 145. OUP Oxford, 2009.

[27] M. Visser, *Lorentzian wormholes: from Einstein to Hawking.* 1995.

[28] L. M. Butcher, "Casimir Energy of a Long Wormhole Throat," *Phys. Rev. D*, vol. 90, no. 2, p. 024019, 2014.

[29] A. C. L. Santos, C. R. Muniz, and L. T. Oliveira, "Casimir Effect in a Schwarzschild-Like Wormhole Spacetime," *Int. J. Mod. Phys. D*, vol. 30, no. 05, p. 2150032, 2021.

[30] C. R. Muniz, V. B. Bezerra, and J. M. Toledo, "Casimir effect in space-times of rotating wormholes," *Eur. Phys. J. C*, vol. 81, no. 3, p. 209, 2021.

[31] G. Alencar, V. B. Bezerra, and C. R. Muniz, "Casimir wormholes in $2+1$ dimensions with applications to the graphene," *Eur. Phys. J. C*, vol. 81, no. 10, p. 924, 2021.

[32] P. H. F. Oliveira, G. Alencar, I. C. Jardim, and R. R. Landim, "Traversable Casimir Wormholes in D Dimensions," 7 2021.

[33] J. Maldacena and A. Milekhin, "Humanly traversable wormholes," *Phys. Rev. D*, vol. 103, no. 6, p. 066007, 2021.

[34] R. Garattini, "Casimir Wormholes," *Eur. Phys. J. C*, vol. 79, no. 11, p. 951, 2019.

[35] L. Flamm, *Beiträge zur Einsteinschen gravitationstheorie.* Hirzel, 1916.

[36] A. Einstein and N. Rosen, "The Particle Problem in the General Theory of Relativity," *Phys. Rev.*, vol. 48, pp. 73–77, 1935.

[37] J. M. Maldacena, "The Large N limit of superconformal field theories and supergravity," *Adv. Theor. Math. Phys.*, vol. 2, pp. 231–252, 1998.

[38] E. Witten, "Anti-de Sitter space and holography," *Adv. Theor. Math. Phys.*, vol. 2, pp. 253–291, 1998.

[39] S. S. Gubser, I. R. Klebanov, and A. M. Polyakov, "Gauge theory correlators from noncritical string theory," *Phys. Lett. B*, vol. 428, pp. 105–114, 1998.

[40] T. Banks, M. R. Douglas, G. T. Horowitz, and E. J. Martinec, "AdS dynamics from conformal field theory," 8 1998.

[41] L. Susskind and E. Witten, "The Holographic bound in anti-de Sitter space," 5 1998.

[42] D. Harlow and D. Stanford, "Operator Dictionaries and Wave Functions in AdS/CFT and dS/CFT," 4 2011.

[43] S. B. Giddings, "The Boundary S matrix and the AdS to CFT dictionary," *Phys. Rev. Lett.*, vol. 83, pp. 2707–2710, 1999.

[44] J. M. Maldacena, "Eternal black holes in anti-de Sitter," *JHEP*, vol. 04, p. 021, 2003.

[45] Y. Takahashi and H. Umezawa, "Thermo field dynamics," *International journal of modern Physics B*, vol. 10, no. 13n14, pp. 1755–1805, 1996.

[46] I. Ichinose and Y. Satoh, "Entropies of scalar fields on three-dimensional black holes," *Nucl. Phys.*, vol. B447, pp. 340–372, 1995.

[47] G. Lifschytz and M. Ortiz, "Scalar field quantization on the (2+1)-dimensional black hole background," *Phys. Rev.*, vol. D49, pp. 1929–1943, 1994.

[48] S. H. Shenker and D. Stanford, "Black holes and the butterfly effect," *JHEP*, vol. 03, p. 067, 2014.

[49] S. H. Shenker and D. Stanford, "Multiple Shocks," *JHEP*, vol. 12, p. 046, 2014.

[50] E. Caceres, A. S. Misobuchi, and M.-L. Xiao, "Rotating traversable wormholes in AdS," *JHEP*, vol. 12, p. 005, 2018.

[51] J. Maldacena and X.-L. Qi, "Eternal traversable wormhole," 2018.

[52] B. Ahn, Y. Ahn, S.-E. Bak, V. Jahnke, and K.-Y. Kim, "Holographic teleportation in higher dimensions," *JHEP*, vol. 07, p. 219, 2021.

[53] S. Fallows and S. F. Ross, "Making near-extremal wormholes traversable," *JHEP*, vol. 12, p. 044, 2020.

[54] S. Hirano, Y. Lei, and S. van Leuven, "Information Transfer and Black Hole Evaporation via Traversable BTZ Wormholes," *JHEP*, vol. 09, p. 070, 2019.

[55] B. Freivogel, D. A. Galante, D. Nikolakopoulou, and A. Rotundo, "Traversable wormholes in AdS and bounds on information transfer," *JHEP*,

vol. 01, p. 050, 2020.

[56] B. Freivogel, V. Godet, E. Morvan, J. F. Pedraza, and A. Rotundo, "Lessons on Eternal Traversable Wormholes in AdS," 2019.

[57] R. van Breukelen and K. Papadodimas, "Quantum teleportation through time-shifted AdS wormholes," *JHEP*, vol. 08, p. 142, 2018.

[58] C. Bachas and I. Lavdas, "Quantum Gates to other Universes," *Fortsch. Phys.*, vol. 66, no. 2, p. 1700096, 2018.

[59] D. Bak, C. Kim, and S.-H. Yi, "Bulk view of teleportation and traversable wormholes," *JHEP*, vol. 08, p. 140, 2018.

[60] S. W. Hawking, "Particle Creation by Black Holes," *Commun. Math. Phys.*, vol. 43, pp. 199–220, 1975. [Erratum: Commun.Math.Phys. 46, 206 (1976)].

[61] J. D. Bekenstein, "Black holes and entropy," *Phys. Rev. D*, vol. 7, pp. 2333–2346, 1973.

[62] J. M. Bardeen, B. Carter, and S. W. Hawking, "The Four laws of black hole mechanics," *Commun. Math. Phys.*, vol. 31, pp. 161–170, 1973.

[63] S. W. Hawking, "Breakdown of Predictability in Gravitational Collapse," *Phys. Rev. D*, vol. 14, pp. 2460–2473, 1976.

[64] D. N. Page, "Information in black hole radiation," *Phys. Rev. Lett.*, vol. 71, pp. 3743–3746, 1993.

[65] S. Ryu and T. Takayanagi, "Holographic derivation of entanglement entropy from AdS/CFT," *Phys. Rev. Lett.*, vol. 96, p. 181602, 2006.

[66] V. E. Hubeny, M. Rangamani, and T. Takayanagi, "A Covariant holographic entanglement entropy proposal," *JHEP*, vol. 07, p. 062, 2007.

[67] T. Faulkner, A. Lewkowycz, and J. Maldacena, "Quantum corrections to holographic entanglement entropy," *JHEP*, vol. 11, p. 074, 2013.

[68] N. Engelhardt and A. C. Wall, "Quantum Extremal Surfaces: Holographic Entanglement Entropy beyond the Classical Regime," *JHEP*, vol. 01, p. 073, 2015.

[69] P. Gao, D. L. Jafferis, and A. Wall, "Traversable Wormholes via a Double Trace Deformation," *JHEP*, vol. 12, p. 151, 2017.

[70] J. Maldacena, D. Stanford, and Z. Yang, "Diving into traversable wormholes," *Fortsch. Phys.*, vol. 65, no. 5, p. 1700034, 2017.

[71] L. Susskind and Y. Zhao, "Teleportation through the wormhole," *Phys. Rev. D*, vol. 98, no. 4, p. 046016, 2018.

[72] W. Cottrell, B. Freivogel, D. M. Hofman, and S. F. Lokhande, "How to Build the Thermofield Double State," *JHEP*, vol. 02, p. 058, 2019.

[73] J. Martyn and B. Swingle, "Product Spectrum Ansatz and the Simplicity of Thermal States," 2018.

[74] J. L. Friedman, K. Schleich, and D. M. Witt, "Topological censorship," *Phys. Rev. Lett.*, vol. 71, pp. 1486–1489, 1993. [Erratum: Phys. Rev. Lett.75,1872(1995)].

[75] M. Visser, "Traversable wormholes: Some simple examples," *Phys. Rev.*, vol. D39, pp. 3182–3184, 1989.

[76] M. Visser, "Traversable wormholes from surgically modified Schwarzschild space-times," *Nucl. Phys.*, vol. B328, pp. 203–212, 1989.

[77] E. Poisson and M. Visser, "Thin shell wormholes: Linearization stability," *Phys. Rev.*, vol. D52, pp. 7318–7321, 1995.

[78] C. Barcelo and M. Visser, "Traversable wormholes from massless conformally coupled scalar fields," *Phys. Lett. B*, vol. 466, pp. 127–134, 1999.

[79] M. Visser, S. Kar, and N. Dadhich, "Traversable wormholes with arbitrarily small energy condition violations," *Phys. Rev. Lett.*, vol. 90, p. 201102, 2003.

[80] B. Bhawal and S. Kar, "Lorentzian wormholes in Einstein-Gauss-Bonnet theory," *Phys. Rev.*, vol. D46, pp. 2464–2468, 1992.

[81] M. Thibeault, C. Simeone, and E. F. Eiroa, "Thin-shell wormholes in Einstein-Maxwell theory with a Gauss-Bonnet term," *Gen. Rel. Grav.*, vol. 38, pp. 1593–1608, 2006.

[82] R. E. Arias, M. Botta Cantcheff, and G. A. Silva, "Lorentzian AdS, Wormholes and Holography," *Phys. Rev.*, vol. D83, p. 066015, 2011.

[83] S. N. Solodukhin, "Restoring unitarity in BTZ black hole," *Phys. Rev.*, vol. D71, p. 064006, 2005.

[84] G. T. Horowitz, D. Marolf, J. E. Santos, and D. Wang, "Creating a Traversable Wormhole," 2019.

[85] Z. Fu, B. Grado-White, and D. Marolf, "A perturbative perspective on self-supporting wormholes," *Class. Quant. Grav.*, vol. 36, no. 4, p. 045006, 2019. [Erratum: Class.Quant.Grav. 36, 249501 (2019)].

[86] M. Van Raamsdonk, "Building up spacetime with quantum entanglement," *Gen. Rel. Grav.*, vol. 42, pp. 2323–2329, 2010. [Int. J. Mod. Phys.D19,2429(2010)].

[87] M. Banados, C. Teitelboim, and J. Zanelli, "The Black hole in three-dimensional space-time," *Phys. Rev. Lett.*, vol. 69, pp. 1849–1851, 1992.

[88] M. Banados, M. Henneaux, C. Teitelboim, and J. Zanelli, "Geometry of the (2+1) black hole," *Phys. Rev.*, vol. D48, pp. 1506–1525, 1993. [Erratum: Phys. Rev.D88,069902(2013)].

[89] D. Nikolakopoulou, "Building traversable wormholes from Casimir energy and non-local couplings," Master's thesis, University of Amsterdam, 2018.

[90] S. H. Shenker and D. Stanford, "Stringy effects in scrambling," *JHEP*, vol. 05, p. 132, 2015.

[91] T. Dray and G. 't Hooft, "The Effect of Spherical Shells of Matter on the Schwarzschild Black Hole," *Commun. Math. Phys.*, vol. 99, pp. 613–625, 1985.

[92] G. Dvali and M. Redi, "Black Hole Bound on the Number of Species and Quantum Gravity at LHC," *Phys. Rev.*, vol. D77, p. 045027, 2008.

[93] N. Kaloper, M. Kleban, A. Lawrence, and M. S. Sloth, "Large Field Inflation and Gravitational Entropy," *Phys. Rev.*, vol. D93, no. 4, p. 043510, 2016.

[94] I. H. Redmount, "Blue-sheet instability of schwarzschild wormholes," *Progress of theoretical physics*, vol. 73, no. 6, pp. 1401–1426, 1985.

[95] N. Bao, A. Chatwin-Davies, J. Pollack, and G. N. Remmen, "Traversable Wormholes as Quantum Channels: Exploring CFT Entanglement Structure and Channel Capacity in Holography," *JHEP*, vol. 11, p. 071, 2018.

[96] D. Berenstein, "Quenches on thermofield double states and time reversal symmetry," 2019.

[97] S. B. Giddings, D. J. Gross, and A. Maharana, "Gravitational effects in ultrahigh-energy string scattering," *Phys. Rev.*, vol. D77, p. 046001, 2008.

[98] D. Anninos, D. A. Galante, and D. M. Hofman, "De Sitter Horizons & Holographic Liquids," *JHEP*, vol. 07, p. 038, 2019.

[99] M. S. Morris, K. S. Thorne, and U. Yurtsever, "Wormholes, Time Machines, and the Weak Energy Condition," *Phys. Rev. Lett.*, vol. 61, pp. 1446–1449, 1988.

[100] M. Visser, "Traversable wormholes: Some simple examples," *Physical Review D*, vol. 39, no. 10, p. 3182, 1989.

[101] M. Chernicoff, E. García, G. Giribet, and E. Rubín de Celis, "Thin-shell wormholes in AdS$_5$ and string dioptrics," 6 2020.

[102] X. O. Camanho, J. D. Edelstein, J. Maldacena, and A. Zhiboedov, "Causality constraints on corrections to the graviton three-point coupling," *Journal of High Energy Physics*, vol. 2016, no. 2, p. 20, 2016.

[103] P. Gao, D. L. Jafferis, and A. C. Wall, "Traversable Wormholes via a Double Trace Deformation," *JHEP*, vol. 12, p. 151, 2017.

[104] J. de Boer, R. Van Breukelen, S. F. Lokhande, K. Papadodimas, and E. Verlinde, "On the interior geometry of a typical black hole microstate," *JHEP*, vol. 05, p. 010, 2019.

[105] A. Almheiri, A. Mousatov, and M. Shyani, "Escaping the Interiors of Pure Boundary-State Black Holes," 3 2018.

[106] J. De Boer, R. Van Breukelen, S. F. Lokhande, K. Papadodimas, and E. Verlinde, "Probing typical black hole microstates," *JHEP*, vol. 01, p. 062, 2020.

[107] Z. Fu, B. Grado-White, and D. Marolf, "Traversable Asymptotically Flat Wormholes with Short Transit Times," *Class. Quant. Grav.*, vol. 36, no. 24, p. 245018, 2019.

[108] B. Freivogel, V. Godet, E. Morvan, J. F. Pedraza, and A. Rotundo, "Lessons on Eternal Traversable Wormholes in AdS," *JHEP*, vol. 07, p. 122, 2019.

[109] A. May and M. Van Raamsdonk, "Interpolating between multi-boundary wormholes and single-boundary geometries in holography," 11 2020.

[110] R. Emparan, B. Grado-White, D. Marolf, and M. Tomasevic, "Multi-mouth Traversable Wormholes," 12 2020.

[111] A. A. Balushi, Z. Wang, and D. Marolf, "Traversability of Multi-Boundary Wormholes," 12 2020.

[112] J. Maldacena and X.-L. Qi, "Eternal traversable wormhole," 2018.

[113] J. Maldacena, "Comments on magnetic black holes," 4 2020.

[114] A. R. Brown, H. Gharibyan, S. Leichenauer, H. W. Lin, S. Nezami, G. Salton, L. Susskind, B. Swingle, and M. Walter, "Quantum Gravity in the Lab: Teleportation by Size and Traversable Wormholes," 11 2019.

[115] S. Nezami, H. W. Lin, A. R. Brown, H. Gharibyan, S. Leichenauer, G. Salton, L. Susskind, B. Swingle, and M. Walter, "Quantum Gravity in the Lab: Teleportation by Size and Traversable Wormholes, Part II," 2 2021.

[116] W. Cottrell, B. Freivogel, D. M. Hofman, and S. F. Lokhande, "How to Build the Thermofield Double State," *JHEP*, vol. 02, p. 058, 2019.

[117] S. Banerjee and J. Kames-King, "Traversable wormholes in AdS and their CFT duals,"

[118] M. Van Raamsdonk, "Cosmology from confinement?," 2 2021.

[119] M. Henningson and K. Sfetsos, "Spinors and the AdS / CFT correspondence," *Phys. Lett. B*, vol. 431, pp. 63–68, 1998.

[120] M. Henneaux, "Boundary terms in the AdS / CFT correspondence for spinor fields," in *International Meeting on Mathematical Methods in Modern Theoretical Physics (ISPM 98)*, pp. 161–170, 9 1998.

[121] A. J. Amsel and D. Marolf, "Supersymmetric Multi-trace Boundary Conditions in AdS," *Class. Quant. Grav.*, vol. 26, p. 025010, 2009.

[122] J. M. Maldacena, J. Michelson, and A. Strominger, "Anti-de Sitter fragmentation," *JHEP*, vol. 02, p. 011, 1999.

[123] V. Balasubramanian and P. Kraus, "A Stress tensor for Anti-de Sitter gravity," *Commun. Math. Phys.*, vol. 208, pp. 413–428, 1999.

[124] S. A. Hartnoll, C. P. Herzog, and G. T. Horowitz, "Holographic Superconductors," *JHEP*, vol. 12, p. 015, 2008.

[125] O. J. Dias, R. Masachs, O. Papadoulaki, and P. Rodgers, "Hunting for fermionic instabilities in charged AdS black holes," *JHEP*, vol. 04, p. 196, 2020.

[126] L. Romans, "Supersymmetric, cold and lukewarm black holes in cosmological einstein-maxwell theory," *Nuclear Physics B*, vol. 383, p. 395–415, Sep 1992.

[127] H. K. Kunduri, J. Lucietti, and H. S. Reall, "Supersymmetric multi-charge AdS_5 black holes," *Journal of High Energy Physics*, vol. 2006, p. 036–036, Apr 2006.

[128] J. B. Gutowski and H. S. Reall, "General supersymmetric AdS_5 black holes," *Journal of High Energy Physics*, vol. 2004, p. 048–048, Apr 2004.

[129] S. Bhattacharyya, S. Minwalla, and K. Papadodimas, "Small hairy black holes in $AdS_5 \times S^5$," *Journal of High Energy Physics*, vol. 2011, Nov 2011.

[130] Y. Chen, V. Gorbenko, and J. Maldacena, "Bra-ket wormholes in gravitationally prepared states," 7 2020.

[131] M. Van Raamsdonk, "Comments on wormholes, ensembles, and cosmology," 8 2020.

[132] A. Lewkowycz and J. Maldacena, "Generalized gravitational entropy," *JHEP*, vol. 08, p. 090, 2013.

[133] X. Dong, A. Lewkowycz, and M. Rangamani, "Deriving covariant holographic entanglement," *JHEP*, vol. 11, p. 028, 2016.

[134] X. Dong, "The Gravity Dual of Renyi Entropy," *Nature Commun.*, vol. 7, p. 12472, 2016.

[135] A. Almheiri, R. Mahajan, and J. Maldacena, "Islands outside the horizon," 10 2019.

[136] A. Almheiri, R. Mahajan, and J. E. Santos, "Entanglement islands in higher dimensions," *SciPost Phys.*, vol. 9, no. 1, p. 001, 2020.

[137] H. Z. Chen, Z. Fisher, J. Hernandez, R. C. Myers, and S.-M. Ruan, "Information Flow in Black Hole Evaporation," *JHEP*, vol. 03, p. 152, 2020.

[138] M. Rozali, J. Sully, M. Van Raamsdonk, C. Waddell, and D. Wakeham, "Information radiation in BCFT models of black holes," *JHEP*, vol. 05, p. 004, 2020.

[139] H. Geng and A. Karch, "Massive islands," *JHEP*, vol. 09, p. 121, 2020.

[140] H. Geng, Y. Nomura, and H.-Y. Sun, "Information paradox and its resolution in de Sitter holography," *Phys. Rev. D*, vol. 103, no. 12, p. 126004, 2021.

[141] H. Z. Chen, R. C. Myers, D. Neuenfeld, I. A. Reyes, and J. Sandor, "Quantum Extremal Islands Made Easy, Part I: Entanglement on the Brane," *JHEP*, vol. 10, p. 166, 2020.

[142] V. Balasubramanian, A. Kar, and T. Ugajin, "Entanglement between two disjoint universes," *JHEP*, vol. 02, p. 136, 2021.

[143] V. Balasubramanian, A. Kar, and T. Ugajin, "Islands in de Sitter space," *JHEP*, vol. 02, p. 072, 2021.

[144] D. Teresi, "Islands and the de Sitter entropy bound," 12 2021.

[145] S. Azarnia, R. Fareghbal, A. Naseh, and H. Zolfi, "Islands in flat-space cosmology," *Phys. Rev. D*, vol. 104, no. 12, p. 126017, 2021.

[146] R. Bousso and E. Wildenhain, "Gravity/ensemble duality," *Phys. Rev. D*, vol. 102, no. 6, p. 066005, 2020.

[147] K. Goto, T. Hartman, and A. Tajdini, "Replica wormholes for an evaporating 2D black hole," *JHEP*, vol. 04, p. 289, 2021.

[148] R. Bousso and A. Shahbazi-Moghaddam, "Island Finder and Entropy Bound," *Phys. Rev. D*, vol. 103, no. 10, p. 106005, 2021.

[149] Y. Chen, V. Gorbenko, and J. Maldacena, "Bra-ket wormholes in gravitationally prepared states," *JHEP*, vol. 02, p. 009, 2021.

[150] T. Hartman, Y. Jiang, and E. Shaghoulian, "Islands in cosmology," *JHEP*, vol. 11, p. 111, 2020.

[151] R. Bousso and E. Wildenhain, "Islands in Closed and Open Universes," 2 2022.

[152] S. R. Coleman and F. De Luccia, "Gravitational Effects on and of Vacuum Decay," *Phys. Rev. D*, vol. 21, p. 3305, 1980.

[153] E. Farhi and A. H. Guth, "An Obstacle to Creating a Universe in the Laboratory," *Phys. Lett. B*, vol. 183, pp. 149–155, 1987.

[154] B. Freivogel, V. E. Hubeny, A. Maloney, R. C. Myers, M. Rangamani, and S. Shenker, "Inflation in AdS/CFT," *JHEP*, vol. 03, p. 007, 2006.

[155] K. Langhoff, C. Murdia, and Y. Nomura, "Multiverse in an inverted island," *Phys. Rev. D*, vol. 104, no. 8, p. 086007, 2021.

[156] S. E. Aguilar-Gutierrez, A. Chatwin-Davies, T. Hertog, N. Pinzani-Fokeeva, and B. Robinson, "Islands in Multiverse Models," 8 2021.

[157] W. Sybesma, "Pure de Sitter space and the island moving back in time," *Class. Quant. Grav.*, vol. 38, no. 14, p. 145012, 2021.

[158] Y. Ling, Y. Liu, and Z.-Y. Xian, "Island in Charged Black Holes," *JHEP*, vol. 03, p. 251, 2021.

[159] W. Kim and M. Nam, "Entanglement entropy of asymptotically flat non-extremal and extremal black holes with an island," *Eur. Phys. J. C*, vol. 81, no. 10, p. 869, 2021.

[160] M. Miyaji, "Island for gravitationally prepared state and pseudo entanglement wedge," *JHEP*, vol. 12, p. 013, 2021.

[161] R. Li, X. Wang, and J. Wang, "Island may not save the information paradox

of Liouville black holes," *Phys. Rev. D*, vol. 104, no. 10, p. 106015, 2021.

[162] N. H. Cao, "Entanglement entropy and Page curve of black holes with island in massive gravity," *Eur. Phys. J. C*, vol. 82, no. 4, p. 381, 2022.

[163] X.-L. Qi, "Entanglement island, miracle operators and the firewall," *JHEP*, vol. 01, p. 085, 2022.

[164] E. Verheijden and E. Verlinde, "From the BTZ black hole to JT gravity: geometrizing the island," *JHEP*, vol. 11, p. 092, 2021.

[165] M.-H. Yu, C.-Y. Lu, X.-H. Ge, and S.-J. Sin, "Island, Page curve, and superradiance of rotating BTZ black holes," *Phys. Rev. D*, vol. 105, no. 6, p. 066009, 2022.

[166] W.-C. Gan, D.-H. Du, and F.-W. Shu, "Island and Page curve for one-sided asymptotically flat black hole," *JHEP*, vol. 07, p. 020, 2022.

[167] R.-X. Miao, "Massless Entanglement Island in Wedge Holography," 12 2022.

[168] A. Karlsson, "Concerns about the replica wormhole derivation of the island conjecture," 1 2021.

[169] P.-J. Hu, D. Li, and R.-X. Miao, "Island on codimension-two branes in AdS/dCFT," *JHEP*, vol. 11, p. 008, 2022.

[170] M.-S. Seo, "Information paradox and island in quasi-de Sitter space," *Eur. Phys. J. C*, vol. 82, no. 12, p. 1082, 2022.

[171] A. Rolph, "Island mirages," *JHEP*, vol. 08, p. 142, 2022.

[172] K. S. Reddy, "A timelike entangled island at the initial singularity in a JT FLRW ($\Lambda > 0$) universe," 11 2022.

[173] I. Lavdas, "Entanglement Islands, AdS-Massive Gravity and Holography," *PoS*, vol. CORFU2021, p. 208, 2022.

[174] G. Yadav and N. Joshi, "Cosmological and black hole islands in multi-event horizon spacetimes," *Phys. Rev. D*, vol. 107, no. 2, p. 026009, 2023.

[175] D. S. Ageev, I. Y. Aref'eva, A. I. Belokon, A. V. Ermakov, V. V. Pushkarev, and T. A. Rusalev, "Entanglement Islands and Infrared Anomalies in Schwarzschild Black Hole," 8 2022.

[176] K. Suzuki and T. Takayanagi, "BCFT and Islands in two dimensions," *JHEP*, vol. 06, p. 095, 2022.

[177] G. Grimaldi, J. Hernandez, and R. C. Myers, "Quantum extremal islands

made easy. Part IV. Massive black holes on the brane," *JHEP*, vol. 03, p. 136, 2022.

[178] A. Saha, S. Gangopadhyay, and J. P. Saha, "Mutual information, islands in black holes and the Page curve," *Eur. Phys. J. C*, vol. 82, no. 5, p. 476, 2022.

[179] K. Hashimoto, N. Iizuka, and Y. Matsuo, "Islands in Schwarzschild black holes," *JHEP*, vol. 06, p. 085, 2020.

[180] J. Hernandez, R. C. Myers, and S.-M. Ruan, "Quantum extremal islands made easy. Part III. Complexity on the brane," *JHEP*, vol. 02, p. 173, 2021.

[181] X. Wang, R. Li, and J. Wang, "Islands and Page curves of Reissner-Nordström black holes," *JHEP*, vol. 04, p. 103, 2021.

[182] G. K. Karananas, A. Kehagias, and J. Taskas, "Islands in linear dilaton black holes," *JHEP*, vol. 03, p. 253, 2021.

[183] Y. Lu and J. Lin, "Islands in Kaluza–Klein black holes," *Eur. Phys. J. C*, vol. 82, no. 2, p. 132, 2022.

[184] H. Geng, A. Karch, C. Perez-Pardavila, S. Raju, L. Randall, M. Riojas, and S. Shashi, "Information Transfer with a Gravitating Bath," *SciPost Phys.*, vol. 10, no. 5, p. 103, 2021.

[185] H. Geng, A. Karch, C. Perez-Pardavila, S. Raju, L. Randall, M. Riojas, and S. Shashi, "Inconsistency of islands in theories with long-range gravity," *JHEP*, vol. 01, p. 182, 2022.

[186] J. de Boer, V. Jahnke, K.-Y. Kim, and J. F. Pedraza, "Worldsheet traversable wormholes," 11 2022.

[187] R. Emparan, B. Grado-White, D. Marolf, and M. Tomasevic, "Multi-mouth Traversable Wormholes," *JHEP*, vol. 05, p. 032, 2021.

[188] A. Al Balushi, Z. Wang, and D. Marolf, "Traversability of Multi-Boundary Wormholes," *JHEP*, vol. 04, p. 083, 2021.

[189] L. Aalsma, A. Cole, E. Morvan, J. P. van der Schaar, and G. Shiu, "Shocks and information exchange in de Sitter space," *JHEP*, vol. 10, p. 104, 2021.

[190] J. G. Cramer, R. L. Forward, M. S. Morris, M. Visser, G. Benford, and G. A. Landis, "Natural wormholes as gravitational lenses," *Phys. Rev. D*, vol. 51, pp. 3117–3120, 1995.

[191] D. F. Torres, E. F. Eiroa, and G. E. Romero, "On the possibility of an astronomical detection of chromaticity effects in microlensing by wormhole

- like objects," *Mod. Phys. Lett. A*, vol. 16, pp. 1849–1861, 2001.

[192] K. K. Nandi, Y.-Z. Zhang, and A. V. Zakharov, "Gravitational lensing by wormholes," *Phys. Rev. D*, vol. 74, p. 024020, 2006.

[193] F. Rahaman, M. Kalam, and S. Chakraborty, "Gravitational lensing by stable C-field wormhole," *Chin. J. Phys.*, vol. 45, p. 518, 2007.

[194] T. K. Dey and S. Sen, "Gravitational lensing by wormholes," *Mod. Phys. Lett. A*, vol. 23, pp. 953–962, 2008.

[195] A. Bhattacharya and A. A. Potapov, "Bending of light in Ellis wormhole geometry," *Mod. Phys. Lett. A*, vol. 25, pp. 2399–2409, 2010.

[196] P. K. F. Kuhfittig, "Gravitational lensing of wormholes in the galactic halo region," *Eur. Phys. J. C*, vol. 74, no. 99, p. 2818, 2014.

[197] K. Jusufi, A. Ovgün, and A. Banerjee, "Light deflection by charged wormholes in Einstein-Maxwell-dilaton theory," *Phys. Rev. D*, vol. 96, no. 8, p. 084036, 2017. [Addendum: Phys.Rev.D 96, 089904 (2017)].

[198] D.-C. Dai and D. Stojkovic, "Observing a Wormhole," *Phys. Rev. D*, vol. 100, no. 8, p. 083513, 2019.

[199] D.-C. Dai and D. Stojkovic, "Reply to "Comment on 'Observing a wormhole'"," *Phys. Rev. D*, vol. 101, no. 6, p. 068302, 2020.

[200] T. Do *et al.*, "Relativistic redshift of the star S0-2 orbiting the Galactic center supermassive black hole," *Science*, vol. 365, no. 6454, pp. 664–668, 2019.

[201] J. H. Simonetti, M. J. Kavic, D. Minic, D. Stojkovic, and D.-C. Dai, "Sensitive searches for wormholes," *Phys. Rev. D*, vol. 104, no. 8, p. L081502, 2021.

[202] M. Kavic, J. H. Simonetti, S. E. Cutchin, S. W. Ellingson, and C. D. Patterson, "Transient Pulses from Exploding Primordial Black Holes as a Signature of an Extra Dimension," *JCAP*, vol. 11, p. 017, 2008.

[203] J. H. Simonetti, M. Kavic, D. Minic, U. Surani, and V. Vijayan, "A Precision Test for an Extra Spatial Dimension Using Black Hole–Pulsar Binaries," *Astrophys. J. Lett.*, vol. 737, p. L28, 2011.

[204] J. Estes, M. Kavic, M. Lippert, and J. H. Simonetti, "Pulsar–black hole binaries as a window on quantum gravity," *Int. J. Mod. Phys. D*, vol. 26, no. 12, p. 1743004, 2017.

[205] M. J. Kavic, D. Minic, and J. Simonetti, "Quantum gravity and BH-NS binaries," *Int. J. Mod. Phys. D*, vol. 27, no. 14, p. 1847007, 2018.

[206] H. Falcke, F. Melia, and E. Agol, "Viewing the shadow of the black hole at the galactic center," *Astrophys. J. Lett.*, vol. 528, p. L13, 2000.

[207] C. Bambi and K. Freese, "Apparent shape of super-spinning black holes," *Phys. Rev. D*, vol. 79, p. 043002, 2009.

[208] C. Bambi, "Can the supermassive objects at the centers of galaxies be traversable wormholes? The first test of strong gravity for mm/sub-mm very long baseline interferometry facilities," *Phys. Rev. D*, vol. 87, p. 107501, 2013.

[209] Y. Mizuno, Z. Younsi, C. M. Fromm, O. Porth, M. De Laurentis, H. Olivares, H. Falcke, M. Kramer, and L. Rezzolla, "The Current Ability to Test Theories of Gravity with Black Hole Shadows," *Nature Astron.*, vol. 2, no. 7, pp. 585–590, 2018.

[210] P. G. Nedkova, V. K. Tinchev, and S. S. Yazadjiev, "Shadow of a rotating traversable wormhole," *Phys. Rev. D*, vol. 88, no. 12, p. 124019, 2013.

[211] T. Ohgami and N. Sakai, "Wormhole shadows," *Phys. Rev. D*, vol. 91, no. 12, p. 124020, 2015.

[212] A. Abdujabbarov, B. Juraev, B. Ahmedov, and Z. Stuchlík, "Shadow of rotating wormhole in plasma environment," *Astrophys. Space Sci.*, vol. 361, no. 7, p. 226, 2016.

[213] R. Shaikh, "Shadows of rotating wormholes," *Phys. Rev. D*, vol. 98, no. 2, p. 024044, 2018.

[214] G. Gyulchev, P. Nedkova, V. Tinchev, and S. Yazadjiev, "On the shadow of rotating traversable wormholes," *Eur. Phys. J. C*, vol. 78, no. 7, p. 544, 2018.

[215] M. Amir, A. Banerjee, and S. D. Maharaj, "Shadow of charged wormholes in Einstein–Maxwell–dilaton theory," *Annals Phys.*, vol. 400, pp. 198–207, 2019.

[216] C. Bambi *et al.*, "Towards Precision Measurements of Accreting Black Holes Using X-Ray Reflection Spectroscopy," *Space Sci. Rev.*, vol. 217, no. 5, p. 65, 2021.

[217] T. Harko, Z. Kovacs, and F. S. N. Lobo, "Electromagnetic signatures of thin accretion disks in wormhole geometries," *Phys. Rev. D*, vol. 78, p. 084005,

2008.

[218] T. Harko, Z. Kovacs, and F. S. N. Lobo, "Thin accretion disks in stationary axisymmetric wormhole spacetimes," *Phys. Rev. D*, vol. 79, p. 064001, 2009.

[219] R. K. Karimov, R. N. Izmailov, and K. K. Nandi, "Accretion disk around the rotating Damour–Solodukhin wormhole," *Eur. Phys. J. C*, vol. 79, no. 11, p. 952, 2019.

[220] S. Paul, R. Shaikh, P. Banerjee, and T. Sarkar, "Observational signatures of wormholes with thin accretion disks," *JCAP*, vol. 03, p. 055, 2020.

[221] A. Tripathi, M. Zhou, A. B. Abdikamalov, D. Ayzenberg, C. Bambi, L. Gou, V. Grinberg, H. Liu, and J. F. Steiner, "Testing general relativity with the stellar-mass black hole in LMC X-1 using the continuum-fitting method," *Astrophys. J.*, vol. 897, no. 1, p. 84, 2020.

[222] A. Tripathi, A. B. Abdikamalov, D. Ayzenberg, C. Bambi, V. Grinberg, and M. Zhou, "Testing the Kerr Black Hole Hypothesis with GX 339–4 by a Combined Analysis of Its Thermal Spectrum and Reflection Features," *Astrophys. J.*, vol. 907, no. 1, p. 31, 2021.

[223] A. Tripathi, Y. Zhang, A. B. Abdikamalov, D. Ayzenberg, C. Bambi, J. Jiang, H. Liu, and M. Zhou, "Testing General Relativity with NuSTAR data of Galactic Black Holes," *Astrophys. J.*, vol. 913, no. 2, p. 79, 2021.

[224] C. Bambi, "Broad Kα iron line from accretion disks around traversable wormholes," *Phys. Rev. D*, vol. 87, p. 084039, 2013.

[225] V. Cardoso and P. Pani, "Testing the nature of dark compact objects: a status report," *Living Rev. Rel.*, vol. 22, no. 1, p. 4, 2019.

[226] V. Cardoso, E. Franzin, and P. Pani, "Is the gravitational-wave ringdown a probe of the event horizon?," *Phys. Rev. Lett.*, vol. 116, no. 17, p. 171101, 2016. [Erratum: Phys.Rev.Lett. 117, 089902 (2016)].

[227] R. A. Konoplya and C. Molina, "The Ringing wormholes," *Phys. Rev. D*, vol. 71, p. 124009, 2005.

[228] R. A. Konoplya and A. Zhidenko, "Wormholes versus black holes: quasinormal ringing at early and late times," *JCAP*, vol. 12, p. 043, 2016.

[229] K. K. Nandi, R. N. Izmailov, A. A. Yanbekov, and A. A. Shayakhmetov, "Ring-down gravitational waves and lensing observables: How far can a wormhole mimic those of a black hole?," *Phys. Rev. D*, vol. 95, no. 10, p. 104011, 2017.

[230] P. Bueno, P. A. Cano, F. Goelen, T. Hertog, and B. Vercnocke, "Echoes of Kerr-like wormholes," *Phys. Rev. D*, vol. 97, no. 2, p. 024040, 2018.

[231] S. Aneesh, S. Bose, and S. Kar, "Gravitational waves from quasinormal modes of a class of Lorentzian wormholes," *Phys. Rev. D*, vol. 97, no. 12, p. 124004, 2018.

[232] J. L. Blázquez-Salcedo, X. Y. Chew, and J. Kunz, "Scalar and axial quasi-normal modes of massive static phantom wormholes," *Phys. Rev. D*, vol. 98, no. 4, p. 044035, 2018.

[233] M. S. Churilova, R. A. Konoplya, and A. Zhidenko, "Arbitrarily long-lived quasinormal modes in a wormhole background," *Phys. Lett. B*, vol. 802, p. 135207, 2020.

[234] C. Bambi and D. Stojkovic, "Astrophysical Wormholes," *Universe*, vol. 7, no. 5, p. 136, 2021.

[235] S.-s. Bao, S. Hou, and H. Zhang, "Searching for wormholes with gravitational wave scattering," *Eur. Phys. J. C*, vol. 83, no. 2, p. 127, 2023.

[236] L. Susskind, "Dear Qubitzers, GR=QM," 8 2017.

[237] P. Gao and D. L. Jafferis, "A traversable wormhole teleportation protocol in the SYK model," *JHEP*, vol. 07, p. 097, 2021.

[238] D. Jafferis, A. Zlokapa, J. D. Lykken, D. K. Kolchmeyer, S. I. Davis, N. Lauk, H. Neven, and M. Spiropulu, "Traversable wormhole dynamics on a quantum processor," *Nature*, vol. 612, no. 7938, pp. 51–55, 2022.

[239] G. Weinstein, "A Comment on "Traversable wormhole dynamics on a quantum processor"," 1 2023.

[240] B. Kobrin, T. Schuster, and N. Y. Yao, "Comment on "Traversable wormhole dynamics on a quantum processor"," 2 2023.

[241] F. Zimmermann, "Future colliders for particle physics —"Big and small"," *Nucl. Instrum. Meth. A*, vol. 909, pp. 33–37, 2018.

[242] G. 't Hooft, "Dimensional reduction in quantum gravity," *Conf. Proc. C*, vol. 930308, pp. 284–296, 1993.

[243] L. Susskind, "The World as a hologram," *J. Math. Phys.*, vol. 36, pp. 6377–6396, 1995.

[244] J. Maldacena and L. Susskind, "Cool horizons for entangled black holes," *Fortsch. Phys.*, vol. 61, pp. 781–811, 2013.

Summary

One of the biggest unresolved problems in modern physics is the formulation of a theory of quantum gravity. The reason is the seeming incompatibility of the theory of general relativity with quantum physics. General relativity describes accurately physics on large scales, such as planets and galaxies, whereas quantum mechanics capture the physics of small scales, such as atoms and subatomic particles. Both theories have been put to the test for many decades. They have both been verified experimentally and their predictions have been found to be correct to a remarkable degree of accuracy. Moreover, they are used in numerous technologies and applications. General relativity is used, among others, in GPS systems where accuracy is important and one needs to account for relativistic phenomena such as time dilation, and in observational astronomy, gravitational lensing is used to make maps of dark matter. Quantum physics also have many applications such as in lasers, MRI scanners, computers and atomic clocks.

However, trying to study gravity in quantum field theory is problematic and the detection of the graviton in a collider is also a distant dream. As Zimmermann illustrates in [241] *"Assuming these fields, the Planck scale of $10^{28}\,eV$ can be reached by a circular or linear collider with a size of about $10^{10}\,m$, or about a tenth of the distance between earth and sun, for either type of collider!"*

A notorious instance where these two theories appear to clash is black holes. From General Relativity we expect that information that falls in the black hole disappears forever. The fate of anything crossing the black hole horizon is sealed. In the 70s, in a series of papers [60–62], it was proven that black holes quantumly, emit radiation and evaporate. Hawking initially thought that even though black holes evaporate, information that falls in is indeed lost forever. However, this violates a core principle of quantum physics: *conservation of information*, leading to the black hole information paradox. Nowadays, we firmly believe that information is not lost in black holes, but the the question of exactly what happens to the information that fell in the black hole after the evaporation is complete, still

remains.

A breakthrough happened when 't Hooft and independently Susskind formulated the holographic principle [242, 243], which says that gravity is emergent from a lower dimensional quantum field theory. In 1997 Maldacena, in his seminal paper [37], proposed the AdS/CFT correspondence, in which a theory of gravity in d dimensional Anti-de-Sitter spacetime is dual to a conformal field theory in one dimension less. This leads us to the following train of thought. A black hole in AdS will be dual to a CFT and CFTs are unitary. This means that information cannot be lost.

One of the reasons that we study wormholes is that they can provide insights about how information can escape black holes. A popular holographic wormhole lives in the bulk of a three dimensional maximally extended AdS black hole, called the BTZ geometry. The BTZ geometry is dual to a maximally entangled state called the thermofield double. At this point it is important to take a moment to discuss entanglement, which is a curious property of quantum physics. Assuming that we entangle a pair of particles by making them interact in some way or produce them by pair creation, they are always going to be "connected", even if they are very far apart. If we measure the quantum state of one, we automatically know the quantum state of the other. Recently, it was proposed by Susskind and Maldacena [244] that entanglement in a holographic system gives rise to a wormhole. The wormhole in the heart of BTZ is such an example. However, it is non-traversable, so we cannot send information through it.

This viewpoint changed in 2016 when Gao, Jafferis and Wall (GJW) [1] constructed the first holographic traversable wormhole. They started with the BTZ black hole and added a non-local coupling. This coupling term creates two negative energy shocks waves that propagate in the bulk and render the wormhole traversable. In chapter 2 of this thesis we studied this wormhole and derived various bounds on how much information can go through it, while staying in the probe approximation. We found that the amount of information that can go through the GJW wormhole is $\mathcal{O}(hr_h/\ell)$, which is a lot smaller than the black hole entropy. Moreover, by coupling many fields instead of only one, we increased the amount of information that can be transferred to be approximately equal to the black hole entropy. Finally, assuming that in the CFT side this protocol is dual to teleportation, we derived an estimate of the information bound from the boundary perspective and compared it to the bulk one.

In chapter 3 we again harnessed the power of the non-local coupling introduced in [1], and constructed a four dimensional eternal AdS wormhole. Starting with two four dimensional magnetically charged Reissner-Nordstrom AdS black holes, we

coupled their dual CFTs. This gives rise to negative energy. When we calculated the backreaction that this negative energy has on our spacetime we found a static traversable wormhole without horizons or singularities. We also found that this wormhole is dual to the ground state of a simple Hamiltonian and for certain values of the parameters of this Hamiltonian we found where the wormhole solution dominates.

In chapter 4 we changed focus and directed our attention on recent developments in the information paradox front. Recently, in a serious of breakthrough papers [4–9] the Page curve of Hawking radiation was recovered within semi-classical gravity, using the island formula. Essentially, what was realized is that in order to correctly calculate the fine grained entropy of the radiation we need to include in the computation a disconnected region that usually lies in the black hole, called the island. The island formula naturally has been applied mostly in black holes, where we have a clear notion of the information paradox.

However, in [10] the authors derived three conditions that are necessary in order to have an island. These rules can be applied in a variety of spacetimes. In [10] they apply it in spatially flat FRW cosmologies that are supported by radiation and cosmological constant. They find that for negative cosmological constant there is a non-trivial island that starts at a large finite value and extends to infinity.

We extended this research and applied this formula to open and closed sliced FRW cosmologies. We found that in the case of negative cosmological constant both for open and closed universes we have non-trivial islands. We concluded that the most important feature that indicates whether or not we have non-trivial islands is the negative cosmological constant.

Samenvatting

Een van de grootste onopgeloste problemen in de moderne natuurkunde is de formulering van een theorie van kwantumzwaartekracht. Dit komt door de schijnbare onverenigbaarheid van de algemene relativiteitstheorie met kwantumfysica. De algemene relativiteitstheorie beschrijft nauwkeurig de fysica op grote schaal, zoals planeten en sterrenstelsels, terwijl kwantummechanica de fysica van kleine schaal vastlegt, zoals atomen en subatomaire deeltjes. Beide theorieën zijn al tientallen jaren op de proef gesteld. Ze zijn allebei experimenteel geverifieerd en hun voorspellingen blijken opmerkelijk nauwkeurig te zijn. Bovendien gebruiken we ze in meerdere technologieën en toepassingen. De algemene relativiteitstheorie wordt onder andere gebruikt in GPS-systemen, waar nauwkeurigheid belangrijk is en men rekening moet houden met relativistische verschijnselen zoals tijddilatatie, en in de waarnemingsastronomie wordt zwaartekrachtlensing gebruikt om kaarten van donkere materie te maken. Kwantumfysica wordt toegepast in onder andere lasers, MRI-scanners, computers en atoomklokken.

Het is echter problematisch om zwaartekracht in de kwantumveldentheorie te bestuderen, en de detectie van het graviton in een deeltjesversneller is nog een verre droom. Zoals Zimmermann illustreert in [241] *"Uitgaande van deze velden, kan de Planck-schaal van $10^{28}\,eV$ worden bereikt door een cirkelvormige of lineaire versneller met een grootte van ongeveer $10^{10}\,m$, ongeveer een tiende van de afstand tussen de aarde en de zon, voor beide soorten versneller!"*

Een berucht geval waarin de twee theorieën lijken te botsen is een zwart gat. Vanuit de algemene relativiteitstheorie verwachten we dat informatie die in het zwarte gat valt voor altijd verdwijnt. Het lot van alles wat de horizon van het zwarte gat passeert, is bezegeld. In de jaren 70 werd echter in een reeks artikelen [60–62] bewezen dat zwarte gaten kwantumstraling uitzenden en daarbij verdampen. Hawking dacht aanvankelijk dat hoewel zwarte gaten verdampen, informatie die erin valt inderdaad voor altijd verloren gaat. Dit is echter in strijd met een kernprincipe van kwantumfysica: behoud van informatie. Zo ontstond de

informatieparadox van zwarte gaten. Tegenwoordig zijn we ervan overtuigd dat er geen informatie verloren gaat in zwarte gaten, maar de vraag blijft wat er precies gebeurt met de informatie die in het zwarte gat is gevallen nadat de verdamping is voltooid.

Een doorbraak vond plaats toen 't Hooft en Susskind onafhankelijk van elkaar het holografische principe formuleerden [242, 243]. Volgens dit principe ontstaat zwaartekracht uit een lager-dimensionale kwantumveldentheorie. In 1997 stelde Maldacena in zijn baanbrekende artikel [37] de AdS/CFT-correspondentie voor, waarin een zwaartekrachttheorie in d-dimensionale Anti-de-Sitter-ruimtetijd duaal is aan een conforme veldentheorie in één dimensie minder. Dit leidt ons tot de volgende gedachtegang: een zwart gat in AdS zal duaal zijn aan een CFT, en CFT's zijn unitair. Dit betekent dat informatie niet verloren kan gaan.

Een van de redenen dat we wormgaten bestuderen, is dat ze inzicht kunnen geven in hoe informatie aan zwarte gaten kan ontsnappen. Een populair holografisch wormgat leeft in het midden van een driedimensionaal maximaal uitgestrekt AdS-zwart gat, in de zogeheten BTZ-geometrie. Deze geometrie is duaal aan een maximaal verstrengelde toestand dat we het thermoveld-dubbel noemen. Op dit punt is het belangrijk even de tijd te nemen om verstrengeling te bespreken, wat een merkwaardige eigenschap is van kwantumfysica. Ervan uitgaande dat we een paar deeltjes verstrengelen door ze op de een of andere manier te laten interageren of ze te produceren met paarvorming, zullen ze altijd "verbonden" zijn, zelfs wanneer ze ver uit elkaar liggen. Als we de kwantumtoestand van de één meten, weten we automatisch de kwantumtoestand van de ander. Onlangs werd door Susskind en Maldacena [244] voorgesteld dat verstrengeling in een holografisch systeem leidt tot een wormgat. Het wormgat in het hart van de BTZ-geometrie is zo'n voorbeeld. Deze is echter niet doorkruisbaar, dus we kunnen er geen informatie doorheen sturen.

Dit standpunt veranderde in 2016 toen Gao, Jafferis en Wall (GJW) [1] het eerste holografische doorkruisbare wormgat construeerden. Ze begonnen met het BTZ zwarte gat en voegden een niet-lokale koppeling toe. Deze koppelingsterm creëert twee negatieve energieschokgolven die zich in de massa voortplanten en het wormgat doorkruisbaar maken. In hoofdstuk 2 van dit proefschrift bestudeerden we dit wormgat en leidde we verschillende grenzen af voor hoeveel informatie er doorheen kan gaan, terwijl we binnen de sondebenadering blijven. We ontdekten dat de hoeveelheid informatie die door het GJW-wormgat kan gaan $\mathcal{O}(hr_h/\ell)$ is, wat een stuk kleiner is dan de entropie van een zwart gat. Daarnaast hebben we, door veel velden te koppelen in plaats van slechts één, de hoeveelheid informatie die kan worden overgedragen vergroot tot ongeveer gelijk aan de entropie van een zwart gat. Ten slotte, in de veronderstelling dat dit protocol aan de CFT-kant duaal is

aan teleportatie, hebben we een schatting afgeleid van de informatiegrens vanuit het grensperspectief en deze vergeleken met de bulk.

In hoofdstuk 3 hebben we opnieuw gebruik gemaakt van de kracht van de niet-lokale koppeling die is geïntroduceerd in [1], en hebben we een vierdimensionaal eeuwig AdS-wormgat geconstrueerd. Beginnend met twee vierdimensionale magnetisch geladen Reissner-Nordstrom AdS zwarte gaten, koppelden we hun dubbele CFT's. Dit leidt tot een negatieve energie. Toen we de terugreactie berekenden die deze negatieve energie heeft op onze ruimtetijd, vonden we een statisch doorkruisbaar wormgat zonder horizonten of singulariteiten. We ontdekten ook dat dit wormgat duaal is aan de grondtoestand van een eenvoudige Hamiltoniaan en voor bepaalde waarden van de parameters van deze Hamiltoniaan vonden we waar de wormgatoplossing domineert.

In hoofdstuk 4 hebben we de focus verlegd en onze aandacht gericht op recente ontwikkelingen op het gebied van de informatieparadox. Onlangs werd in een reeks baanbrekende artikelen [4–9] de Page-curve van Hawking-straling teruggevonden binnen semi-klassieke zwaartekracht, met behulp van de eilandformule. Wat in wezen werd gerealiseerd, is dat om de fijnkorrelige entropie van de straling correct te berekenen we in de berekening een losgekoppeld gebied moeten opnemen dat meestal in het zwarte gat ligt, het eiland genaamd. De eilandformule is natuurlijk vooral toegepast in zwarte gaten, waar we een duidelijk beeld hebben van de informatieparadox.

In [10] hebben de auteurs echter drie voorwaarden afgeleid die nodig zijn om een eiland te hebben. Deze regels kunnen worden toegepast in verschillende ruimtetijden. In [10] passen ze het toe in ruimtelijk vlakke FRW-kosmologieën die worden ondersteund door straling en een kosmologische constante. Ze ontdekken dat er voor een negatieve kosmologische constante een niet-triviaal eiland is dat begint bij een grote eindige waarde en zich uitstrekt tot in het oneindige. We hebben dit onderzoek uitgebreid en deze formule toegepast op open en gesloten FRW-kosmologieën. We ontdekten in het geval van een negatieve kosmologische constante dat er niet-triviale eilanden bestaan in zowel open als gesloten universums. We concludeerden dat de negatieve kosmologische constante het belangrijkste kenmerk is dat aangeeft of we wel of geen niet-triviale eilanden hebben.

Acknowledgements

First and foremost I want to thank my supervisor Ben Freivogel. You set an impossible standard for every future supervisor I'll have. Your expertise, physical intuition and enthusiasm for physics were always matched by your kindness, compassion and humanity. Secondly, I want to thank my co-supervisor Alejandra Castro for being a wonderful teacher to me during my masters years and an inspiration. I would also like to thank Erik Verlinde for letting me participate in the discussions of the master project of Matteo Selle and in this way helping me learn new things and explore different subjects.

A big thank you is also owed to the physicists that have influenced and inspired me earlier in my academic steps Theocharis Apostolatos, Kostas Georgakopoulos, Andreas Kassetas and last but not least Stratos Georgoudis, who truly made me love physics, always challenged me and who when I succeeded in my national exams and entered the Physics department was the first to call me "his colleague".

To Evita, Carlos and Gabri, I cannot begin to express how thankful I am for meeting you and getting to be your office mate and your friend. Thank you for being there for me, in your own completely unique ways. To my colleagues Tony, Ricardo and Suzanne, what an absolute pleasure it was to work with you. You turned annoying days into great ones. Suzanne it was a pleasure not only to work with you but to laugh with you out loud. Tony very few people have the combination of your patience (which I often tried with my questions), kindness, modesty and excellent humor.

Rebecca and Jans I am so thankful we found each other. I am always uplifted and empowered by your company and interesting conversations. Eleni, Gaby and Aeris thank for being there for me through the worst of the pandemic, keeping me sane with your friendship. Thanks to Tarek, Laura, Jacksson, Yukiko, Austin, Mert and John for their friendship and innumerable excellent dinners and barbeques.

Thanks also to Zoe, Christos, Colleen and Vickram for their precious friendship

and company. To Vassilis, thank you for helping me through my masters and igniting my interest in physics, it truly made a difference.

Kostas, Korina, Sol, Dimitra, and Venia thank you for your unfailing support and love throughout the years. To my parents a big thank you for supporting my studies and for believing in me.

A special thanks is due to my husband Alex. Your priceless company, love, friendship and faith in me was a moving force during the years and certainly in the writing of this thesis.